UNIVERSITY
OF TRENTO - Italy
DEPARTMENT OF INDUSTRIAL ENGINEERING

XXXII cycle

Doctoral School in Materials, Mechatronics and Systems Engineering

A MODEL SCAFFOLD FOR ANTERIOR CRUCIATE LIGAMENT TISSUE ENGINEERING

Silvia Chiera

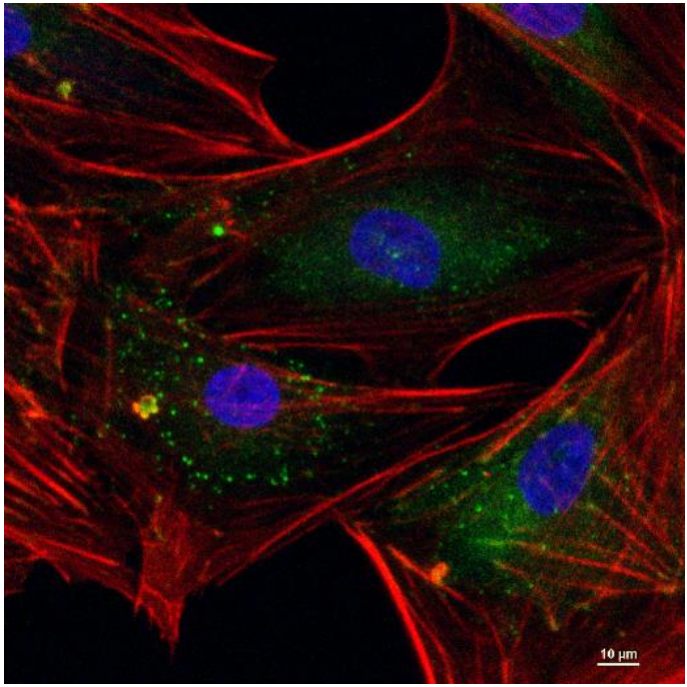

2021

A MODEL SCAFFOLD FOR ANTERIOR CRUCIATE LIGAMENT TISSUE ENGINEERING

Silvia Chiera

E-mail: silvia.chiera.1@unitn.it; chiera.silvia@gmail.com

Approved by:

Prof. Antonella Motta,
Department of Industrial Engineering
University of Trento, Italy.

Prof. Claudio Migliaresi,
Department of Industrial Engineering
University of Trento, Italy.

Ph.D. Commission:

Prof. Nuno Neves,
Department of Polymer Engineering
University of Minho, Portugal.

Prof. Sorada Kanokpanont,
Department of Chemical Engineering
Chulalongkorn University, Thailand.

Prof. Devid Maniglio,
Department of Industrial Engineering
University of Trento, Italy.

University of Trento,

Department of Industrial Engineering

2021

University of Trento - Department of Industrial Engineering

Doctoral Thesis

Silvia Chiera - 2021
Published in Trento (Italy) – by University of Trento

ISBN: - - - - - - - - -

To myself

Abstract

Ligament/tendon disorders and injuries are among the most common health problem influencing the adult and sport population. Anterior cruciate ligament (ACL), is one of the ligaments most injured in the knee, and the soft-to-hard tissue integration (enthesis) shows high rupture rates. To overcome problems related to therapies currently used in medical practice, tissue engineering (TE) has recently emerged as an alternative strategy. TE is a field that applies principles of biology, engineering and medicine toward the development of biological tissue substitutes to restore, repair or improve damaged tissues. Ligament/tendon TE focuses on the combination of specific cell types with a biodegradable scaffold. Once implanted, the scaffold has gradually to degrade, while the tissue is regenerating. The scaffold should be able to promote cell adhesion, differentiation, proliferation and extracellular matrix (ECM) production. Different scaffold materials have been successfully studied for TE application, and among them, silk fibroin has emerged as a promising one.

In this work, silk fibroin has been used to fabricate a ligament scaffold comprising the ligamentous part and the enthesis. The enthesis was fabricated with fibroin sponges with a region of anisotropic porosity (ligament site) and a region of isotropic

porosity (bone site). The enthesis construct was functionalized with heparin molecules to increase the growth factors affinity. Specifically, the effects of TGF-β2 and GDF5 combined with the structural features of the scaffold led to differentiation of AdMSCs. The alignment of the pores and the biological cues synergistically influenced the gene expression and the protein expression. In fact, the tendon/ligament markers were promoted in the anisotropic part of the construct, as well as the cartilage and the enthesis markers in the isotropic and transition part, respectively.

The central part of the ligament was realized with a composite of silk fibroin yarns in a spongeous matrix of silk fibroin, where the yarns have the role to sustain the applied load and the fibroin sponge the role of allowing cell penetration, organization and ECM production. The amount of yarns was decided on the basis of the reported loading of the ligament scaffold after a surgery and during rehabilitation.

A homemade perfusion bioreactor was used to evaluate cell penetration and activity in the scaffold. It was proven that cell culture perfusion stimulation induced cells to populate the model scaffold and to produce ECM components, especially with the presence of TGF-β2 growth factor, indicating the starting point of the regeneration process. Additionally, animal studies have been performed and the inflammatory response was evaluated.

Even if not final, the results indicate that the above strategy could be explored for the fabrication of a full ligament TE scaffold able to bear the physiological loads until the ligament regenerates.

Table of contents

Preface

This thesis reports the research activities conducted during my PhD program, at the BIOtech Research Center and Industrial Engineering Department of the University of Trento, under the supervision of Professor Antonella Motta and Professor Claudio Migliaresi. Parts of the research were performed in collaboration with Trauma Lab (Munich, Germany) under the supervision of Professor Doctor Matijn Van Griensven and Doctor Elizabeth Rosado Balmayor, and at the Department of Engineering of Chonbuck National University (Jeonju, South Korea) under the supervision of Professor Gilson Khang.

The general aim of this work was to develop a silk fibroin model scaffold for ligament tissue engineering. The thesis illustrates the materials and methods adopted, the experiments performed and the results obtained, following the structured chapters:

- Chapter I: *Introduction*. In the first part, an overview of the anatomical structure of anterior cruciate ligament and the interface of ligament-to-bone tissue is reported, with structural and mechanical properties, and their treatments in the current strategies of surgery. In the second part the role of tissue engineering is described, in details related to the regeneration of the ligament and of the interphase between the soft and the hard tissue.

Particular attention is given to silk fibroin, its properties and biomedical applications.

- Chapter II: *Rationale, aims and design of the research activity.* In this chapter, the outline and the aims of the research work are presented to expose the rationality of the thesis.
- Chapter III: *Tissue engineering of tendon/ligament-to-bone insertion*. This chapter describes the work done in collaboration with the group of prof. Van Griensven about a novel strategy for the regeneration of enthesis based on the development of integrated tissue-engineered tendon/ligament-to-bone constructs (scaffolds). The results obtained show the impact of the synergistic effect between the fabrication parameters on the structural properties (porosity gradient) of the constructs and the biochemical cues (growth factors), on cell behaviour and expression of tendon/ligament markers.
- Chapter IV: *A multicomponent model for Anterior Cruciate Ligament (ACL)*. This chapter focuses on the development of a multicomponent model scaffold able to mimic the central ligament part of ACL. The results obtained show the impact of the structural properties on the mechanical role of the scaffold and the biological

effects influenced by a perfusion bioreactor, specifically homemade designed for this purpose, combined with growth factor functionalization.

- Chapter V: *Final remarks and future perspectives*. The conclusions are discussed and possible future developments for ligament tissue engineering applications are suggested.

Chapter I. Introduction

1.1. Anterior Cruciate Ligament (ACL)

Disorders and injuries of ligament tissue are among the most common health problem influencing the adult population and athletes [1,2]. In the United States around 200000 cases of surgical ACL interventions happen every year, and this number may be in expansion considering that the participation in sport activities is increasing [1,3]. Anterior cruciate ligament (ACL) is one of the most studied ligaments in medical history. Descriptions about injuries to ACL are dating back centuries [4].

1.1.1. Structure of ACL

Ligament is a connective tissue that binds bone-to-bone and has the main role in joint stability and locomotion [5,6]. In the case of anterior cruciate ligament (ACL), it binds femur and tibia, its length has a range between 22 and 41 mm and its diameter between 7 and 12 mm, according to age and gender [5,7]. It is a fundamental component of the knee for its remarkable structural properties [5], and it is organized in a multi-unit hierarchical structure composed of collagen molecules, fibrils (150-250 nm), fibre bundles (1-20 μm), subfascicular units (100-250 μm) mainly arranged along their longitudinal axes [6,8]. Subfasciculi,

formed of groups of subfascicular units, are surrounded by loose connective tissue called endotenon, forming fasciculi, mainly composed of collagen II. Groups of fasciculi form fascicles surrounded by epitenon, reaching several millimetres in diameter, and groups of fascicles are delimited by a connective tissue called paratenon [5,8–10], Figure 1. The hierarchical structure surrounded by loose connective tissue allows the ligament to tolerate multiple axial stress and non-linear mechanical deformation [5,9,11].

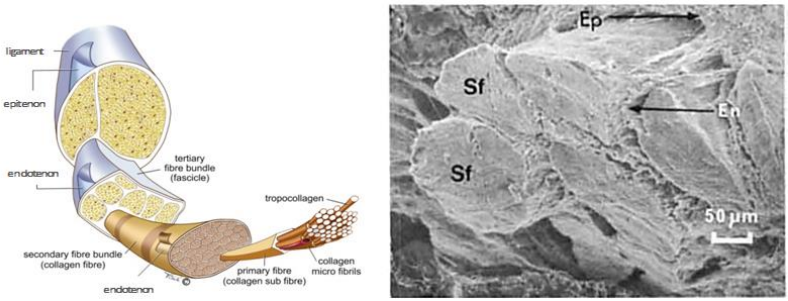

Figure 1: schematic hierarchical structure of ligament (on the left), imaged used with permission. Copyright Vicky Earle, Medical Illustrator. SEM image of smaller subfascicular units (Sf) of human ACL with their connective tissue endotenon (En) and external epitenon (Ep), adapted from [8] (on the right).

The organization of the extracellular matrix (ECM) molecules of ligament at nanometric and micrometric levels is the principal determinant of the physiological function and the mechanical strength of the tissue [6]. Also the biochemical composition gives a contribution to the viscoelastic behaviour and the cellular

composition of the tissue, in fact, as Frank [9] says: “ligaments are approximately two-thirds water and one-third solid”. The principal and the major constituent of the solid part is collagen (primarily composed of collagen I) together with proteoglycans, elastin and other glycoproteins [9,12]. Moreover, the presence of blood vessels is not homogeneous in ligament tissue, which is generally considered a low vascularized tissue, leading to a poor healing capacity [5,13–15]. Another structural characteristic that can impact ligament mechanical behaviour, is the presence of crimps. Crimps are collagen bundle fibres showing a morphological “waviness” along the axis length. In relation to the ligament region and position (for example: anterior-medial (AM) vs posterior-lateral (PL)), it is possible to observe different crimp pattern. According to the crimp angle and length, the biochemical role of the ligament can result in a different behaviour, in fact, crimps contribute to the formation of “toe” region typical of a stress-strain curve, once the ligament is tensed from the rest state [9,12,16–20] .

1.1.1.1. Enthesis structure, function and mechanical properties

Considering the whole structure of ACL, particular attention has to be given to the insertion site of the ligament in to the bone.

The interface between tendon/ligament-to-bone is a specialized tissue called “enthesis”.

According to the bony insertion, the enthesis can consist of a direct or indirect attachment, respectively defined also as fibrocartilaginous or fibrous enthesis [21–23]. Since the former typology has more relevance in the clinical scenario, the current section is describing that type of insertion. A fibrocartilaginous enthesis can be histologically divided in four areas: tendon/ligament (pure dense fibrous connective tissue), unmineralized fibrocartilage (UF), mineralized fibrocartilage (MF) and bone (Figure 2).

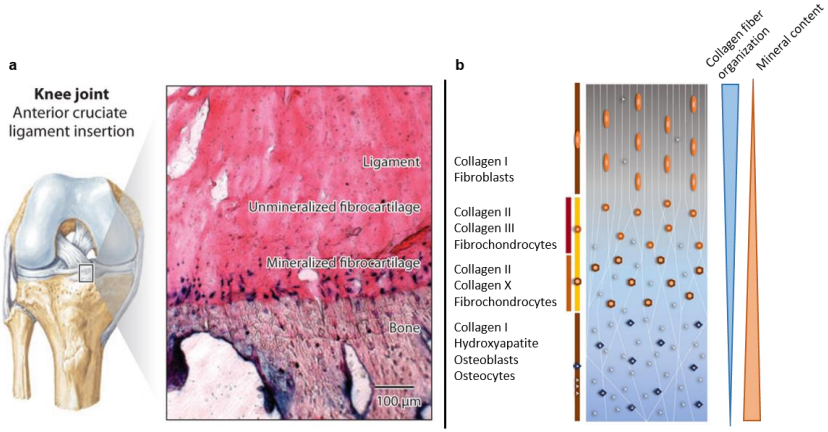

Figure 2: **a**) anterior cruciate ligament (ACL) example of ligament-to-bone interphase where the gradual fibrocartilaginous transition is visible. The histological image reports a stained section of a bovine ACL; image taken from [24]. **b**) fibrocartilage enthesis representation with schematic structure and composition, where is possible to observe the four zones composing the enthesis ECM. The ligament zone consists of fibroblasts and collagen I fibers

highly organized and aligned. The unmineralized fibrocartilage (UF) zone consists of fibrochondrocytes, collagen II and III. The mineralized fibrocartilage (MF) consists of fibrochondrocytes and mainly collagen II, but also collagen X. The mineral content starts to increase moving towards the bone area, with different fibers organization and porosity. This fourth zone consists of mineralized collagen I, osteoblasts and osteocytes. Image adapted from [21].

The extracellular matrix along the four regions is non-homogenous, it is characterized by various cell types, structure, composition and mechanical properties. In fact, the whole enthesis is represented by different collagen fiber alignment organization and mineral content. The former gradually increases from the bone area to the ligament one, while the mineralization steadily increases toward the bone region. The gradient formed by the collagen organization and the mineral content at the microscale is responsible for the gradual transition in force transmission, defining the mechanical properties of the enthesis [21,22,25–27] (Figure 2b). As mentioned by Genin et al. [28], the mineral content is also important for the value of stiffness across the insertion. They also reported that the tissue tensile modulus changes along the enthesis from ~0.45 GPa in the tendon/ligament to ~20 GPa in the bone, nearly two orders of magnitude mismatch. The mineralization is higher at the interphase compared to the tendon/ligament. Nevertheless, it is the interconnectivity between mineral particles that affects the

mineral content, causing an increase in stiffness. In fact, stress can be transferred through the mineral phase, when the amount of mineral particles create enough contact between particles in collagen fibers [28].

1.1.2. Mechanical properties of ACL

The role of ligament and its hierarchical structure is to withstand loads, to perform torsions and elongations. In reality, the biomechanical behaviour of the ACL is characterized by its structural properties. In fact, Woo at al [29] investigated the tensile properties of the complex femur-ACL-tibia (from human cadaver) and they found out that tensile mechanical properties change according to specimen age and orientation. In the Table 1, it is possible to read the collected data in two different orientations (anatomical and tibial) and in three age groups. It is possible to observe that over the course of the age, stiffness and ultimate load significantly decrease in both orientations, that can be explained accordingly to the decrease of the physical condition of the donors. Also the two orientations show differences, but the authors consider the anatomical one, "the realistic representation of the strength of the ACL" [29].

Age group	Specimen orientation	Stiffness (N/mm)	Ultimate load (N)
Younger (22-35)	Anatomical	242 ± 28	2160 ± 157
	Tibial	218 ± 27	1602 ± 167
Middle (40-50)	Anatomical	220 ± 24	1503 ± 83
	Tibial	192 ± 17	1160 ± 104
Older (60-97)	Anatomical	180 ± 25	658 ± 129
	Tibial	124 ± 16	495 ± 85

Table 1: stiffness and ultimate load values of specimen with different age and different test orientation, adapted from [29].

However, the typical representation of the mechanical properties and the viscoelastic behaviour of ligaments subjected to tensile force is a stress-strain curve. An example can be found in Figure 3, in which in the initial non-linear region, it possible to identify the so-called “toe” region, typically representing the effect of the crimp pattern on the rest state of the ligament tissue [16,30]. The toe region is followed by the linear region, in which the crimp patterns of collagen bundles are stretched, whose slope can be analysed to determine the ligament stiffness (N/mm) and Young’s modulus (Pa). Continuing to increase the load applied, then the ultimate load is reached and followed by the rupture of the ligament [6,15,31].

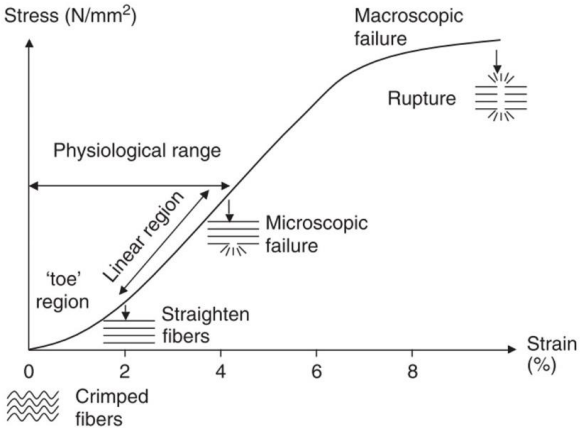

Figure 3: typical ligament stress-strain curve, image from [6].

1.1.3. Current strategies in surgery for ACL treatment

When damages and injuries occur to ligaments, nowadays the common medical procedure adopted is related to the surgical reconstruction [5,32]. As already mentioned, since ligament tissue is low vascularized, the process of regeneration and consequently the healing capacity is practically absent, so the aim is trying to restore the functionality of the tissue as much as possible [33]. For this reason, the current strategies are mainly focused on autografts and allografts [1,7,13,33–36]. The former consist of grafts of tissue from the patient him/herself. Generally, they are preferred to allografts for their availability and ability to reproduce the biomechanical properties of the tissue [1,13].

Sometimes, they can overcome strength and stiffness of natural ACL to succeed complications during healing [37]. Since they are *auto*-grafts, they reduce immunological rejection but they have higher probability to cause donor site morbidity with consequently complications and pain [1,13]. Normally, they are performed with patellar tendon (PT), also known as bone-patellar tendon-bone (BPTB), or hamstring tendons (HT) [1,32,33]. On the other hand, allografts consist of grafts coming from a source different from the patient him/herself, for example another patient or a cadaver. They are considered more suitable grafts for the shorter clinical time needed during surgical operation and for the lower probability to cause donor site morbidity. Nevertheless, they are related to a more frequent immunological response of the patient and to a higher failure rate compared with autografts, besides showing the risk of lack of donors. Usually they are performed with Achilles and tibia tendons [1,13,33]. From the 50s, synthetic materials such as Supramid, Teflon or Dacron, Proplast, carbon fiber graft, ABC graft, Kennedy-LAD, Trevia, Leeds-Keio, Gore-Tex, PDS, EULIT, Polyflex or LARS, have been proposed as alternative grafts for ACL replacement. However, many of them showed high failure rates, making the choice of a synthetic grafts questionable [38].

1.2. Tissue engineering strategy

As mentioned before, allografts and autografts are the most adopted techniques in surgery for ACL repair, even if they are presenting some limitations. Since some decades ago, tissue engineering (TE) has emerged as an alternative solution to overcome problems related to the therapies currently used in medical practice to treat tissue/organ failure. Tissue engineering is a multidisciplinary field that proposes to apply principles of biology, engineering and medicine toward the development of biological tissue substitutes to restore, repair or improve diseased or damaged tissues [39,40]. It can offer potential alternatives managing, in this case, ligament disorders and injuries. The main idea behind tissue engineering is to incorporate specific cell types into a biodegradable scaffold closely resembling the original extracellular matrix (ECM) of the tissue, which can be implanted into a defect and then gradually degrade, while the tissue is regenerating and restoring its functionalities [14].

Tissue engineering is related to a new tissue formation for therapeutic reconstruction through a systematic combination of molecular and mechanical signals. These principles can be schematically resumed in Figure 4. The ability of the human body to repair itself under some limited conditions (tissue/size)

generally concerns nonspecific reparative tissue with subsequent scar formation instead of the regeneration of the specific functional tissue that has been affected. As Williams said: “Tissue engineering is the persuasion of the body to heal itself, achieved by the delivery to the appropriate site of cells, biomolecules and supporting structures: the scaffold” [41]. A scaffold is a temporary supporting structure that provides cells attachment, proliferation and matrix production. It has to biologically function in the implant site and it needs to have specific properties to work as a substitute for the ECM, promoting cellular adhesion and proliferation. Some specific properties that a scaffold should exhibit include biocompatibility, three-dimensionality, porosity, high surface area, appropriate mechanical properties and biodegradability. Biocompatibility refers to the ability of a material to perform with an appropriate host response in a specific situation [42]. The biocompatibility is also affected by the physical morphology and properties that are particularly important in the regulation of cellular activities. The scaffold can also be loaded with growth factors that promote a specific cellular or tissue response that enhances the regenerative process. In such cases, the success of the tissue engineering scaffold will also depend on the ability to provide adequate release kinetics of the various growth factors on multiple timescales referring to their temporal and spatial

expression within complex tissue defects during the healing cascade [43]. Moreover scaffolds should not degrade into harmful residues that could decrease the replicative capacity of the seeded cells and remain stable until a continuous network of ECM is present and then degrade as the network matures [44].

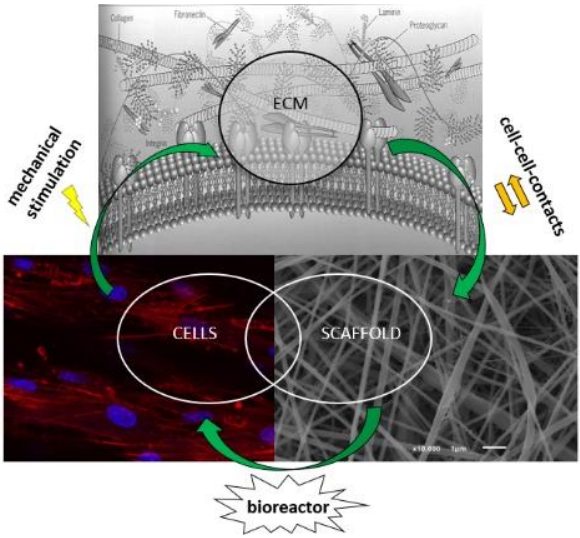

Figure 4: the essential principles for tissue engineering. For the successful generation of functional tissue, the different components (cells, medium and growth factors, scaffold material) must be provided in a suitable environment (formation of cell-cell contacts, mechanical loading, and bioreactor).

1.2.1. Ligament tissue engineering

One of the most important challenges in ligament tissue engineering is to develop scaffolds that mimic the three-dimensional structure of the natural ligament extracellular matrix,

which is a complex fibrous network (from 150 nm to 20 μm diameter fibers). For this reason, a fibrous scaffold is considered the best option to mimic the structure and the mechanical properties for ligament tissue engineering [45–47]. Moreover, the scaffold should be able to promote cell adhesion and differentiation, especially when growth factor and/or bioreactor are combined to trigger cell response into ligament lineage [46–49]. Ligament tissue engineering focuses on the fabrication of scaffold biomaterials that can mimic the hierarchical structure of the ligament to balance the biomechanical properties and the biological performances of the native tissue. Along the time, as mentioned in the article of Nau et al., different types of scaffolds have been developed using natural and synthetic materials, or composite of both of them for ACL TE [47]. In general, synthetic polymers show advantages in the ease of processing and in the higher mechanical properties compared to the ones of natural polymers. On the other hand, natural polymers are used for their biocompatibility, biodegradability, non-toxicity, anti-microbial activity and cell affinity, all properties that are widely used and required in the biomedical field [14,48,50,51]. Petrigliano et al. reviewed the characteristics that a biocompatible scaffold should have, considering the advantages of synthetic and natural polymers in combination with mechanical properties, cellular response and degradation rate, able to provide durable and

compatible constructs [52]. For ligament tissue engineering, Lu et al. made a comparison of different synthetic braided materials and poly L-lactic acid (PLLA) resulted to be the best synthetic polymer in mechanical properties as well as in cell proliferation for ACL TE [53]. Also Cooper et al. focused on PLLA polymer, developing a three-dimensional braided scaffold showing the macrostructure of the whole ACL, from the bony attachment to the intra articular zone, with the exhibition of an optimal porosity for tissue ingrowth [54]. Moreover, they further demonstrated that a braid-twist PLLA scaffold could show viscoelastic properties similar to natural ACL [55]. Buma et al. studied the reconstruction of ACL in an *in vivo* animal study using a braided polydioxanone (PDS) scaffold, but they reported an early loss of mechanical properties not attractive for clinical applications [56]. Liljensten at al. proposed the poly(urethane urea) (PUUR) polymer, because it was shown to have similar loading profile as the human ACL tested post-mortem [57], and also because the PUUR implanted allowed cell migration and neovascularization, indicating tolerance by the host [58].

Besides all these applications of synthetic polymers, there are different natural materials used for ACL TE, for example, collagen, hyaluronic acid (HA), poly(3-hydroxybutyrate) (PHB), poly(3-hydroxybutyrate-co-3-hydroxyvalerate) (PHBV), poly(3-hydroxyundecenoate) (PHUE-O3) and silk fibroin (SF) used with

interesting but controversial results for ligament tissue engineering [48,59]. Irie at al. evaluated an innovative fibrous scaffold for ligament engineering composed of chitosan and hyaluronan that improved the collagen I production and the mechanical strength in *in vivo* studies [60]. Yilgor at al. reported several studies in which collagen, since it is one of the component of the native tissue, is used as scaffold material able to stimulate fibroblast growth and help ligament regeneration [48]. Silk has become of notably importance for ACL TE. In various studies, silk alone or combined with other biopolymers, and in different shapes, has been used for its remarkable properties, from the mechanical and the biological point of view, compared to all the other materials [46,47,61,62].

1.2.1.1. Enthesis tissue engineering

All the characteristics aforementioned have to be considered also for enthesis tissue regeneration (TE), to be emerged as an alternative strategy compared to the limitations that the existing approaches in surgery show. For TE is important to investigate the tissue structure and its function [27], to mimic the damaged tissue that has to be repaired. In the enthesis case, the typical structure adopted is a stratified or multiphase scaffold, able to mimic the diverse organization of the native tissue [24]. Particular attention has to be paid to size and alignment of scaffold pores,

morphology, or fibers, which are all elements that have been shown to influence mechanical properties, and overall the cell behaviour [63]. In fact, it has been shown that topographical cues can affect cell proliferation, morphology, and gene expression [63]. Several research groups tried to fix the enthesis tissue. For example, Ishikawa et al. mixed collagen gel and hydroxyapatite (HA) powder to fix tendon into a bone tunnel. Histological results showed that grafted tendon resulted in direct contact with the new bone (in rabbit), demonstrating that the mix of HA and collagen can be a promising bone substitute [64]. Robertson et al. tried similar technique (in porcine model) but using α-BSM calcium phosphate cement, that could help the fixation of tendon to the bone during the initial phase of healing, able also to increase the stiffness of the graft [65]. Paxton et al. investigated the effect of HA with RGD peptide in polyethylene glycol (PEG) hydrogel to create an *in vitro* tissue interface, which resulted in a construct with no increased mechanical properties, but showed the potential to induce and increase cell adhesion [66]. Spalazzi et al. fabricated a triphasic scaffold with PLGA and a co-culture of osteoblast-fibroblast for ligament-to-bone interface, *in vitro* and *in vivo* (rats), demonstrating the suitability of the scaffold to a multi-tissue regeneration, promoting cell infiltration and matrix production [67,68].

Not only the structure, but also the polymer used to fabricate the scaffold is a relevant feature to consider [69]. As already mentioned in the previous paragraph, silk fibroin has been proven to have a great potential as material for TERM applications [70] and there are also numerous works that demonstrate its use for ligament regeneration [46,47]. Due to its biocompatibility, biodegradability and bioactivity, silk fibroin has been proposed also for enthesis repair [25,71]. In a recent work, Font Tellado et al. [25] combined different topographical cues to study the response of human adipose-derived mesenchymal stem cells (AdMSCs). Changing different pore alignment and morphology, they studied the influence on the cytoskeleton alignment and on the gene expression of AdMSCs. However, in accordance with the principle of tissue engineering [41], tissue regeneration starts not only thanks to the effect of the topographical cues and the biological response of the material, but also with molecular and chemical signals, that can derived from small molecules, peptides, DNA or growth factors (GFs) [21,72]. The latter ones are effective molecules to guide stem cell fate during the regeneration improvement [73].

1.3. Silk as biomaterial

Among the natural materials aforementioned, silk emerged as a good candidate for tissue engineering.

Silk is a natural material of animal origin, produced by various insects (Lepidoptera family) and arachnids to serve for a variety of functions, in different periods of their lifecycles[74]. The domesticated mulberry silkworm *Bombyx mori* is the species that produces most of the silk fibers used nowadays [75,76]. When the silkworm reaches the larvae stage, it starts to extrude the silk 'bave' by spinning glands to build up the cocoon in a continuous way with a unique silk strand almost long 2000 m [74]. The silk bave is composed of two core filaments of fibroin (about 75% in weight), surrounded by a sericin film (20-25% in weight) that coats and sticks together fibroin proteins forming the folded silk strand [74,76], Figure 5. The purity of the silk strand is expressed by fineness into denier (D), that is defined as the mass of 9 km fibers in grams [74]. Fibroin is a fibrillar molecule, made of two protein chains, a light chain (about 26 kDa) and a heavy chain (about 390 kDa) in a ratio 1:1. They are joined by disulphide bonds between two cysteine amino acids [70]. On the other hand, sericin is a globular protein, with molecular weight ranging between 10 to 300 kDa. It is known that sericin can cause immunogenic reaction [77], but with a boiling procedure, known as degumming, it is possible to easily remove this glue-like protein and obtain only fibroin filament [78]. After degumming, silk fibroin can be processed in different ways according to its application. Anyway, silk fibroin can exist in different polymorphic state according to

the amount of different secondary structure combined to form the overall protein “architecture”. Fibroin is water soluble when it has a random coil structure, namely Silk I. To avoid solubilisation, fibroin can be easily crystallized into βsheet structure (Silk II) with heat or methanol treatment, shear stress, water vapour annealing [70,79]. Recently, another insoluble structure of distorted three-fold helices and sheet-like structures was determined (Silk III), at the air/water interface of thin fibroin cast films [80]. The crystalline structure influences also the degradation rate of fibroin, depending on the amount of βstructure [81]. Therefore, different processes induce fibroin structural changes that can result in variation of degradation and mechanical properties as well as bioactivity and biological behaviour of the resulting material [82]. These properties make silk fibroin a good candidate for a scaffold material with high potential to overcome the surgical limitations that affect autografts, allograft and synthetic materials based prostheses.

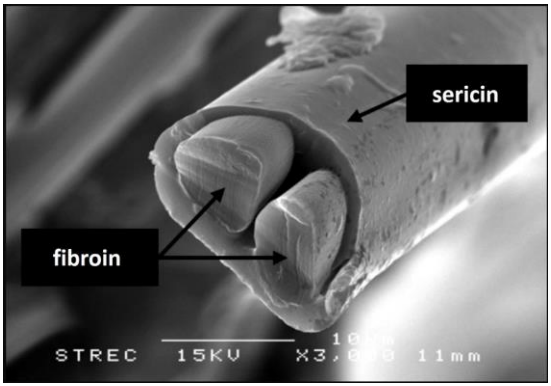

Figure 5: SEM image of silk fiber cross-section (photo courtesy of Rungnapha Yamdech, adapted from www.chulapedia.chula.ac.th).

1.3.1. Silk-based system for ACL tissue engineering

Although natural polymers are usually characterized by weak mechanical properties, unexpectedly silk has shown interesting mechanical properties suitable for ACL tissue engineering. Laurent at al. [46]. and Nau et al. [47] in their recent paper work mentioned studies in which silk is used as biomaterial scaffold to help ligament regeneration, as an effective material for its mechanical properties and for its slow long-term degradation. Altman and Kaplan investigated all the characteristics that make silk an interesting candidate for ACL TE, and particularly they demonstrated that scaffolds fabricated with twisted fibers can mimic the mechanical properties of the native human ACL [83,84]. Combining different textile methods (twisting, braiding, etc.), they

designed SeriACL, a bioengineered silk fibroin graft tested *in vivo* in large animals up to 12 months, indicating stability and promising effect in clinical study [85].

Also Teuschl and colleagues developed a silk-based system to help ACL regeneration: they focused on a method to remove sericin from the ordered matrix of raw silk fiber, which can provoke unfavourable immune responses [77], and on a construction of fiber graft using a wire rope [86]. On the other hand, there are few studies in which silk material is tested *in vivo* as ligament grafts, using small animal models (usually rabbits) [87–90]. However, it should be noted that to transfer the findings from animal *in vivo* experiment to grafts or scaffolds to regenerate human ACL, large animal studies, like pig, goat or sheep models, are preferred to better compare the needed requirements. There are few studies that already tested silk-based systems in large animal studies for ACL grafts [91,92]. For example, Fan at al. tested, in a pig animal model, a silk ligament scaffold seeded with MSCs that resulted in a ligament regeneration after 24 weeks post implantation. Indeed, they were able to obtain ECM component production and the insertion to the bone, beside a tensile strength comparable to ACL native one [91]. Also Nau et al. evaluated the ligament regeneration on sheep study, and upon 12 months they observed not complete silk scaffold degradation, but ECM deposition and cell ingrowth [61].

In conclusion, all these examples of silk applications for ACL regeneration, has given a great potential to this natural material, also for the possible translation into clinical applications.

Chapter II: Rationale, aims and design of the research activity

The wide range of biomedical applications in which silk fibroin-based systems are involved, have demonstrated the versatility of fibroin and the biocompatibility of fibroin-based systems in many studies conducted all around the world.

The aim of this PhD work has been to investigate the use of silk fibroin for the fabrication of a multicomponent model scaffold for ligament tissue engineering application. The dissertation aims to demonstrate that the structural cues that can be obtained during the fabrication of fibroin material, in combination with bioactive molecules (such as growth factor) that can give biochemical signals, can provide additional properties and functionalities. Moreover, the improvement of the mechanical properties and the dynamic stimulation of the constructs can actively control the metabolism of cells on the material, promoting healing outcomes. The experimental activities in this work have been divided in two main lines. The research activities consisted of:

1) Preparation and characterization of silk fibroin scaffold with a porosity gradient to mimic the ligament-to-bone interphase. The use of salt-leaching technique combined with directional freezing and freeze-drying, was optimized to fabricate a scaffold with a gradient

porous structure, from isotropic to anisotropic. Then, a strategy to functionalize the scaffold with heparin was designed and applied to obtain a controlled release of the growth factors. The scaffold was tested in *in vitro* experiments to evaluate the effect of structural cues combined with biochemical cues to induce cell differentiation toward tenogenic/ligamentogenic phenotype. This study was done in collaboration with prof. Van Griensven from Trauma lab, Munich.

2) Design and fabrication of a multicomponent model scaffold able to mimic the central ligament part. The scaffold consisted in silk fibroin yarns reinforcing an anisotropic oriented pores fibroin sponge. The scaffold was stimulated in *in vitro* experiment using a perfusion bioreactor to study the effect of dynamic stimulation on cell penetration and differentiation within the sponge, also with the incorporation of TGF-β2 growth factor to trigger AdMSCs differentiation ligament-specific. Preliminary studies after subcutaneous implantation in rats were done to verify the material inflammation process and cell infiltration. This last *in vivo* evaluation was done at Chonbuk University in the lab of Prof. Gilson Khang.

Chapter III. Tissue engineering of tendon/ligament-to-bone insertion

Part of this chapter is published in: [93]

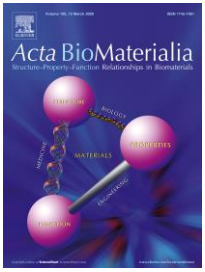

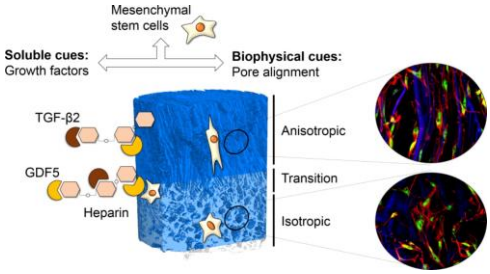

Sònia Font Tellado, Silvia Chiera, Walter Bonani, Patrina S.P. Poh, Claudio Migliaresi, Antonella Motta, Elizabeth R. Balmayor, Martijn Van Griensven

Heparin functionalization increases retention of TGF-b2 and GDF5 on biphasic silk fibroin scaffolds for tendon/ligament-to-bone tissue engineering

Acta Biomaterialia 72 (2018) 150-166

In this chapter a novel approach to regenerate the enthesis tissue based on the synergistic effect of a biomimetic scaffold, stem cells and heparin-based delivery of growth factor is proposed.

My main role in this activity was the confocal imaging evaluation of the cell seeded scaffolds. Moreover, I collaborated to the functionalization and biological evaluation of scaffolds.

3.1. Introduction

In the study area of anterior cruciate ligament repair, the insertion of engineered ligament into bone is a significant concern in the clinical challenge. The interface between tendon/ligament-to-bone is a specialized tissue called “enthesis”, which was discussed in detail in Chapter I. It is an example of soft-to-hard tissue in which tissue engineering and regenerative medicine (TERM) are focusing with promising strategies to allow tissue regeneration [21,24,94].

This specialized tissue interface is necessary to simplify the joint motion and for this reason, its mechanical properties and its tissue arrangement are very important and challenging parameters to be considered for tissue regeneration [22]. The extracellular matrix (ECM) of the enthesis is characterized by a structural gradient, that mainly consists on a mineral gradient and different porosity grade, but also on different type of cells. These components have to be combined to mimic the multi-tissue interface organization. Considering the characteristics just mentioned, the scaffold design has to combine biological and structural cues resembling the properties of the native tissue. Recently, in the current tissue engineering approaches, the use of molecular and chemical signals derived from small molecules, peptides, DNA or growth factors (GFs), are combined in addition

to the effect of the topographical cues and of the biological response of the scaffold material [21,72,73]. Especially growth factors are seen to be effective molecules to guide stem cells differentiation that can improve the regeneration [73].

3.1.1. The role of growth factors

Several studies reported in the review of Font Tellado et al. [21] have addressed the synergistic effect of growth factors on stem cell differentiation for cartilage and bone tissue engineering applications. For example, Cicione et al. obtained chondrogenic differentiation of bone marrow mesenchymal stem cells (MSCs) thanks to the effect of BMP-2, BMP-7 and TGF-β3 [95]. The effects of growth factors on tendon/ligament and fibrocartilage differentiation have been less studied, but there is high probability that tenogenic/ligamentogenic and chondrogenic factors are involved in fibrochondrogenic differentiation of MSCs [24]. Usually, growth factors show some disadvantages such as short half-life, supraphysiological and repeated doses that are required to get therapeutic benefits [73]. To avoid these side effects that lead to high amount of proteins and associated costs, it is necessary to develop and optimize an appropriate delivery system that allows a limited and continued delivery of slight doses of growth factors [96].

Scaffolds can function as platforms to carry growth factors to the injury site [72,97]. Different mechanisms can be adopted to incorporate GFs on scaffolds, such as protein adsorption, surface immobilization and encapsulation into micro- or nanoparticles [21]. Two strategies can be proposed to bind GFs to the biomaterial scaffolds: chemical immobilization and physical encapsulation [98]. The chemical immobilization approach focuses on non-covalent and covalent bonds. In the former case, the bond between GFs and matrix operates between charges or other secondary interactions. The use of proteins, such as heparin, that can be used to chemically or physically modify the surface of the material/scaffold, gives specific biological sites to immobilise GFs. In this way the GFs release rate depends on the electrostatic bonds between molecules and on the environmental conditions. In the covalent incorporation instead, the immobilization is obtained by chemical treatment, resulting in stronger interactions compared to the physical one. The latter approach focuses on the encapsulation, diffusion and pre-programmed release of growth factor from substrate into the surrounding tissue [98].

Since the ECM contains growth factors in the native tissue, recently, it has been suggested that ECM can be used as a releasing system of GFs in response to specific signals [99]. Thus, the ECM can be an option to tightly control growth factor

availability, spatial localization and diffusion [96,99]. Naturally, ECM operates as a storage of GFs and contains the sulfated glycosaminoglycans (GAGs), like heparin, and heparan sulfate which are responsible for and have the ability to bind and release growth factors and also to conserve them from proteolysis [96]. Heparin and heparan sulfate have very similar structure but they differ in the grade of sulfation. Heparin is more sulfated and consequently it has greater negative charges. Heparan sulfate is a proteoglycan naturally present in the ECM of various tissues. Growth factors show specific protein domains called “heparin binding domains”, which allow the GFs to bind heparin through electrostatic bonds. When GFs bind heparin, they increase their half-lives and their biological activity, since their bindings are facilitated to cell surface receptors, avoiding proteolytic degradation [100]. Many studies indicate that various growth factors can be released control by heparin-based delivery systems [93].

3.1.2. Growth factor and TGF-β family

TGF-β(Transforming Growth Factor-β) family of growth factors has been widely investigated for its role on musculoskeletal development, especially for their pro-tenogenic and pro-chondrogenic effects [101]. TGF-β1 and TGF-β3 are key regulators by binding to TGF-β type I and II serine/threonine kinase transmembrane cell receptors [102]. TGF-β family growth factors

can induce different effects on cells depending on their molecular background and level of differentiation. It has been shown that TGF-β2 and 3 signalling is necessary for tendon development in mice embryos [101] and, in mouse, they induce scleraxis (scx) expression, which is a transcription factor responsible for enthesis development [103,104]. To the TGF-β family belong also BMPs (Bone Morphogenetic Proteins), which bind to type I and II TGF-β receptors [101,102]. Among them, BMP2, 6 and 7 can promote both cartilage and bone formation. A subfamily of BMPs showed to have pro-chondrogenic as well as pro-tenogenic/ligamentogenic effects (but only at late phases of tendon development), in particular BMP13 (also known as growth/differentiation factor 5, GDF5) and BMP12 (GDF7) [101]. Interestingly, GDF5 seemed to play an important role during enthesis development and is expressed by enthesis progenitors [105]. Nevertheless, the combination of TGF-β2 and GDF5 factors to evaluate the effect on mesenchymal stem cell differentiation in tissue engineering is less studied compared to the other growth factors in the TGF-β family.

3.2. Materials and Methods

All materials were purchased from Sigma-Aldrich (USA) unless otherwise stated.

3.2.1. Preparation of silk fibroin aqueous solution

Silk fibroin was extracted from white polyhybrid *Bombyx mori* cocoons (Chul Thai Silk Company, Thailand). The cocoons were delaminated and cut in small pieces, submerged in two consecutive alkaline baths (1.5 h in each bath) at 98°C containing 1.1 and 0.4 g/L sodium carbonate (Na_2CO_3) respectively, to remove sericin (degumming). Then, fibroin fibers were washed with deionized water (DI water, produced by using the Elix® Reference 5 water purification system, Merck KGaA, Darmstadt, Germany) and dried overnight under the fume hood. After drying process, fibroin has to show a loss in weight about 25 to 30% to verify the complete removal of sericin. Degummed silk fibers were stored at room temperature and pressure, and low humidity. To prepare fibroin solution in water, silk fibroin was solubilized in 9.3 M lithium bromide (LiBr) solution for 4 h at 65°C. The obtained fibroin solution, appeared as a yellowish, limpid and viscous liquid, was dialyzed against DI H_2O for 3 days using 3,5 kDa MWCO Slide-A-Lyzer dialysis cassettes (Thermo Fisher Scientific, USA), with regular water changes (3 times/day). After dialysis, to concentrate fibroin solution up to 8%, the cassettes were immersed in 25% polyethylene glycol (PEG) (molecular weight = 10kDa). The solution concentration

was measured using NanoDrop (NanoDrop tech, USA). To remove impurities, fibroin solution was centrifuged at 12700 g (Eppendorf 5810R, Eppendorf, Germany) for 20 min at 4°C. Finally, SF aqueous solution was filtered using a glass porous septum to eliminate any solid residue still present. The pH of SF was measured with a Crison pHmeter (Hach Lange, Spain), to assess the typical pH of aqueous fibroin solutions at around 6.5. The process of silk fibroin extraction and processing is summarized in Figure 6, adapted from [78].

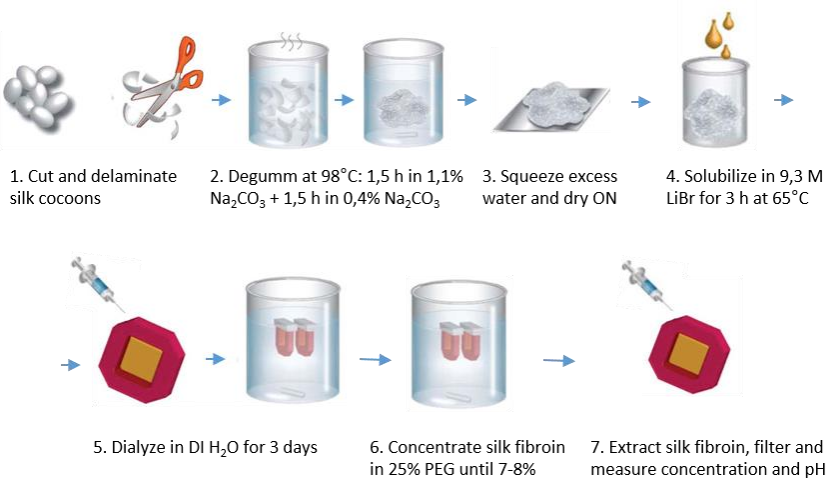

Figure 6: schematic representation of silk fibroin extraction, adapted from [78].

3.2.2. Preparation of biphasic silk fibroin scaffolds

The silk fibroin scaffolds were defined 'biphasic' since they were designed to have aligned (anisotropic) pores mimicking the tendon/ligament-like region and non-aligned (isotropic) pores mimicking the cartilage/bone-like region. The transition area, where a gradual change in pore alignment was expected, should resemble the enthesis-like region.

Biphasic silk fibroin scaffolds were fabricated following the two-step protocol, described in [25], using 8% silk fibroin solution. In summary, in the first step, the isotropic part of the scaffold was produced by solvent casting/particulate leaching using 0,2 gr of NaCl salt crystals (400 - 800 μm) as porogen, that will lead to final pore size of 200 - 300 μm. 200 μl of fibroin solution were poured on NaCl crystals and left at RT to allow gelation. After that, NaCl particles were leached for 3 days in DI water, frozen at -20°C and freeze-dried for 24 hours. Scaffolds obtained were cut in a disc-shape with 8 mm diameter and 5 mm thickness, and were placed at the bottom of a polypropylene (PP) cylinder with 8 mm diameter to start the second step of the protocol. Scaffolds in the PP cylinder were covered with 800 μl of 8% fibroin solution and tightly inserted in a cylindrical polystyrene foam mold, covering only the lateral surface of the cylinder, and placed at -

20°C for 24 h. The polystyrene mold acted as a thermal insulator, generating a temperature gradient along the cylinder, starting from the upper exposed free surface of the fibroin solution. This induced the formation of vertically oriented ice crystals by directional freezing along the main axis of the cylinder. Finally, the frozen scaffolds were lyophilized in an Alpha 1-2 LDplus freeze-dryer (Martin Christ, Germany) for 48 h. The complete biphasic scaffolds (8 mm diameter x 10 mm length) presenting anisotropic and isotropic porosities were treated with 80% methanol (MeOH) to induce a protein conformational change from the silk I to the silk II structure. After treatment, scaffolds were subjected to washes with ddH_2O, another freezing and freeze-drying cycle, they were punched to a final dimension of 4 mm diameter x 8 mm length using biopsy punches (Stiefel, USA) and sterilized with 70% ethanol (EtOH).

3.2.3. Structural characterization of biphasic silk fibroin scaffold

The characterization of the morphology of the scaffold and the alignment of the pores of biphasic silk fibroin scaffolds was performed by micro-computed tomography (μCT) (Skyscan1176, Bruker, Belgium), scanning electron microscopy (FE-SEM) (Phenom Pro, LOT-Quantum Design, Germany) and fluorescent microscopy (BZ-9000, Keyence, Japan).

The equipment used for micro-computed tomography was a Skyscan1176 µCT (Bruker, USA), at 40kV with a voxel size of 9µm. Scaffold dimensions were of 8mm diameter x 10mm length (n=6). To measure scaffold porosity, a built-in algorithm of µCT software (Bruker, USA) was used to create 3D images and then consequently perform the analysis. The structure of the scaffolds was also characterized by FE-SEM, performing transversal or longitudinal cross-sections. Prior to imaging, scaffolds were placed on stubs and coated with Pt/Pd alloy (80/20) using a Q150R sputter coater (LOT-Quantum Design, Germany). Pore morphology and alignment of both anisotropic and isotropic silk fibroin scaffolds were observed by staining with DAPI (4',6-diamidino-2-phenylindole) following the manufacturer's instructions, using fluorescence microscopy.

3.2.4. Functionalization of biphasic silk fibroin scaffolds with heparin

Biphasic silk fibroin scaffolds were functionalized using heparin sodium salt from porcine intestinal mucosa. Covalent binding between carboxyl groups in heparin and primary amines in fibroin was performed with carbodiimide chemistry. The crosslinkers used were 1-ethyl-3-(3dimethylaminopropyl) carbodiimide hydrochloride (EDC) and N-hydroxysuccinimide (NHS) (Carl Roth, Germany). First, scaffolds were incubated in

0.1 M 2-(N-morpholino) ethanesulfonic acid (MES) buffer (pH 5.8) for 30 min at room temperature (RT) under shaking. Next, heparin was dissolved to a final concentration of 3% in MES buffer and sterilely filtered using 0.2 µm filters (Sarstedt, Germany). EDC and NHS were added at a final concentration of 0.25 M and 0.125 M, respectively, to activate carboxyl groups in heparin molecules. The reaction was conducted for 15 min at RT under shaking and quenched with 0.2 M 2-mercaptoethanol. Subsequently, each scaffold reacted with 1 ml of 3% activated heparin solution for 4 h at RT under shaking. Scaffolds having reacted with activated heparin are hereafter termed “scaffolds crosslinked with heparin” or “heparin-crosslinked scaffolds”. Naked scaffolds (termed “unmodified scaffolds”) and scaffolds having reacted with 3% non-activated heparin solution (without EDC/NHS, termed “scaffolds non-crosslinked with heparin” or “non-crosslinked scaffolds”) were used as controls. All scaffolds were washed 5 times with MES buffer and 3 times with ddH_2O to remove excess of heparin. Scaffolds used for growth factor loading and cell culture were additionally incubated for 3 days in ddH_2O to ensure complete removal of unbound heparin. All reactions and washing steps were performed in sterile conditions.

3.2.5. Quantification of heparin binding efficiency and release

Heparin release was quantified after washing with MES buffer and ddH_2O. Each scaffold was incubated in 1 ml of ddH_2O and 100 µl were taken after 1 h, 3 h, 1 d, 3 d and 7 d for quantification. 100 µl of fresh ddH_2O were replenished at every measuring point. Heparin quantification was done using a Blyscan Sulfated Glycosaminoglycan (GAG) assay (Bicolor, United Kingdom) according to the manufacturer's instructions. Heparin binding efficiency and release were quantified in non-crosslinked and heparin-crosslinked scaffolds (n = 6 for each group). Heparin binding efficiency was determined indirectly by measuring the amount of unreacted heparin in MES buffer after the conjugation reaction (before washing). The amount of heparin released after 3 days was used to estimate the amount of heparin remaining bound to scaffolds used for growth factor binding and cell culture after 3 days washing. This was done by subtracting the heparin released at 3 days from the total heparin incorporated after conjugation.

3.2.6. Growth factors binding to biphasic silk fibroin scaffolds

Human recombinant TGF-β2 and GDF5 (Peprotech, USA) were added to the silk fibroin scaffolds (unmodified, non-crosslinked with heparin and crosslinked with heparin) (n = 3 for each group). Growth factor loading was performed by incubating the scaffolds in 500 µl of a PBS solution containing 200 ng/ml of TGF-β2 or GDF5 (single growth factor loading) or 100 ng/ml TGF-β2 plus 100 ng/ml GDF5 (double growth factor loading). The reaction was performed at RT for 3 h under shaking.

3.2.7. Quantification of TGF-β2/GDF5 binding efficiency and release

Binding efficiency and release profile of TGF-β2/GDF5 from biphasic silk fibroin scaffolds (unmodified, non-crosslinked with heparin or crosslinked with heparin) (n = 3 for each group) were quantified by ELISA. Growth factor release was quantified by incubating each scaffold in 1 ml Dulbecco's Modified Eagles Medium (DMEM) supplemented with 2% fetal calf serum (FCS) and 1% Penicillin/Streptomycin (P/S) at 37°C to simulate cell culture conditions. 100 µl of medium were taken for quantification after 1 h, 3 h, 1 d, 3 d, 7 d or 14 d and replenished with 100 µl fresh medium. TGF-β2 was quantified using a TGF-

β2 ELISA kit (Diaclone, France) and GDF5 using a DuoSet DY853 GDF ELISA kit (R&D, USA) following the manufacturer's instructions. Binding efficiency was calculated indirectly by quantifying the amount of unbound TGF-β2/GDF5 in PBS after the conjugation reaction.

3.2.8. In vitro evaluations

3.2.8.1. AdMSCs culture on biphasic silk fibroin scaffolds

Biphasic silk fibroin scaffolds were punched to a final dimension of 4 mm diameter x 8 mm length using disposable biopsy punches (Integra Miltex, USA). Prior to cell culture, scaffolds were sterilized with 70% ethanol, washed with PBS and incubated in growth medium overnight at 37°C to improve cell attachment. Human adipose tissue was obtained from healthy donors after written informed patient's consent according to the guidelines of the Local Ethics Committee of ''Klinikum Rechts der Isar'' at the Technical University of Munich, Germany. AdMSCs isolation was performed as described in Schneider et al. [106]. AdMSCs were seeded on the scaffolds at a density of 4 x 10^5 cells/scaffold. Seeding was performed in a small volume (60 µl) to improve seeding efficiency. To ensure homogenous cell distribution on the scaffolds, seeding was performed on both

scaffold sides (anisotropic and isotropic, 30 µl on each side). After seeding, scaffolds were incubated for 2 h at 37°C to facilitate cell attachment. Cells were cultured either in growth medium or in high glucose DMEM containing 2% FCS and 1% P/S (AdMSCs low serum medium). Since the aim of the project was more focused on evaluating AdMSCs differentiation, low serum medium was used to promote differentiation over proliferation. Medium was changed every 2 days.

3.2.8.2. Immunofluorescence and confocal microscopy

AdMSCs morphology, cytoskeletal alignment and distribution on biphasic silk fibroin scaffolds were analysed by immunofluorescence staining. In particular, the presence of collagens was evaluated to check the influence of the growth factor binding with the topographical surface of the scaffold. The presence of collagen types I, II and III was analysed in silk fibroin scaffolds crosslinked with heparin and unloaded or loaded with TGF-β2/GDF5.

The following antibodies were used (Abcam, Germany). Primary: collagen I (ab34710, 1:500), collagen II (ab34712, 1:200) and collagen III (ab7778, 1:200). Secondary: IgG goat anti-rabbit, conjugated with Alexa Fluor 488 (ab150077, 1:1000). All antibodies were diluted in 1% bovine serum albumin (BSA) in

PBS. After 14 days of culture on scaffolds in low serum medium, AdMSCs were fixated with 4% formaldehyde in PBS for 30 min at RT and permeabilized with 0.2% Triton X-100 in PBS for 20 min at RT. Next, scaffolds were incubated in 1% BSA in PBS for 1 h at RT. Subsequently, scaffolds were cut in transversal sections (2mm thickness) and stained with primary antibodies overnight at 4°C. Next, samples were washed 3 times in PBS and stained with secondary antibody at RT for 1h. Finally, scaffolds were washed with PBS and stained with Alexa Fluor 594 Phalloidin (Thermo Fisher Scientific, USA) and DAPI following the manufacturer's instructions.

3.2.8.3. Gene expression

Gene expression of tendon/ligament, enthesis and cartilage differentiation markers was analysed in biphasic silk fibroin scaffolds. AdMSCs were cultured for 14 days on the scaffolds in growth medium or low serum medium (scaffolds crosslinked with heparin unloaded or loaded with TGF-β2/GDF5). Next, the scaffolds were washed in PBS and cut in 3 parts (anisotropic, transition, isotropic) to analyse gene expression in each region separately. The transition was defined as the region 0.5 mm up and 0.5 mm down from the detectable porosity change. Each part was cut in small pieces and stored at -80°C in TRIreagent for at least 24 h. Next, RNA isolation in TRIreagent was

performed by chloroform extraction following the manufacturer's instructions. RNA quantity and quality was measured with NanoDrop. Reverse-transcription to cDNA was performed using a first strand cDNA synthesis kit (Thermo Scientific, USA) according to the manufacturer's instructions. The thermocycler used was a C1000 Touch Thermal Cycler (Eppendorf, Germany). Quantitative analysis of gene expression was performed by quantitative polymerase chain reaction (qPCR). 30 ng of sample cDNA were used per reaction. The thermocycler used was a CFX96 Real Time System thermocycler (BioRad, USA). Sso Fast EvaGreen supermix (BioRad, USA) was used as a detection reagent. The primers used and their sequences are shown in Table 2. Results from heparin-crosslinked scaffolds were expressed as fold change relative to the housekeeper and to unloaded scaffolds (heparin-crosslinked without growth factors) ($2^{-\Delta\Delta CT}$).

Target gene	Forward (5' → 3')	Reverse (5' → 3')	Function
Aggrecan	TCGAGGACAGCG AGGCC	TCGAGGGTGTAGC GTGTAGAGA	Major proteoglycan in the articular cartilage, responsible for chondrocyte interactions and for hydrated gel structure.

βTubulin	GAGGGCGAGGAC GAGGCTTA	TCTAACAGAGGCAA AACTGAGCACC	Housekeeping gene, found in microtubules of cytoskeleton.
Collagen I A1 (Col I)	AGCGGACGCTAA CCCCCTCC	CAGACGGGACAGC ACTCGCC	Col type I is a fibril-forming collagen found in most connective tissues and is abundant in bone and tendon
Collagen II (Col II)	AACCAGATTGAGA GCATCCG	ACCTTCATGGCGTC CAAG	Major component of hyaline cartilage.
Collagen III (Col III)	TACTTCTCGCTCT GCTTCATCC	GAACGGATCCTGA GTCACAGAC	Fibrillar collagen extensively found in connective tissue.
Mohawk	TGGTTTGCTAATG CAAGACG	CCTTCGTTCATGTG GGTTCT	Important marker in tendon/ligament development
Scleraxis	CAGCCCAAACAG ATCTGCACCTT	CTGTCTTTCTGTCG CGGTCCTT	Transcription factor related to tenogenesis and upregulation of col I
SRY-box 9 (Sox9)	GAGCCGAAAGCG GAGCTGGAA	ACAGCTGCCCGCT CCAAGTG	Transcription factor related to chondrogenic differentiation.
Tenascin – C	TCAAGGCTGCTA CGCCTTAT	GTTCTGGGCTGCCT CTACTG	Protein of tendon/ligament ECM and enthesis.

Table 2: primers used for qPCR. Primer sequences used for quantitative polymerase chain reaction (qPCR). βTubulin was used as a housekeeper.

3.2.9. Statistical analysis

Statistical analysis of quantitative data was performed using GraphPad Prism version 5.00 (GraphPad software, USA). Statistical significance was considered at $p < 0.05$. Data were analysed with One-way analysis of variance (ANOVA) and Tukey's correction.

3.3. Results and discussion

3.3.1. Morphology and pore alignment of biphasic scaffolds

The biphasic silk fibroin scaffold was fabricated as described in Materials and Methods, paragraph 3.2.2. The fabrication method was optimized by Font Tellado et al. in their previous work in 2017 [25], in which they showed that between the two protocols proposed for scaffold fabrication, the one starting with the fabrication of isotropic porosity (so called type B in [25]) resulted in a continuous construct.

In fact, the lamellar porosity penetrates more gradually the isotropic region, forming a mixed porosity identified as a transition region. This zone is able to mimic the enthesis area, and resemble the gradual changes of collagen molecule alignment in the native tissue. Plus, the biphasic silk fibroin

scaffold was composed of an anisotropic part with aligned porosity corresponding to the tendon/ligament, and of an isotropic area, with non-aligned pores, corresponding to the cartilage/bone part. The structure and its porosity is visible from SEM and confocal pictures reported in Figure 7.

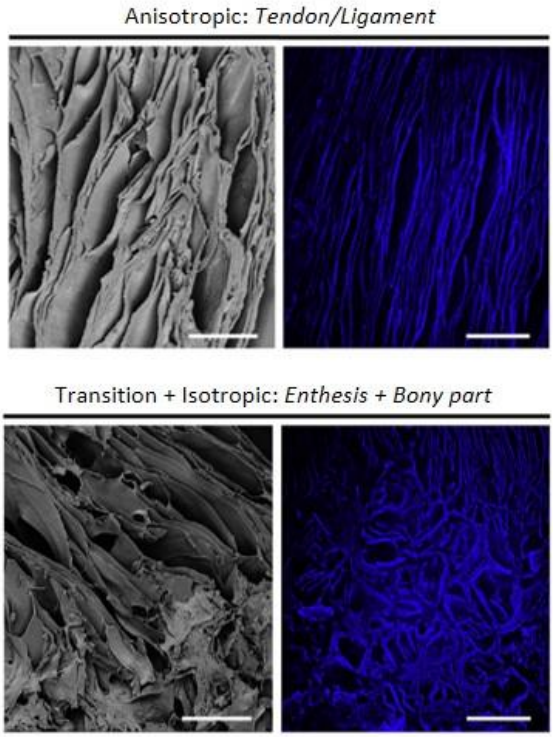

Figure 7: in this panel there are four images: the images on the left side show FE-SEM images, the images on the right side show fluorescence images by confocal microscopy. All images are about structure and pore morphology of anisotropic (upper part) and transition + isotropic (lower part) parts of the biphasic scaffold. The former structure shows an aligned porosity, whereas the latter shows a merge of aligned pores entering in a non-aligned and round

porosity, mimicking the transition region ligament/tendon-to-bone insertion. Scale bars = 300 μm (first and third images) or 500 μm (second and fourth images). Image adapted from [93].

It is possible to notice that the anisotropic region is characterized by vertical aligned pores, obtained thanks to the directional freeze and freeze-drying technique [107], while the isotropic part shows round and open pores, obtained by salt leaching technique, more resembling the bone structure [108]. Total porosity and pore sizes were measured along the Z axis of the scaffold using μCT scan and algorithm built-in for 3D structure analysis. From the data obtained in collaboration with Font Tellado et al. [93], pore size distribution is similar in all three areas of the scaffold (anisotropic, transition, isotropic). On average, 80-90% of the pores ranged between 100-300 μm. The open porosity across the scaffold structure was maintained at 65-70% with irrelevant close porosity, indicating high interconnectivity among the pores (Figure 8). It is known that porosity can influence important parameters such as diffusion of oxygen and nutrients, and mechanical properties. It has also been shown that pores can directly affect cytoskeleton alignment and gene expression [25,109].

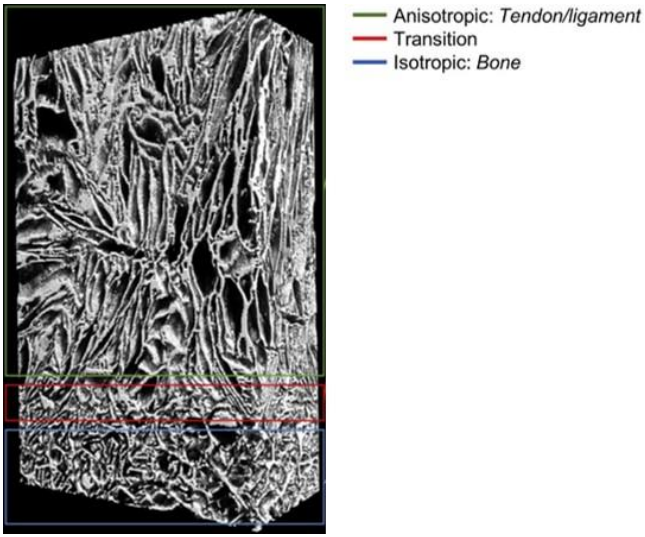

Figure 8: micro-computed tomography reconstruction of biphasic silk fibroin scaffold. Three different colours highlight the three areas characterising the biphasic scaffold: anisotropic (tendon/ligament, green), transition (enthesis, red) and isotropic (bone, blue). Image from [93].

3.3.2. Heparin and growth factors binding evaluation

The idea, developed in collaboration with the group of prof. Van Griensven [93], to functionalize silk fibroin scaffold with heparin was triggered from the wide use of heparin as a suitable molecule to immobilize various growth factors with reasonably elevated affinity, extensively reviewed in [110]. This is the case of the used growth factors, TGF-β2 and GDF5, that display heparin-binding domains.

The evaluation of heparin functionalization on the binding and release of TGF-β2 and GDF5 was done by comparing three groups: unmodified scaffolds, scaffolds non-crosslinked with heparin and scaffolds crosslinked with heparin.

Heparin binding to fibroin was improved with the use of EDC/NHS crosslinkers, which thanks to the carbodiimide chemistry, resulted in a covalent binding between the carboxyl groups in heparin and primary amines in silk fibroin scaffold. Even after 3 days washing, the amount of heparin remaining bound to the scaffold (26%) was higher on the crosslinked scaffold compared to the non-crosslinked one (Graph 1). However, it was not possible to increase the efficiency of heparin binding probably because of the low availability of the primary amines in the silk fibroin scaffold [70].

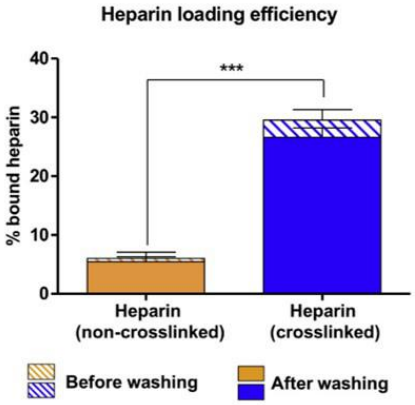

Graph 1: representation of heparin loading efficiency of non-crosslinked scaffold (without EDC/NHS) and crosslinked scaffold (with EDC/NHS). The graph also shows the bound heparin before and after 3 days washing in

ddH_2O. The % of bound heparin is in relation to the initial amount used for conjugation (30 mg/ml); n = 6. Statistical significance is indicated with asterisks (***$p < 0.001$). Image from [93].

With the aim to adopt the heparin as a delivery system for growth factors, it was important to measure the heparin release in ddH_2O. Along 3 days of washing, the heparin release was faster in the non-crosslinked scaffolds compared to the crosslinked one, but not in a statistically significant way. Heparin release between 3 and 7 days was negligible, and for this reason, the scaffolds used for growth factor incorporation during the cell culture experiments were washed for 3 days in water to ensure complete removal of unbound heparin [93].

The growth factors binding on scaffold showed high incorporation efficiency for all three groups of scaffold tested, but the growth factor kinetics were different among them. In fact, for TGF-β2, after 24 h the unmodified and the non-crosslinked scaffold released almost half of the growth factor incorporated, whereas the crosslinked scaffold released only 21%. The latter value just increased about 5 points until 14 days of release, meaning that the growth factor firmly bound to the heparin incorporated into the scaffold.

The scaffolds unmodified and non-crosslinked with GDF5 released almost the 80% after 24 h, while on the crosslinked

scaffold only 10% was released. Value that was quite maintained (18%) after 14 days (Graph 2).

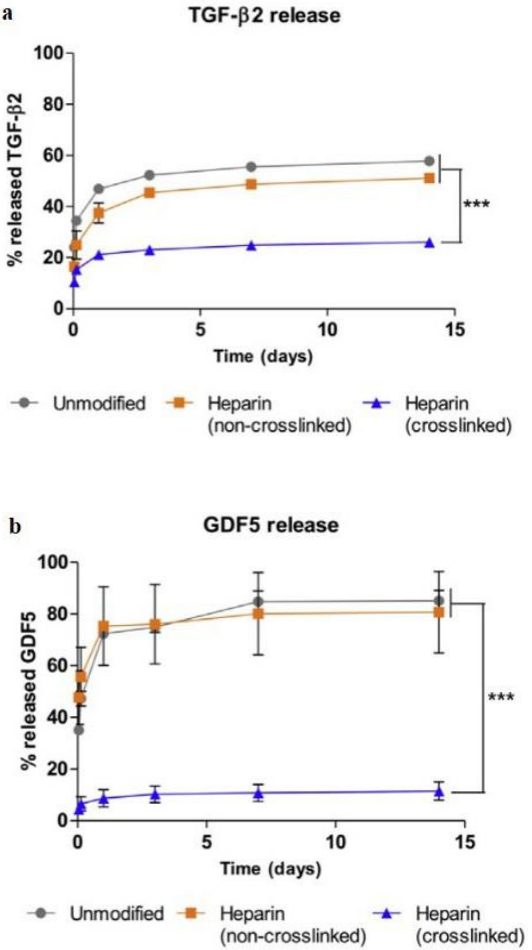

Graph 2: curve of growth factors release of three groups of scaffolds: unmodified, non-crosslinked and crosslinked with heparin. The two graphs show cumulative release corresponding to **a**) TGF-β2 growth factor and **b**) GDF5 in relation to the total amount of growth factor loaded; n = 3. Statistical significance is indicated with asterisks (***$p < 0.001$). Images from [93].

In general, TGF-β2 and GDF5 resulted incorporated with high efficiency on the three groups of scaffold tested, probably because of the electrostatic interactions between fibroin (negatively charged) and growth factors (positively charged). On the other hand, the three scaffold groups showed different release trends: in fact, unmodified and non-crosslinked scaffolds rapidly lost the growth factors, probably because the GFs quickly diffused out in presence of aqueous solution as a typical behaviour of proteins when adsorbed to porous matrices [111]. On the contrary, the crosslinked scaffold lost a very low amount of growth factor, since the electrostatic interactions between heparin binding domains on TGF-β2/GDF5 and heparin molecules are strong and stable [96,100], and they can increase protein stability, retention and half-life [112]. In particular, it is possible to notice that TGF-β2 was slightly more released compared to GDF5, suggesting that the latter GF has a higher affinity for heparin then TGF-β2 that may have a higher affinity for fibroin. Indeed, multiple parameters can influence interactions between proteins and other molecules, such as molecular weight and isoelectric point [112]. However, similar results confirming the release trend of growth factor are reported in previous works [113,114].

Thanks to the results obtained, the crosslinked heparin scaffold was chosen for all the further *in vitro* evaluations.

3.3.3. Gene expression analysis of AdMSCs cultured up to 14 days on biphasic scaffolds

The effect of TGF-β2, GDF5 and the combination of both, was evaluated through AdMSCs gene expression analysis. Gene expression data from growth factor-loaded scaffolds was expressed as fold change respect to unloaded scaffolds, for each scaffold region (anisotropic, transition and isotropic). For the analysis, genes related to tendon/ligament markers (scleraxis (scx), collagen I, mohwak and tenascin C), cartilage markers (SRY-box 9 (sox9), collagen II and aggrecan) and enthesis markers (sox9, scx, collagen II, collagen III, tenascin C and aggrecan) were tested. Figure 9 shows the expression of each gene in the three regions of the scaffold. The growth factor effect is represented by a colour (TGF-β2 = orange, GDF5 = blue, TGF-β2 + GDF5 = black), the GF influence on each region of the scaffold is represented by a shade of the colour chosen.

The expression of scx was not significantly different in scaffolds loaded with TGF-β2/GDF5 compared to unloaded scaffolds along the 14 days, except at day 7 in the isotropic region loaded with both growth factors (Figure 9A). Despite scx is expressed in tendon/ligament tissues throughout development, on the anisotropic construct could not enhance its expression. A similar behaviour was observed by Caliari et al. [115], who did not find

positive interactions between scaffold anisotropy and treatment with GDF5 or GDF7 on scx expression.

The expression of sox9 showed similar levels in unloaded scaffolds in most of the conditions and scaffold regions (Figure 9E). At 7 days, sox9 displayed an upregulation (3-fold) in the isotropic region of scaffolds loaded with TGF-β2 and GDF5. At 14 days, sox9 showed some upregulations but not statistically significant. The highest upregulation of sox9 expression happened in the transition region of scaffolds containing both growth factors in comparison to unloaded scaffolds.

During the first 7 days, the expression of collagen I tended to be downregulated compared to unloaded scaffolds, although without statistically significance (Figure 9B). At 14 days, collagen I expression was upregulated (12-fold) in the anisotropic region of scaffolds containing TGF-β2. The combination of TGF-β2 and GDF5 resulted in a significantly downregulation in the isotropic compared to the anisotropic and transition regions of the scaffolds. The collagen I expression was significantly lower in the transition region of scaffolds loaded with GDF5.

Collagen II showed upregulated expression (3-fold) at 7 and 14 days in the isotropic region of scaffolds loaded with TGF-β2 and GDF5 (Figure 9F). Collagen II expression was also upregulated in the anisotropic area of scaffolds loaded with GDF5 or TGF-β2

and GDF5, and in the transition region of scaffolds loaded with TGF-β2 at day 14 (3-fold).

The expression of mohawk showed a similar trend to collagen I, in fact, for the first time point, the mohawk expression was either downregulated or similar to unloaded scaffolds. At 14 days, the gene showed upregulation (3-fold) in the anisotropic region of scaffolds containing TGF-β2 and in the transition region of scaffolds containing TGF-β2 and GDF5 (6-fold) (Figure 9C). In addition, mohawk expression was downregulated in the isotropic region of scaffolds loaded with both growth factors without any statistically significant differences.

Aggrecan expression was upregulated in all conditions of isotropic scaffold at day 7 (Figure 9G). There are differences statistically significant when comparing the anisotropic and isotropic regions of scaffolds loaded with TGF-β2 or TGF-β2 and GDF5 at day 7. In addition, aggrecan expression in the anisotropic region of scaffolds loaded with TGF-β2 and GDF5 was significantly downregulated compared to the same region in unloaded scaffolds. On the contrary, aggrecan expression at 14 days tended to be upregulated in all the conditions of anisotropic regions compared to unloaded scaffolds, although differences were not statistically significant.

At 7 days, tenascin C expression followed a similar tendency to the other tendon/ligament markers (collagen I and mohawk) in

which expression levels were either similar or lower than in unloaded scaffolds (Figure 9D). In addition, the gene expression was significantly downregulated in the anisotropic part of scaffolds loaded with TGF-β2 and GDF5 compared to unloaded scaffolds. On the other hand, at 14 days, tenascin C was upregulated in the anisotropic region of scaffolds loaded with growth factors (all conditions). In addition, in scaffolds loaded with TGF-β2 and GDF5, tenascin C was significantly upregulated in the anisotropic compared to the transition and isotropic regions.

The expression of collagen III was downregulated in all growth factor-loaded scaffolds at 7 days (Figure 9H). There were some statistically significant differences at the transition region of scaffolds loaded with TGF-β2 ($p<0.05$) and in all regions of scaffolds loaded with TGF-β2 and GDF5. At 14 days, collagen III expression was upregulated (3 to 5-fold) in the anisotropic region of scaffolds loaded with growth factors (all conditions). In addition, collagen III was also upregulated in the transition region of scaffolds containing TGF-β2 (6-fold) or TGF-β2 and GDF5 (7-fold) and in the isotropic region of scaffolds containing TGF-β2 and GDF5 (8-fold), without any statistically significant differences.

Notably to said that, in presence of TGF-β2, upregulation of collagen I, mohawk and tenascin C has been observed in the

anisotropic part, corresponding to tendon/ligament-like region. On the other hand, the presence of GDF5 seemed to be correlated with collagen II production in the anisotropic region, indicating a possible pro-fibrochondrogenic effect.

It is possible to assess that the combination of the two growth factors promoted the expression of sox9, collagen II, collagen III and aggrecan at the transition region (enthesis). TGF-β2 and GDF5 are key regulators of tendon/ligament and cartilage development, therefore they may be encouraging for fibrochondrogenic differentiation, since their combination seems to induce the expression of chondrogenic and tenogenic/ligamentogenic markers in the transition area.

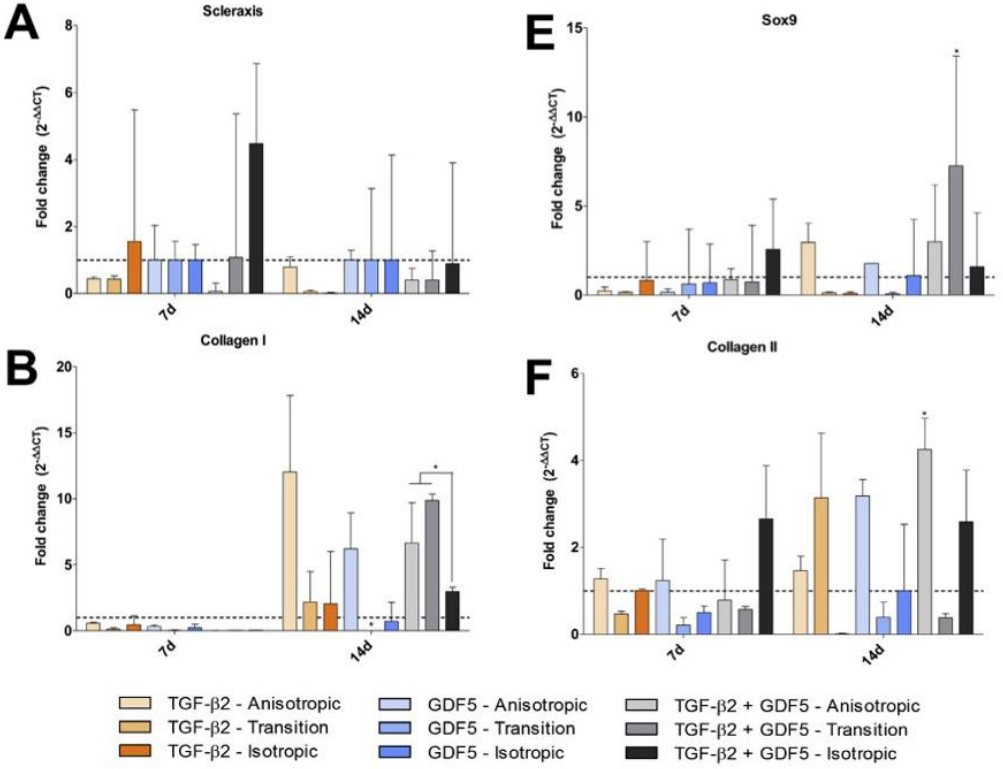
A
Scleraxis
Fold change (2^-ΔΔCT)
7d
14d
B
Collagen I
E
Sox9
F
Collagen II
TGF-β2 - Anisotropic
TGF-β2 - Transition
TGF-β2 - Isotropic
GDF5 - Anisotropic
GDF5 - Transition
GDF5 - Isotropic
TGF-β2 + GDF5 - Anisotropic
TGF-β2 + GDF5 - Transition
TGF-β2 + GDF5 - Isotropic

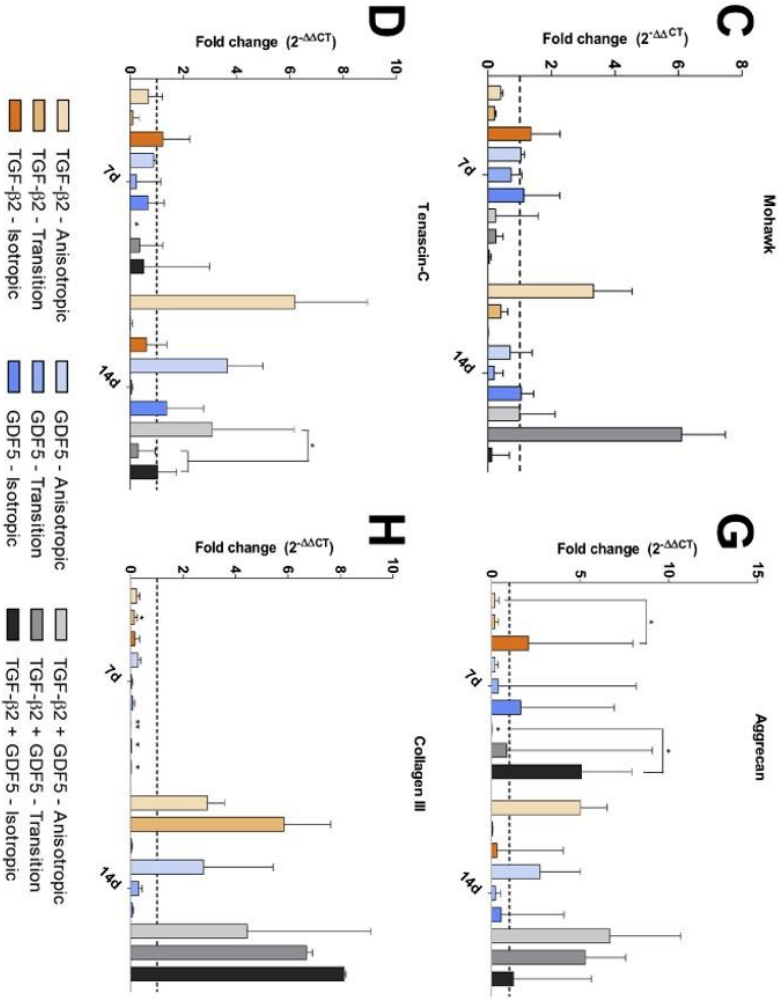

Figure 9: gene expression analysis of AdMSCs culture up to 14 days, influenced by scaffold structure and growth factors. Target genes are scleraxis (A), collagen I (B), mohawk (C), tenascin C (D), SRY-box 9 (sox9) (E), collagen II (F), aggrecan (G) and collagen III (H). Housekeeper gene is β Tubulin. It was analysed the effect of each growth factor, and the combination of the two, on each one of the three groups in which the scaffold has been divided (anisotropic, transition, isotropic). The fold change was calculated

normalizing the target gene expression to the housekeeper gene in unloaded scaffolds (dashed line). Statistical significance is indicated with asterisks. *p < 0.05, **p < 0.01. Asterisks on top of a bar indicate statistical significance respect to unloaded scaffolds. Image from [93].

3.3.4. Immunofluorescence analysis on collagen deposition on biphasic scaffold

To check if the growth factors increased the deposition of collagens, immunofluorescence images were taken after 14 days of culture to analyse the presence of collagen I, II and III on the three scaffold regions (anisotropic, transition and isotropic). Collagen molecules are stained green, the scaffold matrix blue and the actin cytoskeleton red. In all the figures (Figures 10, 11, 12), the *A row* pictures show low magnification images of whole scaffold transversal sections, while *B* and *C* are high magnification images of the anisotropic and isotropic regions of the scaffolds, where it is possible to appreciate the cytoskeletal alignment of AdMSCs. The images show how the porosity of the scaffolds influenced the alignment of cell cytoskeleton. In the anisotropic region, cells are elongated and aligned, whereas in the isotropic one, apparently, the cell alignment seems to be not present (Fig.10, 11, 12).

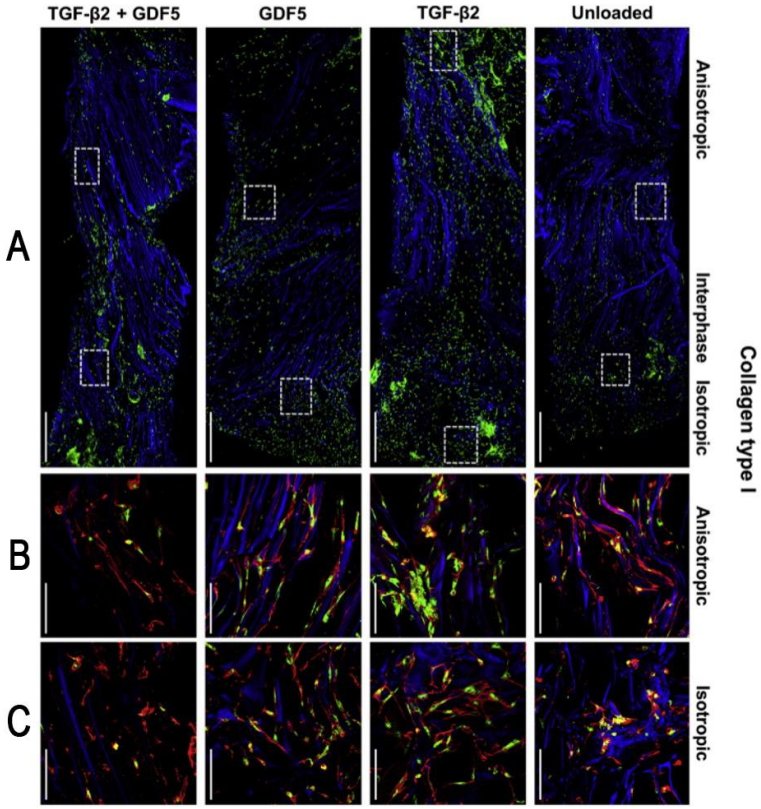

Figure 10: collagen I staining on different areas of biphasic scaffold (anisotropic, interphase, isotropic), in different growth factor conditions (unloaded, TGF-β2, GDF5 or both). The panel shows images of collagen I deposition after 14 days of AdMSCs culture. Images in the **A** row are corresponding to the transversal sections of the whole biphasic scaffold (blue staining), where collagen I is in green staining. Scale bars = 1 mm. In **B** and **C** rows, images are magnifications of the dashed squares on the transversal sections, showing how cell cytoskeleton (red) follows the two porosities (anisotropic and isotropic). Scale bars = 200 μm. Image adapted from [93].

Figure 10 shows collagen I deposition. At first sight on the transversal section images, it is possible to appreciate that collagen I is more abundant in the scaffold containing TGF-β2 compared to the other groups, especially in the anisotropic and in the isotropic regions (external ends) than the transition one (inner region). Collagen I levels appeared similar in unloaded scaffolds and scaffolds containing GDF5 or TGF-β2 and GDF5.

Collagen II content is shown in Figure 11. From the transversal sections, it is clear that the scaffold showing higher content of collagen II is the one loaded with GDF5 compared to the other groups. It seems to be more concentrated in the anisotropic and in the transition region, respect to the isotropic one. The scaffold containing TGF-β2 and GDF5 shows more abundant collagen II staining than the unloaded and TGF-β2 groups, in particular at the transition and isotropic regions. On the other hand, collagen II seems to decrease to the anisotropic area, since in the high magnification images cannot be detected. In the unloaded group, collagen II concentrates at the isotropic region. The scaffold containing TGF-β2 shows the lowest collagen II content among groups.

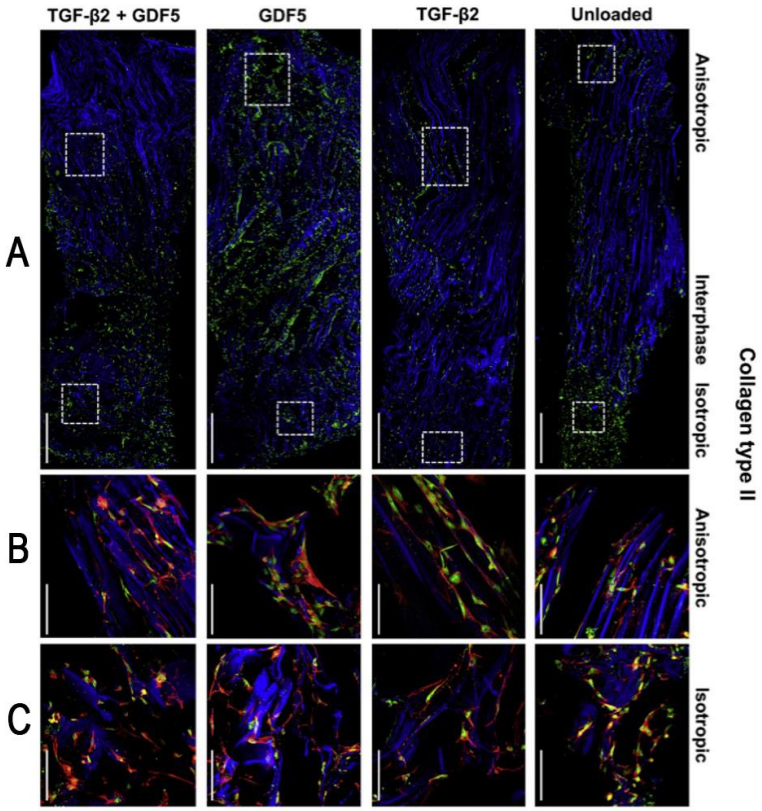

Figure 11: collagen II staining on different areas of biphasic scaffold (anisotropic, interphase, isotropic), in different growth factor conditions (unloaded, TGF-β2, GDF5 or both). The panel shows images of collagen II deposition after 14 days of AdMSCs culture. Images in the **A** row are corresponding to the transversal sections of the whole biphasic scaffold (blue staining), where collagen II is in green staining. Scale bars = 1 mm. In **B** and **C** rows, images are magnifications of the dashed squares on the transversal sections, showing how cell cytoskeleton (red) follows the two porosities (anisotropic and isotropic). Scale bars = 200 μm. Image adapted from [93].

Figure 12 shows collagen III content, which appears to be the highest in the scaffold loaded with TGF-β2 and GDF5, reasonably distributed in a homogeneous way. Collagen III and cell clusters can be observed especially at the transition area and at the anisotropic area close to the transition (row A). Values that are confirmed also from the gene expression analysis (Figure 9H). However, also unloaded and GDF5 treated scaffolds show collagen III deposition, particularly in the interphase-isotropic region. On the contrary, TGF-β2 loaded one showed very poor presence of collagen III.

As a general consideration, it is evident that the incorporation of TGF-β2 had a tenogenic/ligamentogenic effect combined with the anisotropic region of the scaffold, not only for protein expression but also for gene expression (Figure 9), as well as the synergistic effect of both GFs mainly in the isotropic region resulted in a chondrogenic effect.

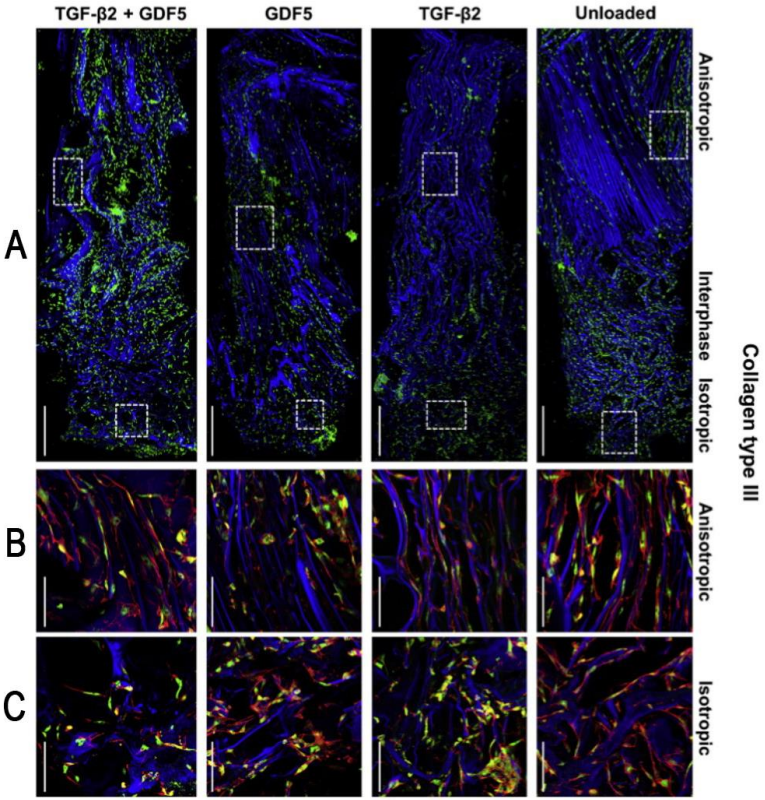

Figure 12: collagen III staining on different areas of biphasic scaffold (anisotropic, interphase, isotropic), in different growth factor conditions (unloaded, TGF-β2, GDF5 or both). The panel shows images of collagen III deposition after 14 days of AdMSCs culture. Images in the **A** row are corresponding to the transversal sections of the whole biphasic scaffold (blue staining), where collagen III is in green staining. Scale bars = 1 mm. In **B** and **C** rows, images are magnifications of the dashed squares on the transversal sections, showing how cell cytoskeleton (red) follows the two porosities (anisotropic and isotropic). Scale bars = 200 μm. Image adapted from [93].

3.4. Conclusions

Enthesis, defined as the interphase between soft and hard tissue, nowadays has shown surgical importance for its limitations in treatments for tendon/ligament-to-bone repair and regeneration.

In this chapter and in the published work done in collaboration with prof. Van Griensven and his laboratory [93], a new approach was proposed mainly focused on the combination of topographical and biological cues of the scaffold to induce cell differentiation for tissue regeneration. The scaffold fabricated consisted of two integrated and interconnected parts that together form a transition region resembling the enthesis. In particular, the scaffold could mimic the extracellular matrix of the enthesis, resembling the collagen fiber organization and the mineral content. The different porosities of the ligament/bone sites and their transition zone allowed cell penetration, differentiation and proper collagen production.

The innovative approach focused on the functionalization of silk scaffold with heparin molecules. The heparin functionalization showed an increased growth factor affinity, able to release low doses of growth factor and keep higher their local concentration and bioactivity [96,97]. TGF-β2 and GDF5 were incorporated with high efficiency on the three regions of the scaffold thanks to

electrostatic bonds to heparin. The use of growth factors led AdMSCs toward differentiation after 14 days of culture, as promising result for enthesis regeneration, showing a synergistic effect with the different porosity present on the scaffold structure. In fact, alignment, morphology and size of pores in the different scaffold areas demonstrated to have direct effect on cell morphology, ECM synthesis and gene expression. The scaffold structure probably influenced the diffusion and the local concentration of the growth factors, besides to the diffusion of nutrients and oxygen.

In particular, the combination of TGF-β2 with the highly porous lamellar-like structure induced the upregulation of tendon/ligament markers and collagen I production, as well as the GDF5 induced the cartilaginous marker in the transition region and collagen II production in the anisotropic region. The combination of the two growth factors instead, increased the collagen III production in the interphase and the cartilaginous gene expression.

Finally, this work gave a preliminary result mainly based on a biological response of the effect of structural and biological cues for enthesis regeneration. It would be interesting to evaluate the biphasic scaffold *in vivo*, but overall improve its structure considering the mechanical properties that the scaffold can achieve to mimic the ones of the native tissue, considering the

potential of silk fibroin natural polymer, for a better evaluation and improvement of a enthesis tissue engineering strategy.

Chapter IV. A multicomponent model for Anterior Cruciate Ligament (ACL)

The current chapter focuses on the ligamentous part of the scaffold. The requirement is an augmentation model scaffold able to ensure the regeneration of the ACL in its whole structure, while assuring the required mechanical properties and the bioactive potential, to start the regenerative process.

4.1. Introduction

4.1.1. The use of silk fibroin fibers in ligament regeneration

As already introduced in chapter I, silk fibroin is one of the nature-derived polymers, having a great attention in the field of tissue engineering (TE), due to its attractive characteristics. It has tunable bioactivity, degradability and mechanical properties, intrinsic functionality, it can be processed in aqueous solution and it can be chemically modified. Different processing methods have been developed in order to obtain constructs with different characteristics depending on the biomedical field application [14,48,50,51]. Many research groups described various silk-based scaffolds with different morphologies and architecture, depending on the application considered, such as films,

hydrogels, sponges, non-woven mats and fibers [70,116,117]. In ligament TE, silk fibroin fibers have already been used for the fabrication of prostheses and also for ligament augmentation, since a fibrous scaffold has been considered one of the best candidate to mimic the native tissue [46]. In fact, the fiber-organized structures can resemble the hierarchical structure of the native ECM, the diameter and the orientation of the collagen fibers, and they can provide the mechanical properties required in the ligament directionality [46] which can also influence cellular functions and behaviour [118–120].

Silk fibroin fibers can be native or made by regenerated fibroin. The term regenerated refers to constructs that are produced, after degumming, from fibroin solutions [121,122], where fibroin is denatured, losing its secondary protein structure and adopting the random coil conformation. Regenerated fibers show relevant advantages over native silk fibers: their morphology and properties (such as secondary structure of the protein) can be tuned according to the application, and biomolecules can be conjugated/mixed to silk fibroin in solution. On the other hand, native silk fibers show high crystallinity and consequently, high stability [123]. In fact, there are several works describing the use of native silk fibers or silk fibroin fibers for tendon/ligament tissue engineering, but some critical issues still need to be solved. For example, Altman et al. [83] developed a silk wire rope matrix

mimicking the native mechanical properties of ACL, but the geometry of the matrix did not induce cell infiltration to the inner part of the bundles composing the rope. Teuschl et al. [61] fabricated a silk fiber-based scaffold to induce *in vivo* ACL regeneration, after 12 months they observed some collagen deposition. Horan et al. [85] provided a bioresorbable scaffold to recover the functional integrity of ACL, describing the situation *in vitro* and *in vivo* and the importance of cell ingrowth. Laurent et al. [46] reported various fabrication methods of fibers used for ACL scaffolds, among those electrospinning, a technique widely used for its capacity to produce fibers ranging from nano to micrometer of diameter. Electrospinning has been considered one of the most versatile and effective technology to produce nanofibers from various polymeric materials with different dimensions, functional components and controlled fiber morphology [124]. Nevertheless, with this technique it is difficult to reach the necessary mechanical properties[125–127].

Recently, for this reason, many researchers, such as Altman and Teuschl, adopted the braiding/twisting method as effective to improve some mechanical properties, such as stiffness and ultimate tensile strength [61,83,126]. Nowadays, textile industrial strategies can be used to process fibers playing a considerable role in biomedical engineering [128,129], since they can offer various

weaving methods that lead to constructs suitable for cell activities [61,126,130].

4.1.2. The role of bioreactor in ligament tissue engineering

Tissue engineering (TE) is a field that applies principles of biology, engineering and medicine toward the development of biological tissue substitutes to restore, repair or improve damaged tissues [39,40]. To do this, TE focuses on the combination of specific cell types with a biodegradable scaffold, resembling the original extracellular matrix (ECM) of the damaged tissue, to restore its functionalities [14]. Once implanted, the scaffold has gradually to degrade, while the tissue is regenerating. The scaffold should be able to promote cell adhesion and differentiation, especially when growth factor and/or bioreactor are combined to trigger cell response. The human body can be considered the physiological bioreactor able to sustain and give the right support to all tissues and organs.

Bioreactors are important devices in TE, they can control the environmental conditions in which the scaffold is operating. In particular, the most significant role is to mimic the mechanism of the physiological conditions for a 3D scaffold-structure, simulating the living organism to encourage tissue regeneration, enhancing the formation of ECM.

The parameters that a bioreactor should precisely control are temperature, medium pH, gas exchange, O_2 level, CO_2 level, humidity, nutrient transport, waste removal and mechanical-biochemical stimuli. Some of these parameters have to respect the standard cell culture conditions (for example: the temperature at 37°C, the CO_2 at 5%, the pH at 7.2-7.4), but they can be adjusted according to the application.

Beyond the external environment, the place where all these parameters merge is the culture chamber (of primary importance), where the cells on the scaffold receive the stimulation. This is a sterile environment where the scaffold is confined and the medium flow has to diffuse to allow nutrients supply, waste removal, and gas exchange.

Samples in the bioreactor can be cultivated under biochemical and mechanical signals mimicking the *in vivo* physiological environment to improve the tissue engineering construct. The mechanical stress induced can lead to different effects on the cells generating various biological responses. In fact, the biomechanical interactions between cells and scaffolds can critically influence cell behaviour [131].

The principle of the bioreactor can be applied to help the *in vitro* development of new tissues, but also *in vivo* [132].

According to the type of bioreactor, different stimuli can be applied in relation to physiological condition that has to

resemble. The stimuli produced by the bioreactor can induce the formation and deposition of extracellular matrix. Concerning the type of stimulation that is needed, different bioreactors can be used. Several types of bioreactors are commercially available for tissue engineering, but not only (food industry, agriculture, etc.) [133]. In TE, the bioreactor is mainly used to mimic the physiological condition of the musculoskeletal tissue, where the mechanical forces are important modulators of cell physiology. There are various bioreactor settings, depending on the application, the type of stimulation and the flow profile. Thereinafter listed in Table 3 the most commonly used bioreactors [134]

Type of bioreactor	Function
Spinner Flask	Common bioreactor with turbulent flow, able to increase nutrient, waste removal and oxygen diffusion. Typical used for articular and bone tissue engineering.
Rotating Wall Vessel (RWV)	Rotating bioreactor with cylindrical chamber where the scaffold is cultured and the medium is filled. Introduced by NASA since it is able to generate a micro gravitational environment.
Rotating Wall Perfusion Vessel Bioreactors (RWPV):	Rotating bioreactor that induces perfusion on scaffolds, widely used in cartilage tissue engineering. It is a variation of RWV bioreactor.

Perfusion Bioreactor	Bioreactor allowing nutrient transport and waste removal through the culture medium flow constrained to pass along the scaffold section.
Concentric Cylinder Bioreactor (CCBR)	The shear stress produced by the turbulent flow is reduced, to increase cell efficiency and decrease cell damages.
Rotating-Shaft Bioreactor (RSB)	The culture is carried out in two phases, with two independent pumps, one for the medium perfusion, the other for the gas exchange. The shear stress generated is less than one produced by CCBR.

Table 3: list of typical bioreactors used in tissue engineering and their functionalities.

There is not the ideal bioreactor design, it has to be tailored for a specific individual purpose, considering both tissue and application. However, the apparatus may be designed with the possibility of a fast removal for external analysis.

4.1.2.1. Perfusion bioreactor

In this paragraph, the attention will focus on perfusion bioreactor, since it has been usually involved in the stimulation of ligament scaffolds [86,135] and it is the typology used in this chapter.
The perfusion is a necessary process to let the cells survive, as the body fluids penetrate inside tissues to supply oxygen and nutrients, while removing wastes.

When the tissues are naturally avascular (for example, ligament tissue), the nutrient delivery throughout the tissue-engineered construct in static condition must occur by diffusion. Providing a dynamic medium flow, the nutrient exchange and the cell growth can be enhanced. The perfusion bioreactor is basically a system in which the culture medium circulates through a culture vessel. According to the different settings of this type of bioreactor, several benefits can be achieved. For example, with the automatic replenish of the medium, the culture chamber can be connected to a medium reservoir in a closed loop or in a more complex methodology. In this way the system allows the medium circulation through the scaffold chamber with constant gas exchange. It is important to consider how the perfusion occurs through the interior structure of the scaffold, and which will be the effect on cell migration.

During the perfusion, cells are also exposed to the shear stress induced by the flow. The shear stress is considered an advantageous signal for tissue regeneration, since it can stimulate the mechanotransduction pathways [136]. In these terms, the mechanical stress is transduced into biochemical signals to regulate cell functions.

Therefore, many parameters have to be considered to design a perfusion system, to provide the adequate culture condition to the scaffold.

The first parameter is the medium flow pathway. The medium has to be restricted to follow a unidirectional flow, otherwise the flow will follow the path with less resistance, and the perfusion of the entire scaffold cannot be guaranteed.

Another important variable that has to be controlled is the flow rate of the medium. The optimal value has to consider the design of the bioreactor, the structure of the scaffold and the cell type used. It can influence the shear stress applied to the construct, according to the architecture and the porosity of the scaffold. Moreover, it can affect cell adhesion, cell proliferation and gene expression [132,137].

Other relevant parameters are the ones mentioned at the beginning of the previous paragraph: pH, oxygen tension, temperature, nutrient availability, and waste removal. Nutrient supply and waste removal can be addressed by medium change, but since the perfusion system is closed, frequent medium change is slightly complicated. For this reason, sometimes a two-reservoir system is used, while the bioreactor is normally working, the medium can be changed [138] (Figure 13). Also pH and gas exchange have to be maintained using permeable materials. However, keeping the perfusion bioreactor in the incubator, will help to maintain uniform and controllable the cell culture conditions.

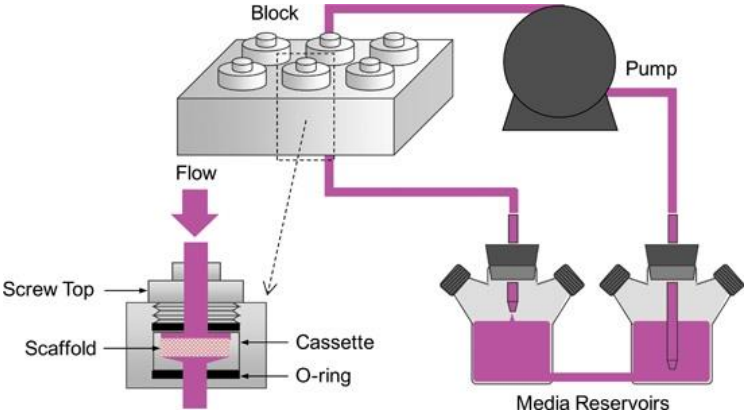

Figure 13: example of perfusion bioreactor at two-reservoir system, where the medium is forced to pass through a porous scaffold. Image from [139].

Since perfusion bioreactors are usually used for dynamic cell culture or long term cell culture, another parameter to consider is the seeding method. Different seeding techniques can influence the initial cell seeding efficiency and cell distribution on the scaffold. The seeding can be performed in static condition (the most prevalent technique) but also in perfusion condition. Different methodologies will affect the cell seeding efficiency also according to the structure of the scaffold and probably the cell type used [140,141].

In conclusion, the perfusion bioreactor can provide an effective environment to mimic the *in vivo* situation, meaning that it is a powerful instrument to be used in tissue engineering applications, in particular for ligament tissues [135].

4.2. Materials and Methods

All materials were purchased from Sigma-Aldrich (USA) unless otherwise stated.

4.2.1. Silk fibroin aqueous solution preparation

The procedure to prepare silk fibroin aqueous solution is described in the paragraph 3.2.1. of chapter III. After dialysis, the silk fibroin solution was used at 4%, making a dilution with DI water.

4.2.2. Fabrication of multicomponent scaffold

The multicomponent scaffold was fabricated combining the anisotropic silk fibroin sponge with native yarns produced by Chul Thai Silk Company (Thailand) with 130/150 Denier (D) and 302 twists (Figure 14), as a core structural component.

Figure 14: silk fibroin hank from Chul Thai silk Company, Thailand.

The dimensions decided for the diameter and for the length of the multicomponent model scaffold were 9,5 mm and 30 mm respectively, referring to the average values reported in the literature of the natural ACL [5,7]. To build up the multicomponent structure of the scaffold, a simple system was designed to keep the yarns equally distanced among each other, to allow anisotropic porosity formation for cell migration. A polypropylene (PP) cylinder (9.5 mm diameter x 30 mm length) was used with plugs with holes, fabricated by a 3D printer using PLA (polylactic acid) material, as shown in the picture below (Figure 15). Once the yarns are positioned into the holes, the cylinder can be filled with 4% aqueous silk fibroin solution, and subjected to directional freeze and freeze-drying technique, as described in chapter III.
Briefly, the cylinder containing fibroin solution and silk yarns is positioned in a polystyrene foam and at -20°C for 24 hours, to induce vertical ice crystals formation. The polystyrene mold acted as a thermal insulator, generating a temperature gradient along the cylinder, starting from the upper exposed free surface of the fibroin solution (using to the plug with bigger holes to allow water evaporation, Figure 15, n°3). The method induced the formation of vertically oriented ice crystals by directional freezing along the main axis of the cylinder. Finally, the frozen scaffolds were lyophilized (freeze-dryer Lio-5P 4k, 5pascal, Italy) for 48 h. The complete multicomponent scaffolds presenting yarns and

anisotropic porosity were treated with 80% methanol (MeOH) to induce a protein conformational change from the silk I to the silk II structure. After treatment, scaffolds were subjected to washes with ddH_2O (to remove MeOH residuals), another freezing and freeze-drying cycle (to maintain the structure) and sterilized with 70% ethanol (EtOH).

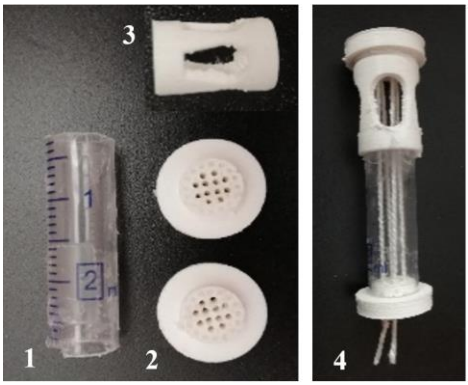

Figure 15: components of the system to fabricate the multicomponent scaffold: n°1 is the PP cylinder (30 mm length, 9,5 mm diameter), n°2 are the plugs with holes, n°3 is the top plug. In the n°4 is possible to see all the system built up, with the plugs n°2 that keep the yarns equally distanced inside the n°1, with n°3 plug on the top that allows the temperature gradient to start but also the water to evaporate during the last passage of freeze-drying during the fabrication process.

4.2.3. Tensile mechanical properties of yarns

To evaluate the tensile mechanical properties, silk fibroin yarns were tested by a universal mechanical testing machine (Instron

4502, USA). The analyses were performed with a strain rate of 50 mm/min, a cell load of 1 kN and an extensometer (contact type). The specimens were fixed to round grips (Figure 16a) and an extensometer was applied to avoid sample sliding directly on the specimen (Figure 16b). The samples were pre-tensioned to 2 N. Specimen thickness (~1 mm diameter) was determined by confocal microscopy imaging to increase measurement accuracy. The test was performed on dry and wet fibers. Kept in DI water at 37°C for at least 16 h (overnight). The test was performed at RT and with 50% of humidity. Load-displacement curves were obtained and stiffness was calculated from the initial linear part of the curves. At least seven specimens were tested per condition.

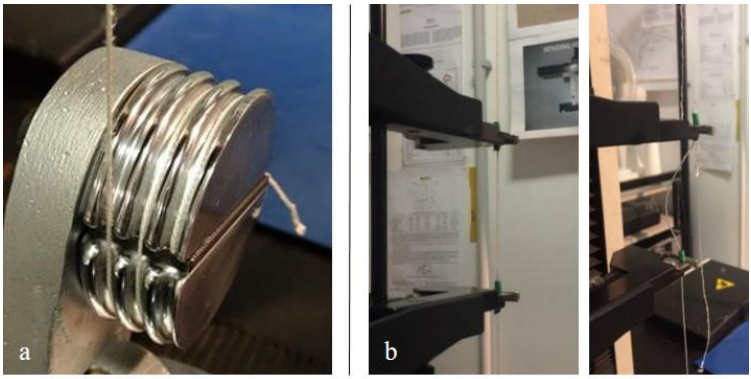

Figure 16: **a**) round grips, especially used to fix rope-like samples during tensile test; **b**) extensometer applied to the specimen, before and after its rupture.

4.2.4. Characterisation of the multicomponent scaffolds

4.2.4.1. Microstructure evaluation by electron microscopy and micro-tomography

The morphology and the porosity of the multicomponent scaffold were analysed by scanning electron microscope (Zeiss supra 40, Germany), after coating the samples with Pt/Pd alloy (80/20) using a Q150R sputter coater (LOT-Quantum Design, Germany), and by micro-computed tomography (µCT) (Skyscan1176, Bruker, Belgium). The µCT equipment was used at 40kV with a voxel size of 9 µm. Scaffold dimensions were of 9,5 mm diameter x 10 mm length (n=3). To measure scaffold porosity, a built-in algorithm of µCT software (Bruker, USA) was used to create 3D images and then consequently perform the analysis.

4.2.4.2. Scaffold stability in aqueous environment

To verify the scaffold stability in aqueous environment, the weight loss was measured, also in preparation for long-term cell culture. The samples (9,5 mm diameter x 10 mm length) placed in a 24-well plate were immersed in 2 ml of DI H_2O up to 10 weeks at 37°C. Then, samples were washed two times in DI

H_2O, frozen, lyophilized and weighted to check if a loss in weight was detected. The initial dry weight of scaffolds (W_0) and the dry weight after different time points (Wt) were recorded. The weight loss of the samples was calculated using the equation: weight loss (%) = (W_0 – Wt)/ W_0 × 100%. At least 3 samples per each time point were measured.

4.2.5. Functionalization of multicomponent silk fibroin scaffolds with heparin

Multicomponent silk fibroin scaffolds were functionalized using heparin sodium salt from porcine intestinal mucosa following the procedure described in the paragraph 3.2.4. of the previous chapter, with the aim to create covalent bonds between carboxyl groups in heparin and primary amines in fibroin, by carbodiimide chemistry.

4.2.5.1. Quantification of heparin binding release

Similarly to the procedure reported in the paragraph 3.2.5., heparin release was quantified for a total period of 28 days. After functionalization and washes with MES buffer and ddH_2O, each scaffold was incubated in 1 ml of ddH_2O and 100 µl were taken after 1 h, 3 h, 1 d, 3 d, 7 d, 14 d and 28 d for quantification. 100 µl of fresh ddH_2O were replenished at every measuring point. Heparin quantification was done by a dimethylmethylene blue

(DMB) assay, using and following the instructions reported by the protocol related [142]. Heparin binding efficiency and release were quantified in heparin-crosslinked scaffolds (n = 4). To determine the binding efficiency of heparin, the amount of unreacted heparin was measured indirectly in MES buffer after the conjugation reaction (before washing). The time of 3 days was still considered to evaluate the heparin quantity available for growth factor binding and cell culture, after 3 days washing. The calculation was done by subtracting the heparin released at 3 days from the total heparin incorporated after functionalization.

4.2.6. TGF-β2 growth factor binding to multicomponent silk fibroin scaffolds

To induce ligament differentiation of AdMSCs, human recombinant TGF-β2 was chosen for its role in the musculoskeletal system and incorporated into the multicomponent silk fibroin scaffolds crosslinked with heparin (n = 4). Growth factor loading was performed following the method reported in the paragraph 3.2.6., chapter 3.

4.2.6.1. Quantification of TGF-β2 binding efficiency and release

ELISA assay was used to calculate and quantify the binding efficiency and release of TGF-β2 growth factor from the

functionalized scaffolds (n = 4). Growth factor release was performed following the instructions reported in the paragraph 3.2.7., up to 28 days. TGF-β2 was quantified using a TGF-β2 ELISA kit (Invitrogen, Austria) following the manufacturer's instructions. To estimate the binding efficiency, the amount of unbound TGF-β2 was indirectly calculated by quantifying the amount of unbound growth factor in PBS after the conjugation reaction.

4.2.7. In vitro evaluations on multicomponent scaffolds

In vitro tests were done to evaluate the ability of the scaffold to promote cell adhesion, cell metabolic activity, ECM molecules production (collagens) and phenotype-specific gene expression. In the first part of the results presented in this chapter, the abilities aforementioned were evaluated on the multicomponent scaffold not functionalized, while in the second part of the result section, the *in vitro* tests were repeated following the same methods herein reported, but on the functionalized scaffold with heparin and TGF-β2 growth factor to observe the effect on the AdMSCs culture. To perform these analyses, adipose tissue derived mesenchymal stem cells (AdMSCs) were cultured up to 4 weeks in different cell culture conditions.

4.2.7.1. Adipose-derived MSCs culture

The dimensions of multicomponent scaffolds used for cell culture were of 9,5 mm diameter x 10 mm length (cylindrical shape). Prior to cell culture, scaffolds were sterilized with 70% ethanol and washed with PBS. Adipose tissue derived mesenchymal stem cells (AdMSCs) were kindly provided by the Technical University of Munich, Germany, isolated according to the guidelines of the Local Ethics Committee of ''Klinikum Rechts der Isar'' and with the method described in Schneider et al. [106]. AdMSCs were seeded on the upper surface of the dry scaffolds to improve cell attachment at a density of 3 x 10^5 cells/scaffold. Seeding was performed in a small volume of cell culture medium (80 µl) to improve seeding efficiency. After seeding, scaffolds were incubated for 30 min at 37°C to facilitate cell attachment. Cells were cultured as reported in the paragraph 3.2.8.1. All experiments were performed with AdMSCs at passage 3 (p3).

4.2.7.2. Static versus perfusion culture condition

To assess cell penetration along the structure of the multicomponent scaffold in the first part of the chapter, and the effect of TGF-β2 on the AdMSCs culture in the second part, a perfusion system was specially designed to allow cell culture medium permeation through the scaffold, consisting in a

homemade bioreactor made with (Figure 17): impulse pumps, controlled by a multi-function timer (Brodersen, Unic XT Recycler), giving impulses close enough to simulate a continuous flow pumping 0,2 ml/min according to the scaffold cross section (calculation adapted from literature [137]); sterile chambers (Ebers P3D-10) (Fig.16, a) with internal diameter of 9-11 mm, perfectly matching with the diameter of the scaffolds; sterile filters of 0,22 µm (Sarstedt); 50 ml syringes (Exelmed) used as medium storage containers; adapters and connectors, including needles (Nipro needle 19G) and marprene tubes, with 0,8 mm of internal diameter and 1,2 mm of external diameter (Fig. 17b and c). The medium was recirculated, and changed every three days. The final set up of the homemade bioreactor is shown in Figure 18.

Figure 17: different components used to build up the homemade bioreactor: **a**) sterile chambers in which the scaffold was inserted; **b**) marprene tube and needle and **c**) various connectors.

Figure 18: final set up of the homemade bioreactor, using the components reported in Fig. 17. In the image, it is possible to observe as the syringes work as medium storage to allow the recirculation of the medium (clockwise direction, black arrows) and to keep the system self-sustaining for long time.

The impact of the perfusion system was compared with samples cultured in static condition.

One of the aspects that should be evaluated, before starting a perfusion culture, is to define the post-seeding time needed to promote cell adhesion and adhesion stability before the perfusion stimulus is introduced.

4.2.7.3. AdMSCs metabolic activity

The metabolic activity of AdMSCs seeded on multicomponent scaffold was measured using the resazurin salt (Chemodex)

solution, a homemade working solution (similar to AlamarBlue assay [143]). When resazurin enters the cells, blue precipitates appear on the scaffolds as a consequence of resazurin reduction into fluorescent resorufin in the cytoplasm (Figure 19). At each time point (day 14 and day 28) the cell culture medium was replaced with medium containing resazurin solution (10% v/v) and data were recorded after 3 hours (simplified protocol in Table 4).

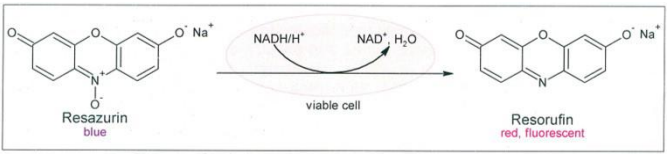

Figure 19: chemical structure and reaction of resazurin to resorufin.

Resazurin assay	
Resazurin solution preparation	0,025 gr of resazurin salt in to 100 ml of PBS w/o Mg^{2+}
reagent composition	Resazurin solution 10% (v/v) in cell culture medium
medium composition	DMEM high glucose + FBS inactivated 10% (v/v) + Glutamine 1% + P/S 1%
assay support	96-well plates
repetitions	4 samples for group
incubation time	3 h
data record	fluorescence excitation wavelength: 535 nm fluorescence emission wavelength: 590 nm
notes	protect samples from light

Table 4: schematic protocol to measure the metabolic activity of AdMSCs with resazurin assay.

4.2.7.4. AdMSCs differentiation by gene expression evaluation

Gene expression of tendon/ligament differentiation markers was analysed on multicomponent silk fibroin scaffolds. AdMSCs were seeded on scaffold and cultured for 14 and 28 days. Next, the scaffolds were washed in PBS, cut in small pieces and stored at -80°C in TRIreagent for at least 24 h. Next, RNA isolation in TRIreagent was performed by chloroform extraction following the manufacturer's instructions. RNA quantity and quality was measured with NanoDrop. Reverse-transcription to cDNA was performed using a first strand cDNA synthesis kit (iScript™ Reverse Transcription Supermix, BioRad, USA) according to the manufacturer's instructions. Quantitative analysis of gene expression was performed by quantitative polymerase chain reaction (qPCR). 30 ng of sample cDNA were used per reaction. The thermocycler used for both procedures was a CFX96 Real Time System thermocycler (BioRad, USA). SsoAdvanced™ Universal SYBR® Green supermix (BioRad, USA) was used as a detection reagent. The primers used and their sequences are shown in Table 5. Results were expressed as fold change relative to the housekeeper gene ($2^{-\Delta CT}$).

Target gene	Forward (5' → 3')	Reverse (5' → 3')	Function
βTubulin	GAGGGCGAGGA CGAGGCTTA	TCTAACAGAGGCAAA ACTGAGCACC	Housekeeping gene, found in microtubules of cytoskeleton.
Collagen I A1 (Col I)	AGCGGACGCTAA CCCCCTCC	CAGACGGGACAGCA CTCGCC	Col type I is a fibril-forming collagen found in most connective tissues and is abundant in bone and tendon
Collagen III (Col III)	TACTTCTCGCTCT GCTTCATCC	GAACGGATCCTGAGT CACAGAC	Fibrillar collagen extensively found in connective tissue.
Scleraxis (Scx)	CAGCCCAAACAG ATCTGCACCTT	CTGTCTTTCTGTCGC GGTCCTT	Transcription factor related to tenogenesis and upregulation of col I
SRY-box 9 (Sox9)	GAGCCGAAAGCG GAGCTGGAA	ACAGCTGCCCGCTCC AAGTG	Transcription factor related to chondrogenic differentiation.
Tenomodulin (TND)	ATTCAGAAGCGG AAATGGCACTGA	TAGGCTTTTCTGCTG GGACCCAA	Gene highly expressed in tendon, upregulated by Scx.

Table 5: primers used for qPCR. Primer sequences used for quantitative polymerase chain reaction (qPCR). βTubulin was used as a housekeeper gene.

4.2.7.5. Collagen production and assembling by imaging

AdMSCs morphology and migration/distribution on multicomponent silk fibroin scaffolds were evaluated at 2 and 4 weeks after seeding. In addition, the production and distribution into matrices of collagen I and III was evaluated on the seeding area and in the longitudinal section of the scaffold, by using the following immunofluorescence staining antibodies (Abcam, Germany). Primary: collagen I (ab34710, 1:500), and collagen III (ab7778, 1:200). Secondary: IgG goat anti-rabbit, conjugated with Alexa Fluor 594 (a11037, Life Tech, 1:1000 in PBS). All primary antibodies were diluted in 1% bovine serum albumin (BSA) in PBS. After 14 and 28 days of culture on scaffolds, AdMSCs were fixated with 4% formaldehyde in PBS for 40 min at RT and permeabilized with 0.2% Triton X-100 in PBS for 30 min at RT. Next, scaffolds were incubated in 1% BSA in PBS for 1 h at RT. Subsequently, scaffolds were stained with primary antibodies overnight at 4°C. Next, samples were washed 3 times in PBS and stained with secondary antibody at RT for 1 h, shaking. Finally, samples were washed with PBS and stained with Alexa Fluor 488-Phalloidin (Thermo Fisher Scientific, USA) and DAPI following the manufacturer's instructions to detect cytoskeleton structure and nuclei, respectively.

4.2.8. In vivo evaluation: impact on the inflammatory response

4.2.8.1. Histological analysis of the inflammatory response

In vivo evaluation was performed by implanting the multicomponent silk fibroin scaffolds in rats under the skin. All the animal experiments were performed in accordance with the guidelines and approval of Chonbuk National University Animal Care Committee, Jeonju, Republic of Korea (CBNU 2016-50). The surgery has proceeded under general anaesthesia (Dormitor/Alfaxan), and all attempts were made to minimize animal suffering.

Male rats (6 weeks of age) were anesthetized with intramuscular injection. The hairs on the rat's back were removed using an electric shaver. The surgical site was disinfected with povidone-iodone. Samples (5 mm in length and 9,5 mm in diameter) sterilized with 70% of EtOH, were implanted into the subcutaneous dorsum of rats (n = 3). Animals were sacrificed after 14 and 28 days after implantation, and the scaffolds removed with the surrounding tissue.

Samples were washed two times with DI H_2O and then fixed with 10% neutral buffered formalin for 48 h. Then, samples were washed again in DI H_2O and kept in PBS at 4°C until embedding

in paraffin for histological sectioning. Samples were sectioned at 10 µm thickness and stained with a specific antibody, CD68 antibody (ED-1, Santa Cruz Biotechnology, USA) used for the staining of tissue macrophages by following the manufacturer's protocol. Briefly, slide glasses were washed with PBS and quenched endogenous peroxidase activity by incubating with 1% hydrogen peroxide. The specimens were incubated with blocking reagent to prevent nonspecific binding for 1 h at room temperature. The 8 µg/mL primary antibody was diluted in blocking reagent and the samples have been incubated with the primary antibody at 4°C overnight. The samples were then incubated with HRP-conjugated mouse IgG kappa binding protein (m-IgG$_K$ BP-HRP, Santa Cruz Biotechnology, USA), which was diluted in blocking reagent with the ratio of 1:25, for 90 min at room temperature and washed with PBS for two times. The slides were stained with a 3-amino-9-ethylcarbazole (AEC) chromogen kit for 20 min at room temperature. The sections were washed in deionized H_2O and dehydrated with 90% ethanol and 100% ethanol. Also haematoxylin and eosin (H&E) staining was performed according to the manufacturer's instruction.

4.2.9. Statistical analysis

Statistical analysis of quantitative data was performed using GraphPad Prism version 7.00 (GraphPad software, USA).

Statistical significance was considered at $p<0.05$. Data were analysed with Two-way analysis of variance (ANOVA) and Tukey's correction.

4.3. Results and discussion

4.3.1. Characterization of silk fibroin yarns

The smallest unit composing the yarn is the silk bave, the basic filament produced by the silkworm. To estimate how many baves were composing the native silk fibroin yarn, the latter was embedded in an epoxy resin and cut with a microcutter to get the cross section, procedure known as "*conventional method*" and described in [144]. The use of a fluorescent dye helped the detection of the cross section area of each bave in the yarn (Fig. 20b), that was analysed using the software ImageJ and resulted about 0,001 mm^2. Therefore, counting a total number of 1800 baves in the yarn, the total cross section area of the yarn is about 2 mm^2. These dimensions easily mimic the ones of collagen fascicles consisting the ECM of the ligament tissue [8]. Moreover, the subdivisions of the yarn (Fig. 20a) resembles the native hierarchical architecture of the ligament, which plays an important structural and functional role in the stability of the ligament, as already stated in chapter I and shown in Figure 1.

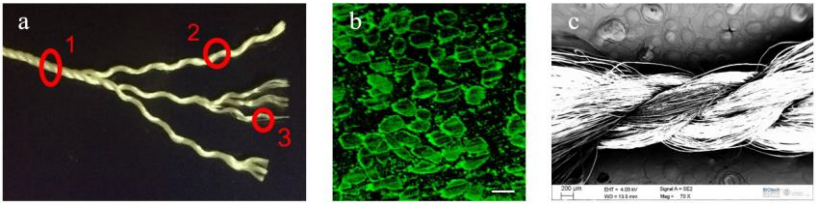

Figure 20: **a**) subdivision of a yarn composing the silk fibroin hank; where n°1 is called yarn, n°2 is called fiber and n°3 is called fibril, composed of baves; **b**) group of bave stained with a fluorescent dye to detect the cross-section area, scale bar = 20 µm; **c**) FE-SEM image of the torsions of the fibers composing the yarn.

4.3.2. Mechanical properties of the silk fibroin yarns

The yarns composing the multicomponent scaffold were subjected to uniaxial tensile test in dry and wet conditions. Representative Load-Strain curves are presented in the graphs reported in Figure 21. The strain was calculated as a ratio between the displacement of the sample during the traction and the length of the sample tested. The strain at break obtained in the two conditions ranged between 20-25%. The replicates of the samples among the same condition were showing similar values of load at break, with few differences in the standard deviation. For this reason, in Figure 21 are reported just representative curves and not all the samples tested ($n \geq 7$).

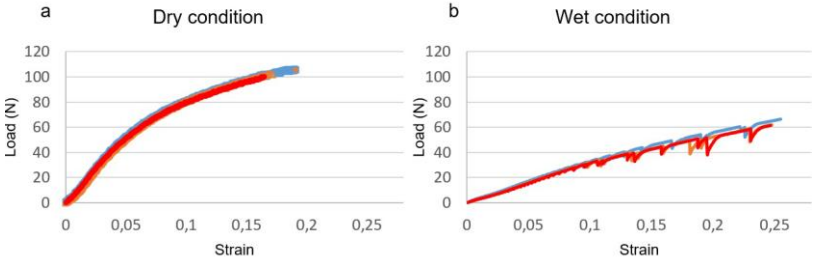

Figure 21: graphs obtained during the tensile mechanical test. **a**) representative curves of yarn tested in dry condition; **b**) representative curves of yarn tested in wet condition (in H_2O, overnight).

From the linear region of the curve, it was possible to calculate the stiffness as a ratio of load and extension, and the values are reported in the Table 6. Stiffness more than elastic modulus is in fact representative of the true mechanical behaviour of a real body, depending on its size. These data were calculated considering the length of the sample tested equal to 30 mm, resembling the average length of the natural ACL [29]. Observing the curves, there is an evident reduction of mechanical properties of the yarns in wet condition, in fact, the stiffness has fallen by a quarter, from 37 ± 1 N/mm in dry condition to 9 ± 1 N/mm in wet condition, due to the water plasticization of the fibroin. The value of the load at break was also calculated, which slightly decreased from 102 ± 3 N in dry condition to 78 ± 2 N in wet condition, values reported in Table 6.

The results obtained from the tensile test indicate that, to reach the natural values of ACL stiffness and load at break (reported in the last column of Table 6), is necessary to consider the insertion of 27 silk fibroin yarns in the multicomponent scaffold.

	Dry	Wet	Natural ligament[29]
Stiffness (N/mm)	37 ± 1	9 ± 1	242 ± 28
Load at break (N)	102 ± 3	78 ± 2	2160 ± 157

Table 6: in the first two columns there are the mechanical properties values of yarn tested in the two conditions. In the last column there are the values of stiffness and load at break of the native ACL.

4.3.3. Fabrication and characterization of the multicomponent scaffolds

The multicomponent scaffold was fabricated as described in Materials and Methods, paragraph 4.2.2. In literature, one of the most recent works dealing with ACL regeneration dates back to 4 years ago from Teuschl and colleagues [61]. They proposed a silk fiber-based scaffold that poorly regenerated due to the lack of void volume, around fibers, to let cell ingrowth. For this reason, we decided to provide a matrix around the yarns to let the cells adhere, penetrate and migrate through the pores and along the yarns, to reach the inner part of the scaffold and to start the regeneration process before yarn degradation. The basic idea came from the concept developed by prof. Migliaresi in a

previous work [145], in which, to reproduce a synthetic model of tendon, he and his collaborators proposed a composite material consisting of poly(ethylene terephthalate) (PET) fibers and poly(2-hydroxyethyl metacrylate) (PHEMA) matrix. While the fibers should give the mechanical contribution to the structure, the matrix has the key role to start the regeneration process, allowing cell infiltration.

Considering the stress at break of an ACL, 27 silk fiber yarns would be needed. However, 27 yarns would occupy most of the volume of the scaffold (about 85% in a scaffold sizing as the natural ACL) and this would impede cell infiltration. Nevertheless, loads applied after a surgery and during the rehabilitation process are much lower than the ACL strength and evaluable in about 445 N [31,146]. These mechanical conditions could be matched in the model ligament by using just 6 silk fibroin yarns. In our scaffold we have decided to use 12 yarns to achieve a mechanical strength double than the one that would be applied after a surgery and also to overcome unexpected early yarn failure due to degradation.

It is clear that reducing the number of yarns, the stiffness of the model ligament decreases proportionally. This fact could be overcome by using yarns with a lower twisting degree and should be considered if the aim is to make an isostiff scaffold. Even so, the condition on the strength is by far stricter.

An overview of scaffold morphology and pore alignment was performed using the µCT 3D volume reconstruction and FE-SEM images. The scaffold typically shows a cylindrical shape due to the polypropylene (PP) cylinder used during the fabrication.

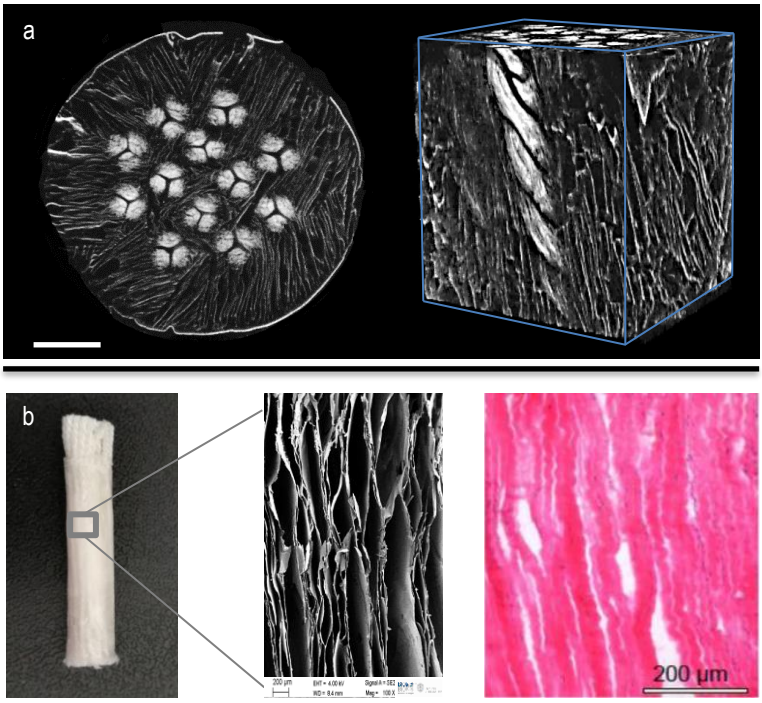

Figure 22: **a**) µCT 3D reconstruction of multicomponent scaffold. It is possible to observe, on the left side, the upper surface corresponding to the cross-section area where the yarns are visible; and on right, the inner structure where the yarns are integrated in the silk fibroin sponge with elongated pores. Scale bar = 2 mm. **b**) FE-SEM image of the vertical porosity characterizing the silk fibroin sponge fabricated with the freeze-drying method, resembling the structure of the native ECM of the human ACL (staining haematoxylin-eosin), adapted from [147], scale bar = 200 µm.

From transversal and longitudinal cross-section images (Figure 22a), it can be appreciated that the yarns are equally distributed in the core giving mechanical support to the scaffold structure and the porous fibroin sponge is homogeneously distributed around them offering void volume to let the cells adhere, migrate and proliferate. Indeed, the lamellar structure of the vertically aligned pores was successfully developed using the freeze-drying technique.

The architecture of the pores depends on the ice crystals shape formed following the solution concentration and freezing temperature, according to the freezing kinetics induced by the temperature gradient [107,148]. In fact, the ice crystal formation started from the surface (coldest region) through the temperature gradient, in the vertical direction, along the z-axis. In some areas of the scaffold, it is possible to find pores differently oriented due to the nucleation of ice crystals in different orientation. Each nucleus originates a group of ice crystals which will correspond to a group of lamellas with a specific orientation [107]. In general, the microstructure seems to mimic the ECM of the natural ACL, as it is possible to observe the comparison in the Figure 22b.

The overview of pore alignment and morphology is also shown by μCT 3D volume reconstruction (Fig. 22a). The vertically aligned pores with lamellar structure is visible as well as in FE-SEM images. Thanks to the 3D structural analysis software, it

was possible to calculate the percentage of the open porosity in the scaffold corresponding to a pore interconnection, that is around 60-80% with pore diameters ranging between 100-300 μm, resembling the values obtained from Font et al. [93].

The stability of the multicomponent scaffold was determined by incubating the samples in DI H_2O at 37°C up to 10 weeks. Weight loss was calculated every two weeks. During the first two weeks the weight of the scaffold remained stable, and then it started to slightly decrease until reaching the ~7% loss after 10 weeks (Graph 3). This loss is due to regenerated sponge degradation, since it has a less crystalline structure, as reported in literature [123,149].

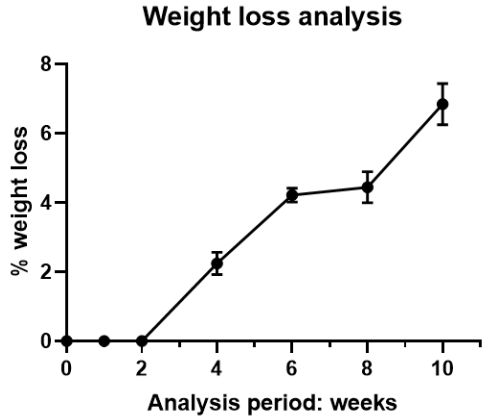

Graph 3: weight loss measurements in percentage for 10 weeks, where samples were in DI H_2O at 37 °C. Error bars represent standard deviation (n = 3).

4.3.4. Biological characterizations

4.3.4.1. In vitro evaluation by culturing AdMSCs in static and in perfusion condition

AdMSCs were cultured on multicomponent scaffolds up to 4 weeks to check cell migration, metabolic activity and gene expression. To promote cell penetration along the structure of the multicomponent scaffold, a perfusion system was designed, using a homemade bioreactor, to allow cell culture medium diffusion through the scaffold. A bioreactor system should consider some parameters to successfully address its role. Following the concepts aforementioned in the introduction of the current chapter, it was decided to apply the perfusion stimulation on the model scaffold to enhance the nutrient exchange, the cell migration and penetration. The flow rate of 0,2 ml/min was calculated according to the dimensions of the samples tested and adapted to the results obtained by Cartmell et al. in their work [137], showing that this flow rate may help cell differentiation compared to the other values proposed.

The bioreactor chamber used was sterile and made of materials allowing the gas exchange, as well as all the other components. The medium flow was directed throughout the scaffold, since the scaffold diameter was perfectly corresponding to the diameter of the bioreactor chamber, not allowing the medium to flow around

the scaffold, but through it. The perfusion bioreactor was placed in the incubator at 37°C of temperature and 5% of CO_2. The system was used for a long-term culture (28 days).

To compare the efficiency of the perfusion system, scaffolds were also cultured in standard static condition, placing the samples in the bioreactor chamber to ensure the same environmental conditions.

4.3.4.2. Cell seeding efficiency

To assess cell distribution, morphology and penetration along the multicomponent scaffold, confocal microscopy images were detected by cutting the scaffold along the z axis, to analyse the internal part of the scaffold, as shown in the Figure 23:

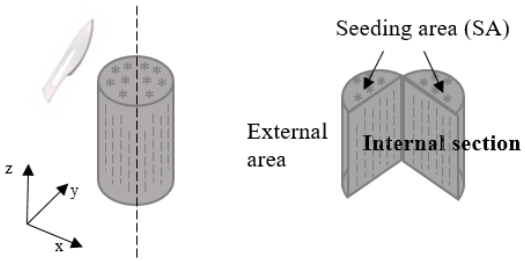

Figure 23: schematic representation of how the multicomponent scaffold was cut to be analysed by immunofluorescence imaging. Images were taken of the upper surface area, called the seeding area (SA) and of the internal part to actually observe the penetration of the cells along the length of the scaffold.

From literature it is known that the perfusion flow can induce stress on cells right after seeding, causing detachment and leading to a low cell seeding efficiency [138]. Therefore, we decided to evaluate the time to maintain static cell culture conditions before starting the culture in perfusion.

To avoid further difficulties, the seeding was performed directly on the scaffold already positioned inside the bioreactor chamber. Cell adhesion was evaluated after 1, 2, and 3 days in static condition before starting the perfusion, in comparison with samples seeded and directly stimulated in perfusion condition. In Figure 24 the results of the experiment are reported, showing that 2 days of static cell culture were enough to guarantee a strong adhesion of cells and their permanence on the substrate once put into perfusion cell culture condition.

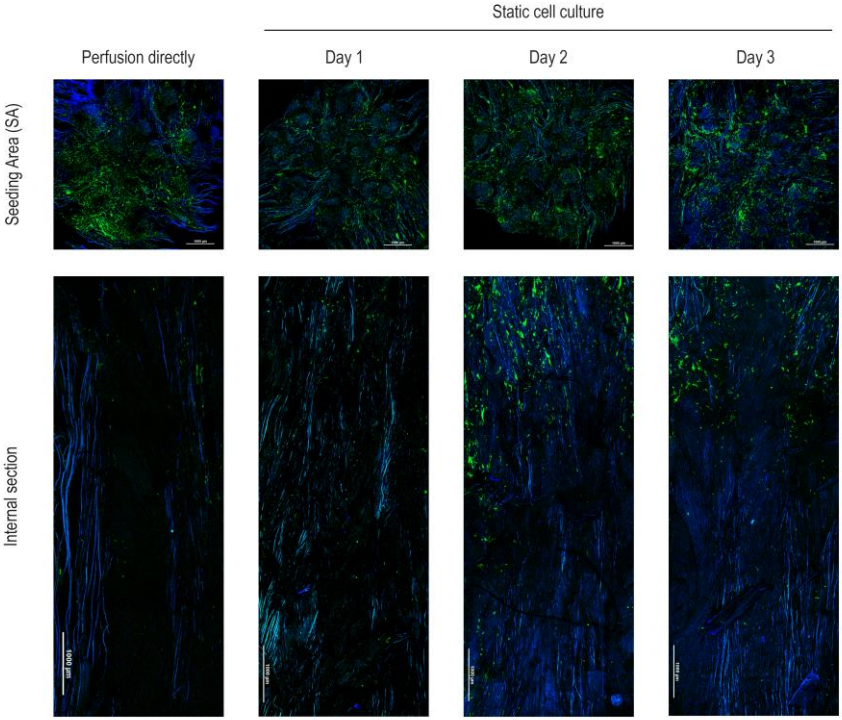

Figure 24: confocal images of samples cultured in static condition for 1 day, 2 days and 3 days before the perfusion stimulation. The cell adhesion was compared with a sample cultured directly in perfusion condition. Cytoskeleton is stained in green, nuclei and silk fibroin scaffold are visible in blue. Scale bars = 1000 µm.

4.3.4.3. Cell metabolic activity

One of the phenomena that has to be evaluated after seeding, besides cell adhesion, is the metabolic activity, to evaluate the interaction among the cells and the substrate scaffold.

To investigate the impact of the two types of cell culture conditions on AdMSCs, the cell metabolic activity was measured by Resazurin assay. As Graph 4 shows, in general, AdMSCs metabolic activity significantly increased from day 14 to day 28 and from static to perfusion cell culture conditions. In detail, the metabolic activity of AdMSCs at day 14 resulted significantly higher in the perfusion condition than in the static one. Similar results are shown at day 28, in which the metabolic activity follows the same significant trend. However, in both cell culture conditions the values of metabolic activity increased from day 14 to day 28, even if not in a significant way. This means that during the culturing period, cells were metabolically active, in fact, it is well known that higher metabolic activity causes a larger absorbance value as well as a larger percentage of resorufin (reduced resazurin) [150,151]. The difference between static and perfusion results may indicate that the flow produced by the perfusion bioreactor, stimulates the metabolic activity of the cells.

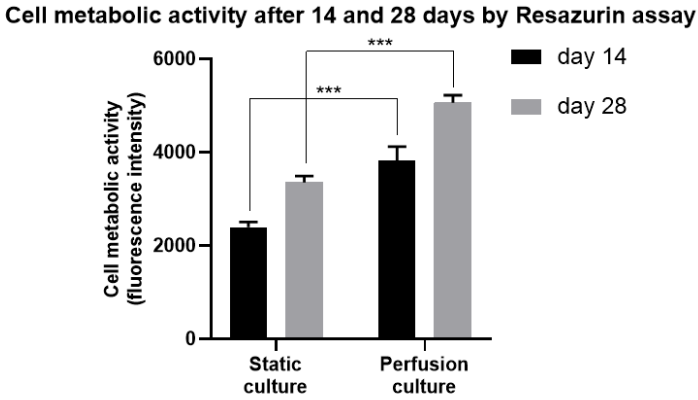

Graph 4: metabolic activity of cells cultured on the scaffolds in static and in perfusion conditions, measured after 14 and 28 days. Values expressed as resazurin fluorescence intensity. The values are represented as mean with SD (n = 4). (***) indicates statistically significant difference at $p < 0.001$.

4.3.4.4. Gene expression analysis

The expression of genes related to the selected tendon/ligament markers (collagen I (col I), collagen III (col III), scleraxis (scx), SRY-box 9 (sox9) and Tenomodulin (TND)) was evaluated on AdMSCs cultured up to 4 weeks on samples in static and in perfusion conditions (Graph 5). Gene expression data were expressed as fold change respect to the housekeeper gene, β tubulin.

In both time points, TND expression was not detectable (nd) in static cell culture, and in perfusion cell culture the value was almost close to 0.

Sox9 expression was downregulated in both cell culture conditions at both time points. It seems that in perfusion condition the value is slightly higher, but not in a significant way. Scx expression followed the same tendency of sox9, it was downregulated in static and in perfusion conditions, at 14 and 28 days.

Collagen I expression was slightly upregulated in both culture conditions. In static cell culture condition, the expression at day 14 and at day 28 is significantly higher compared to the expressions of scx, sox9 and TND. In perfusion condition, the expression is significantly lower compared to collagen III at day 14, but especially at day 28.

Collagen III expression was almost 2-fold upregulated in static cell culture at day 14 and 28, and in perfusion condition at day 14. The expression at day 28 in perfusion condition was almost 4-fold upregulated, in fact, it is significantly higher compared to the expression of col III at day 14, and compared to the expression of col I at both time points.

As a general overview, it is possible to assess that the static cell culture, without mechanical stimulation, did not show upregulation in gene expression related to tendon/ligament markers, as expected. On the other hand, the perfusion cell culture condition did not improve in a significant way the expression of genes related to tendon/ligament differentiation.

Despite the scx is expressed in tendon/ligament tissues throughout development, it could not enhance its expression, even in perfusion condition. A similar behaviour was observed in the previous chapter, where the interaction with biphasic scaffold and growth factors did not promote the scx expression. The downregulated expression of sox9 indicates that there is a very poor chondrogenic response of AdMSCs on the scaffold, in static and in perfusion condition. Moreover, TND expression is a specific marker of tendons and ligaments, but recently it has been discovered that scx is necessary for TND expression [152]. Therefore, the downregulation of scx may be a consequence for the downregulated values of TND expression.

Notably to say that, collagen I and collagen III expressions were significantly upregulated in both cell culture conditions. Especially collagen III in perfusion condition showed upregulated expression (~4-fold) at day 28.

Since collagen III is one of the major component of the ligament ECM, it may indicate that AdMSCs stimulated in perfusion condition were induced to produce more ECM structural molecules. This is supported by the results obtained from Resazurin assay (Graph 4), showing cells with increased metabolic activity. It is possible to assess that the perfusion cell culture may stimulate the cell metabolic activity to increase, triggering the basic ECM molecules synthesis but not driving cell

differentiation. About this, Wagner and colleagues studied different cell culture conditions of AdMSCs. They observed that the presence of growth factors promoted the expression of ligamentous marker, but AdMSCs cultured in standard culture medium, showed an increased expression of collagen III up to 28 days [153]. Comparing collagen III expression with the ACL fibroblasts, cultured as a positive control, they considered collagen III as a nonspecific marker of fibrogenic differentiation [153,154].

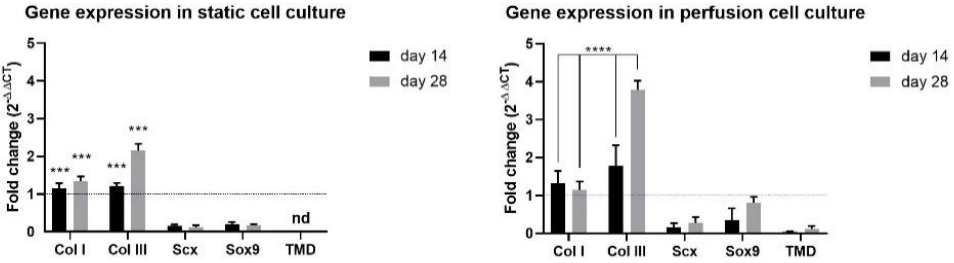

Graph 5: gene expression analysis of AdMSCs culture up to 28 days, influenced by different cell culture conditions. Target genes are collagen I (col I), collagen III (col III), scleraxis (scx), SRY-box9 (sox9), and tenomodulin (TND). Housekeeper gene is βTubulin. The fold change was calculated normalizing the target gene expression to the housekeeper gene. nd = not detectable. Statistical significance is indicated with asterisks. ***$p < 0.001$, ****$p < 0.0001$.

4.3.4.5. Immunofluorescence evaluation of collagens deposition

To investigate if the two types of cell culture conditions induced different effects on AdMSCs culture, immunofluorescence images were taken after 14 and 28 days to analyse the presence of collagen I and III, the actin cytoskeleton organization, the cell distribution and penetration.

Figure 25, 26, 27 and 28 show immunofluorescence staining of collagens type I and III. Collagen molecules are stained in red, the scaffold matrix in blue and the actin cytoskeleton in green. The left panels show low magnification images of the seeding area (top) and the whole internal section of the scaffold (bottom). The right panels show high magnification images, where more details can be appreciated.

First of all, confocal images showed that cells adhered and highly proliferated on the seeding area (SA), covering almost homogenously all the SA surfaces in both cell culture conditions (static and perfusion), and at both time points (day 14 and day 28). Cells are elongated, they adhered on the sponge lamellae and also among the fibrils composing the yarns, not only in the SA but also in the internal section of the scaffold, where it is possible to appreciate the cytoskeletal alignment of AdMSCs. The images in fact, show how the porosity of the scaffolds

influenced the alignment of cell cytoskeleton (Figure 25, 26, 27, 28).

[Note: the black crack that is visible in the middle of each SA picture is due to the cut that is done before the staining to allow it to penetrate inside the scaffold; not all the internal section images show the same homogeneous cell distribution since the acquisition depends on how was done the cut of the scaffold to allow staining penetration].

Figure 25 and 26 show collagen I and collagen III deposition (respectively) in static and in perfusion cell culture conditions at day 14.

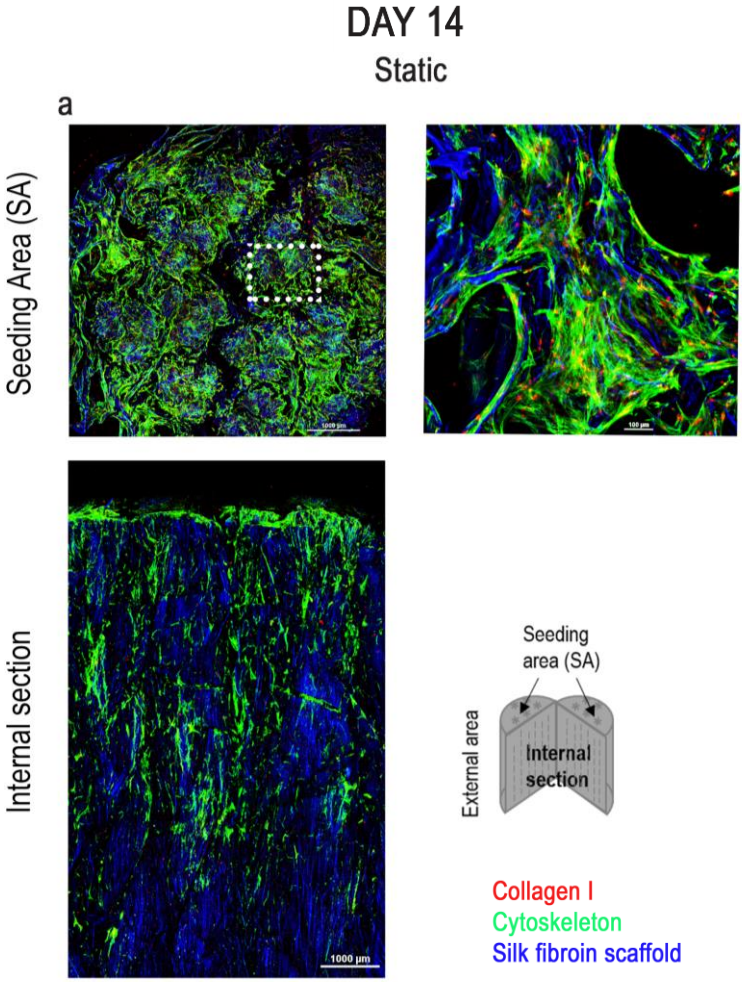

Figure 25a: confocal images of samples cultured in static condition for 14 days. In the upper part of each panel, there are images showing the seeding area (SA), low and high magnification (left and right, respectively). In the lower part, there are images corresponding to the internal section of the scaffold. Collagen I is stained in red, cytoskeleton in green, nuclei and silk fibroin scaffold are visible in blue. Scale bars for low magnification images (left column of each panel) = 1000 µm. Scale bars for high magnification images (right column of each panel) = 100 µm.

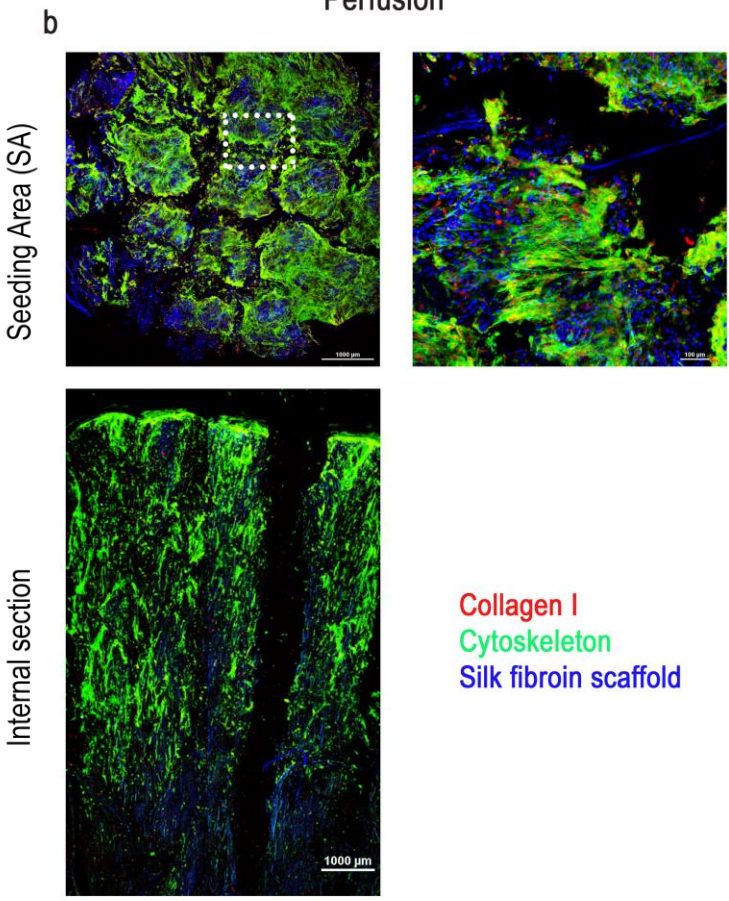

Figure 25b: confocal images of samples cultured in perfusion condition for 14 days. In the upper part of each panel, there are images showing the seeding area (SA), low and high magnification (left and right, respectively). In the lower part, there are images corresponding to the internal section of the scaffold. Collagen I is stained in red, cytoskeleton in green, nuclei and silk fibroin scaffold are visible in blue. Scale bars for low magnification images (left column of each panel) = 1000 µm. Scale bars for high magnification images (right column of each panel) = 100 µm.

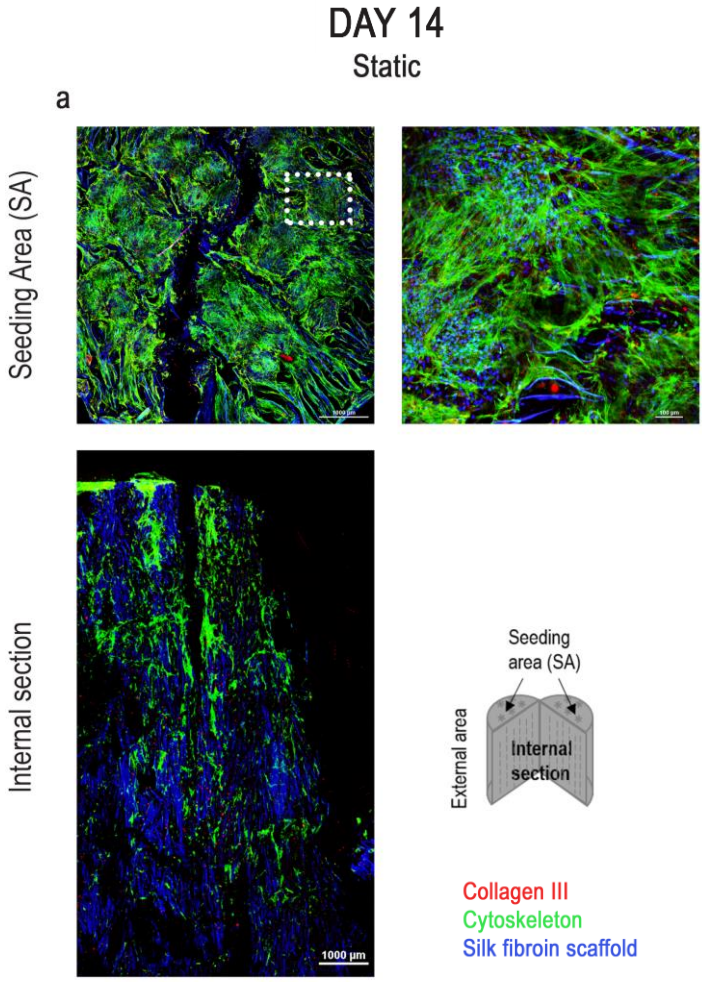

Figure 26a: confocal images of samples cultured in static condition for 14 days. In the upper part of each panel, there are showing the seeding area (SA), low and high magnification (left and right, respectively). In the lower part, there are images corresponding to the internal section of the scaffold. Collagen III is stained in red, cytoskeleton in green, nuclei and silk fibroin scaffold are visible in blue. Scale bars for low magnification images (left column of each panel) = 1000 µm. Scale bars for high magnification images (right column of each panel) = 100 µm.

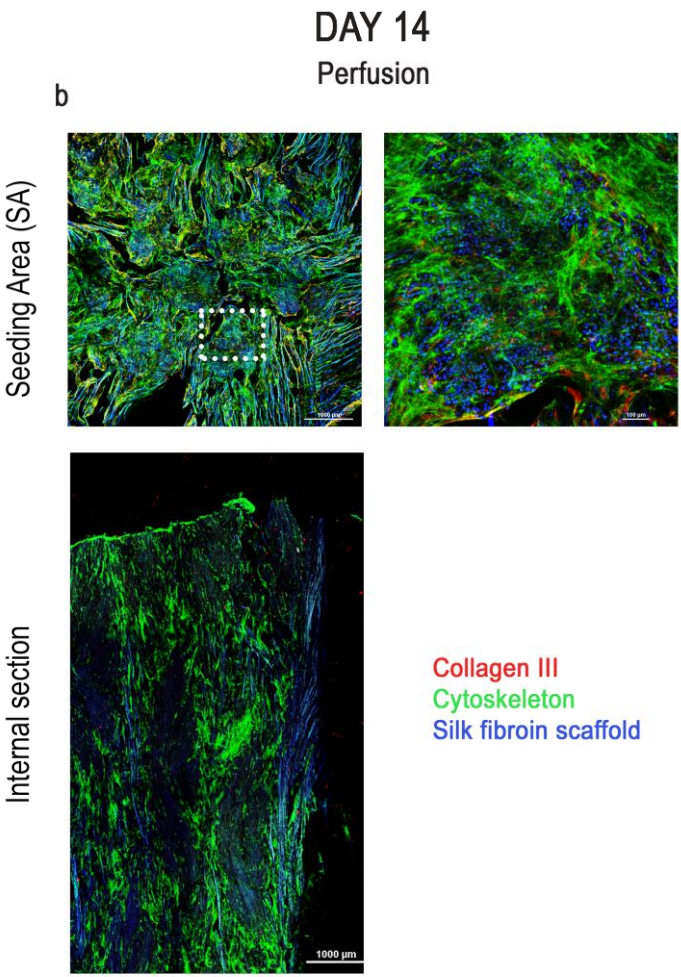

Figure 26b: confocal images of samples cultured in perfusion condition for 14 days. In the upper part of each panel, there are showing the seeding area (SA), low and high magnification (left and right, respectively). In the lower part, there are images corresponding to the internal section of the scaffold. Collagen III is stained in red, cytoskeleton in green, nuclei and silk fibroin scaffold are visible in blue. Scale bars for low magnification images (left column of each panel) = 1000 µm. Scale bars for high magnification images (right column of each panel) = 100 µm.

At first sight, the SA cells adhered on the sponge lamellae and among the fibrils of the yarns, almost reaching the confluence. Moreover, cells penetrated inside the scaffold even if not occupying the entire section, as the internal section images show.

The signals of collagen I and collagen III were clearly visible in the high magnification images, indicating that collagens were expressed in both cell culture conditions. In general, the perfusion condition does not appear to have interfered with the collagen deposition, if not slightly with collagen III at day 14. These results can be easily compared with qPCR values, indicating that the collagens markers are present not only at the gene level, but also at the protein level. Surely, it can be noticed that the perfusion condition stimulated cell migration into the majority of the structure. This was probably due to the enhanced nutrients supply inside the scaffold compared to the static condition.

Figure 27 and 28 show the content of collagen I and III (respectively) after 28 days of culture in static and in perfusion conditions.

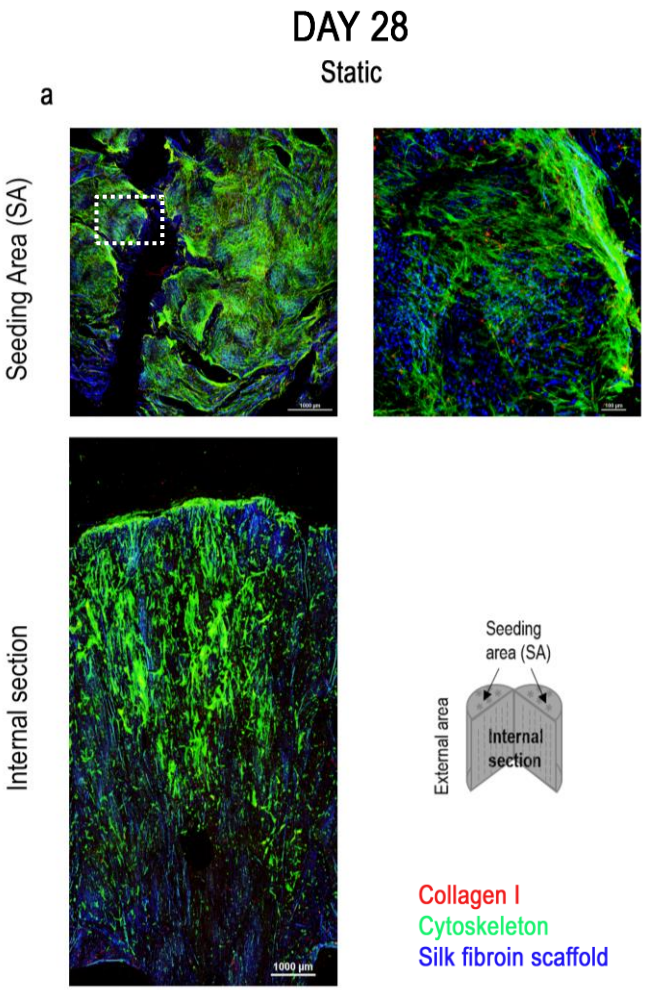

Figure 27a: confocal images of samples cultured in static condition for 28 days. In the upper part of each panel, there are images showing the seeding area (SA), low and high magnification (left and right, respectively). In the lower part, there are images corresponding to the internal section of the scaffold. Collagen I is stained in red, cytoskeleton in green, nuclei and silk fibroin scaffold are visible in blue. Scale bars for low magnification images (left column of each panel) = 1000 µm. Scale bars for high magnification images (right column of each panel) = 100 µm.

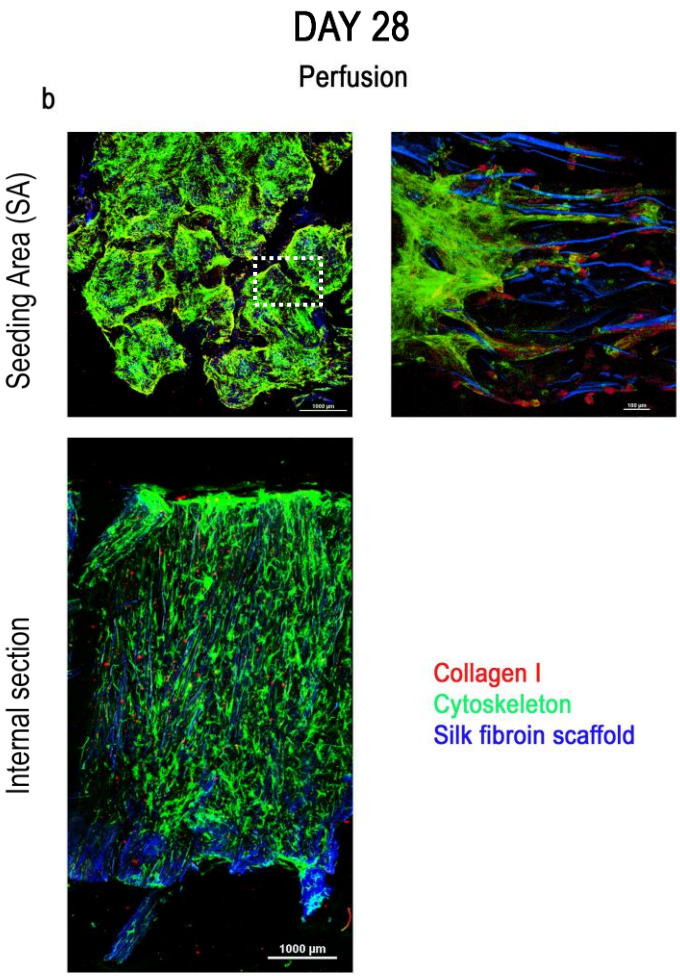

Figure 27b: confocal images of samples cultured in perfusion condition for 28 days. In the upper part of each panel, there are images showing the seeding area (SA), low and high magnification (left and right, respectively). In the lower part, there are images corresponding to the internal section of the scaffold. Collagen I is stained in red, cytoskeleton in green, nuclei and silk fibroin scaffold are visible in blue. Scale bars for low magnification images (left column of each panel) = 1000 µm. Scale bars for high magnification images (right column of each panel) = 100 µm.

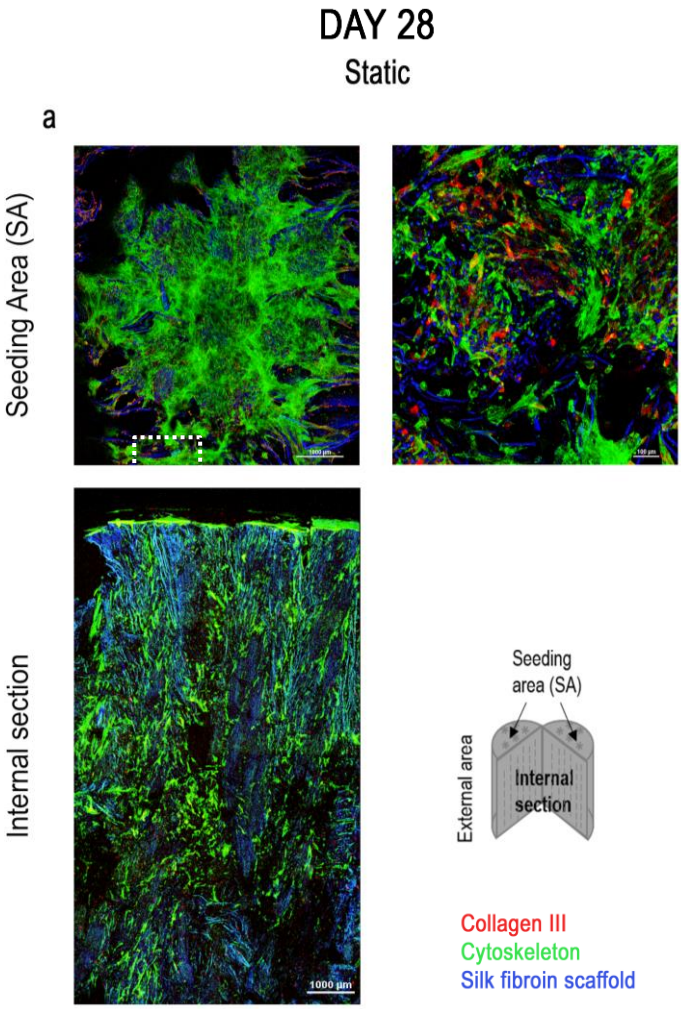

Figure 28a: confocal images of samples cultured in static condition for 28 days. In the upper part of each panel, there are showing the seeding area (SA), low and high magnification (left and right, respectively). In the lower part, there are images corresponding to the internal section of the scaffold. Collagen III is stained in red, cytoskeleton in green, nuclei and silk fibroin scaffold are visible in blue. Scale bars for low magnification images (left column of each panel) = 1000 µm. Scale bars for high magnification images (right column of each panel) = 100 µm.

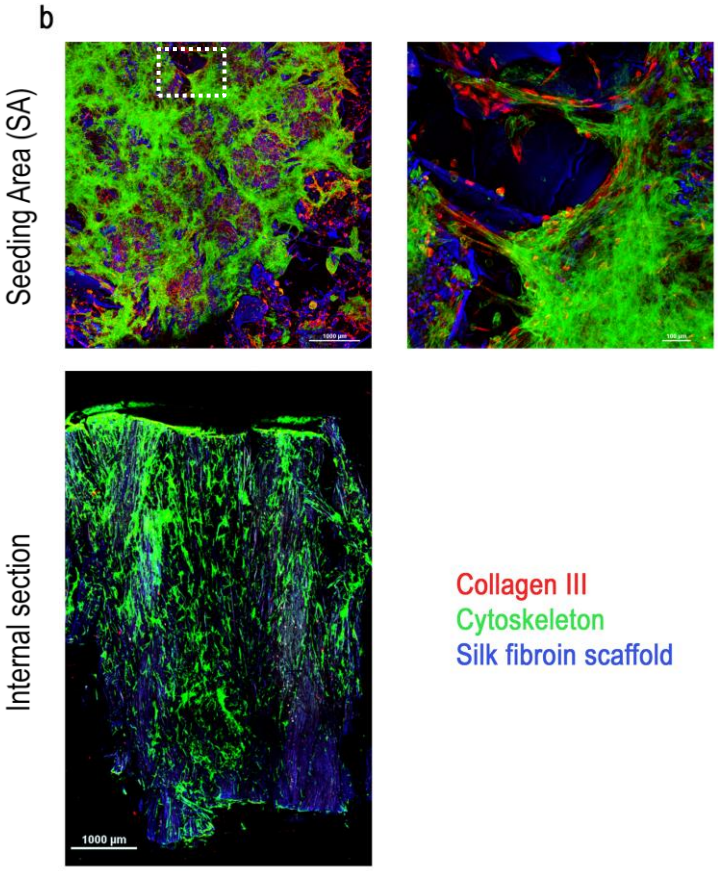

Figure 28b: confocal images of samples cultured in perfusion condition for 28 days. In the upper part of each panel, there are showing the seeding area (SA), low and high magnification (left and right, respectively). In the lower part, there are images corresponding to the internal section of the scaffold. Collagen III is stained in red, cytoskeleton in green, nuclei and silk fibroin scaffold are visible in blue. Scale bars for low magnification images (left column of each panel) = 1000 µm. Scale bars for high magnification images (right column of each panel) = 100 µm.

As a general overview, in both figures it is possible to observe that the number of cells increased, meaning that from day 14 to day 28, AdMSCs grew and proliferated on and inside the scaffold, in both cell culture conditions. This result may indicate an increase in the cell metabolic activity, which can be supported from the data in Graph 4, where is noticeable the increase in metabolic activity at day 28 in static and in perfusion conditions.
As shown in Figure 27, collagen I deposition was mainly visible at high magnification images, indicating a signal hidden by the strong cytoskeleton fluorescence. On the other hand, collagen III was highly expressed, visible with a strong signal even at low magnification, in Figure 28.
Moreover, as it happened at day 14, it seems that cell penetration inside the scaffold increased, enough to colonize the entire inner structure. Qualitatively, from image 28, it seems that cell penetration is slightly more evident in perfusion condition than in the static one, as well as the amount of cells. These results may indicate that the perfusion condition enhanced the nutrients supply inside the scaffold, promoting cell proliferation even after 28 days of culture. Additionally, these observations reflect the gene expression data (Graph 5) where is clearly evident that the collagens protein level follows the same trend, especially the one of collagen III, supported by its upregulated gene level at day 28, in perfusion condition.

4.3.5. Functionalization of multicomponent silk fibroin scaffold

4.3.5.1. Heparin binding efficiency and release

Heparin is a polysaccharide that has been exploited for its incorporation into biomaterials, mainly for drug delivery systems. Its structure is prone to chemical modifications but also can easily bind growth factors [100,110]. Heparin was incorporated in the multicomponent scaffold with the strategy to release low doses of growth factor during time, following the methodology investigated in chapter 3, where the carbodiimide chemistry applied by EDC/NHS crosslinkers, was able to provide a covalent binding between the primary amines of silk fibroin and the carboxylic groups of heparin. The percentage of heparin binding efficiency on the heparin-crosslinked multicomponent scaffold after functionalization was 35,6 ± 0,6% (corresponding to 10,6 ± 0,2 mg heparin/scaffold).

Since the purpose was to adopt heparin as a delivery system, it was important to measure heparin release in ddH_2O during the estimated time of cell culture (over a period of 28 days).

The heparin release in ddH_2O was expressed as a percentage respect to the amount of bound heparin after functionalization (before washing) and it is shown in Graph 6.

During the first 24h the heparin released reached a value of 22%, however, in the following time points the rate of the release steadily decreased in a range of 25-32% from day 3 until day 28. Since the faster release of heparin happened in the first three days of analysis, the scaffolds used for the incorporation of growth factors, were washed for 3 days in water to remove the unbound heparin [93]. Indeed, after 3 days of washing, the amount of heparin remaining bound to the scaffold was about ~32%.

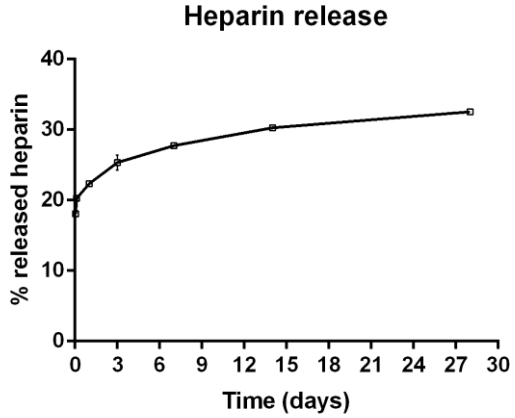

Graph 6: curve of heparin release of crosslinked multicomponent scaffolds. The graph shows the cumulative release of heparin along 28 days in relation to the effective amount of heparin loaded (29,8 ± 0,2 mg/ml). The values are represented as mean with SD (n = 4).

As already experienced in the chapter 3, the efficiency of heparin binding did not result in a high percentage, probably due to the low availability of the primary amines in the silk fibroin scaffold

[70]. However, the heparin efficiency and release can depend on the structure and the composition of the scaffold. In fact, the diffusion of initial heparin solution can be influenced by the porosity of the scaffold, and consequently with the presence of the yarns.

4.3.5.2. TGF-β2 incorporation to the multicomponent silk fibroin scaffold

Growth factors play a key role in the process of tissue engineering, since they are bioactive molecules that can influence cell behaviour. Heparin has the ability to bind a broad range of growth factor, in particular, is know that it can create strong interactions with TGF-β family, which is involved in the musculoskeletal development [100].

TGF-β2 was incorporated into the multicomponent heparin-crossliked scaffold to observe the effect on AdMSCs culture. The binding efficiency of TGF-β2 to the heparin crosslinked on the scaffold, is based on the electrostatic interactions between the negative charges of the polysaccharide and the positive charges of the GF. The scaffold showed high incorporation efficiency, as 80% compared to the initial amount loaded. To observe the possible effect of TGF-β2 during the cell culture over a period of 28 days, a release curve was performed (Graph 7).

It is possible to observe from that in the first 24 h the release reached only 6%. From day 3 to day 14, an 8% of GF is released, but from day 14 to 28 the release seemed to be quite stable, maintained among 14-16%. These results suggested that the growth factor firmly bound the heparin incorporated into the scaffold [100].

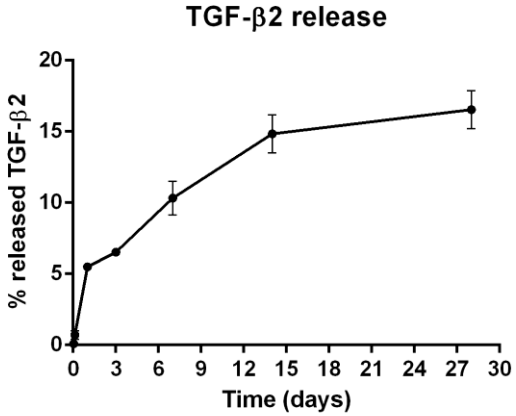

Graph 7: curve of TGF-β2 growth factor release along 28 days of multicomponent scaffold crosslinked with heparin in relation to the total amount of growth factor loaded. The values are represented as mean with SD (n = 4).

4.3.6. Biological characterizations of functionalized multicomponent scaffold

The same biological characterizations performed on the multicomponent scaffold in the first part of the "Results" paragraph are repeated on the functionalized multicomponent

scaffold to study and observe the effect of the TGF-β2 growth factor on AdMSCs culture, with the contribution of the perfusion stimulation on the topographical cues of the model scaffold.

4.3.6.1. Cell metabolic activity

The metabolic activity was measured by Resazurin assay, to examine the influence of TGF-β2 functionalized scaffold on the cell activity in the two type of culture conditions (Graph 8).
As a general overview, the AdMSCs metabolic activity increased from day 14 to day 28. In detail, the metabolic activity of AdMSCs at day 14 resulted comparable in both of static and perfusion conditions, while at day 28 the perfusion condition showed higher values than in the static one, but not in a significant way.
In particular, the metabolic activity at day 28 in perfusion condition is significantly higher compared to day 14. This result could indicate that the flow produced by the bioreactor combined with the effect of the growth factor stimulate the cell activity.

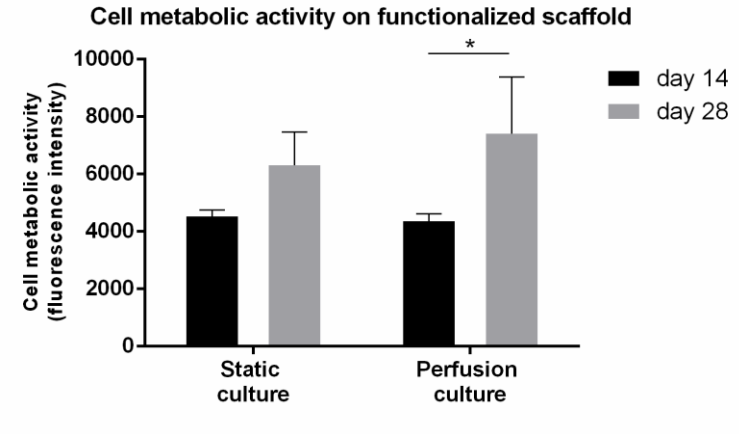

Graph 8: metabolic activity of cells cultured on the functionalized scaffolds in static and in perfusion conditions, measured after 14 and 28 days. Values expressed resazurin fluorescence intensity. The values are represented as mean with SD (n = 4). (*) indicates statistically significant difference at $p < 0.1$.

4.3.6.2. Gene expression analysis

To investigate the possible effect of TGF-β2 in addition to the perfusion stimulation of the bioreactor, on the expression related to tendon/ligament markers, genes of (collagen I (col I), collagen III (col III), scleraxis (scx), SRY box9 (sox9), and Tenomodulin (TND)) were analysed up to 4 weeks of culture on samples in static and in perfusion conditions. Gene expression data were expressed as fold change respect to the housekeeper gene, β-tubulin (Graph 9).

In both time points and in both cell culture conditions, TND expression was downregulated, more at day 28 than at day 14.

Similar situation was for the expression of sox9 that showed a general downregulation, mainly at day 14 in static condition.

The expression of collagen I was slightly upregulated in both culture conditions. In static cell culture condition, the expression of collagen I at day 28 was slightly more upregulated than the one at 14 days, and it was significantly higher compared to the expression of TND and sox9. At the contrary, the expression in perfusion condition is more than 2-fold upregulated at day 14, with a slight decrease at day 28.

Collagen III expression reached 2 and 3-fold upregulation respectively at day 14 and 28 in static condition. The value at day 14 showed a slight significance in the upregulation compared to the expression of scx at day 14. The expression at day 28, instead, is significantly higher among the expressions of scx, sox9 and TND.

The expression of collagen III in perfusion condition, at day 28 was almost 5-fold upregulated, in fact, it is slightly higher compared to the expression of col III at day 14, but is significantly higher compared to the expression of all the other genes.

Scx expression was slightly upregulated in static condition at day 28, while in perfusion condition, following the same tendency of collagen III, it was 3-fold upregulated at day 14 and almost 6-fold upregulated at day 28.

As a general overview, it is possible to assess that the static cell culture, besides the GF incorporation and without mechanical stimulation, did not show a relevant upregulation in the gene expression related to tendon/ligament markers, as expected. On the other hand, the perfusion cell culture condition improved in a significant way the expression of genes related to tendon/ligament differentiation. Worthy of attention is the expression of scleraxis, a marker involved in tendon/ligament tissue development, that showed significant upregulation in perfusion condition, especially at day 28. Its expression could be enhanced thanks to effect of TGF-β2 combined with the perfusion stimulation.

The downregulated expression of Sox9 indicates that there is a very poor chondrogenic response of AdMSCs on the scaffold, in static and in perfusion condition. Moreover, TND is a specific marker of tendon and ligament lineage, and recently it has been discovered that its expression is upregulated by scleraxis [152]. Therefore, with higher gene expression values of scx, it could be expected an upregulation of TND expression.

Notably to say that, collagen I and collagen III expressions were significantly upregulated in both cell culture conditions. Especially collagen III in perfusion condition showed upregulated expression (~5-fold) at day 28.

The results of gene expression analysis may indicate that AdMSCs stimulated in perfusion condition with the influence of TGF-β2 were induced to produce ECM structural molecules, like collagen III, and toward a differentiation lineage.

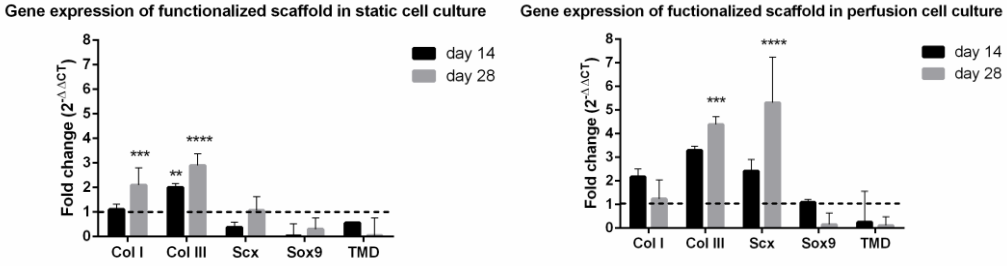

Graph 9: gene expression analysis of AdMSCs cultured on functionalized multicomponent scaffolds up to 28 days, influenced by different cell culture conditions. Target genes are collagen I (col I), collagen III (col III), scleraxis (scx), SRY-box9 (sox9), and tenomodulin (TND). Housekeeper gene is β Tubulin. The fold change was calculated normalizing the target gene expression to the housekeeper gene. Statistical significance is indicated with asterisks. **p < 0.01, ***p < 0.001, ****p < 0.0001.

4.3.6.3. Immunofluorescence evaluation of collagen deposition

Immunofluorescence images were taken after 14 and 28 days to analyse the actin cytoskeleton organization, the cell distribution, migration and the presence of collagen I and III, to investigate if the two types of cell culture conditions induced different effects

on the AdMSCs culture on the functionalized multicomponent scaffolds.

Figure 29, 30, 31 and 32 show immunofluorescence staining of collagens type I and III. Collagen molecules are stained in red, the scaffold matrix in blue and the actin cytoskeleton in green. The left part of each panels shows low magnification images of the seeding area (top) and the whole internal section of the scaffold (bottom). The right part of the panels shows high magnification images, where more details can be appreciated.

In general, confocal images showed that cells adhered on the seeding area (SA), covering quite homogenously all the SA surfaces in both cell culture conditions (static and perfusion), and at both time points (day 14 and day 28). Cells adhered on the sponge lamellae and also among the fibrils composing the yarns, not only in the SA but also in the internal section of the scaffold, where it is possible to appreciate AdMSCs migration (Figure 29, 30, 31, 32).

[Note: the black crack that is visible in the middle of each SA picture is due to the cut that is done before the staining to allow it to penetrate inside the scaffold; not all the internal section images show the same homogeneous cell distribution since the acquisition depends on how was done the cut of the scaffold to allow staining penetration].

Figure 29 and 30 show collagen I and collagen III deposition (respectively) in static and in perfusion cell culture conditions at day 14.

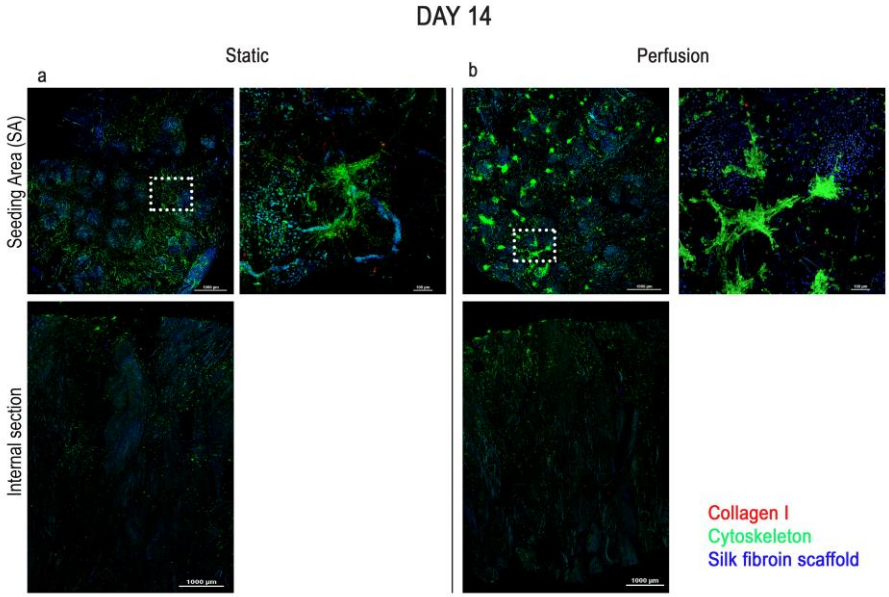

Figure 29: confocal images of functionalized samples cultured in static **a**), and in perfusion **b**) conditions for 14 days. In the upper part of each panel, there are showing the seeding area (SA), low and high magnification (left and right, respectively). In the lower part, there are images corresponding to the internal section of the scaffold. Collagen I is stained in red, cytoskeleton in green, nuclei and silk fibroin scaffold are visible in blue. Scale bars for low magnification images (left column of each panel) = 1000 µm. Scale bars for high magnification images (right column of each panel) = 100 µm.

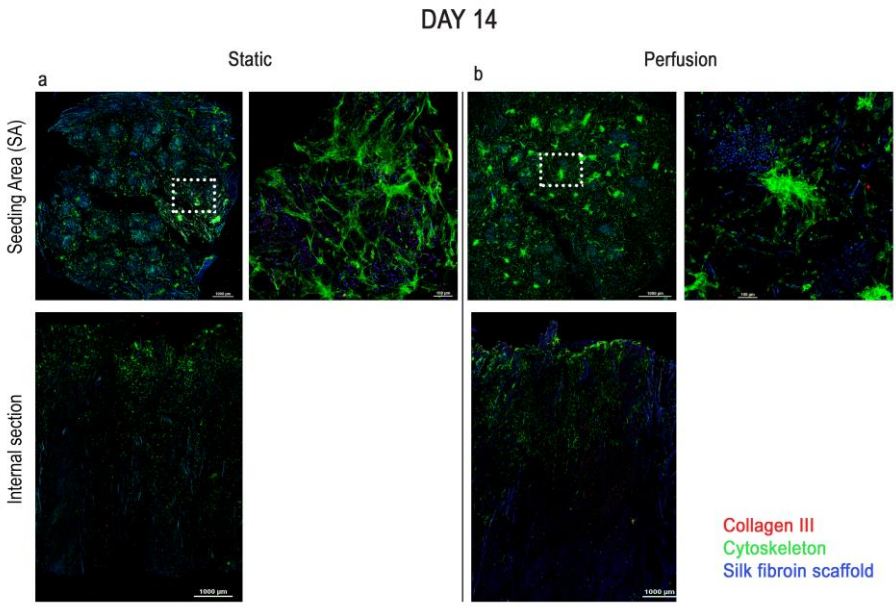

Figure 30: confocal images of functionalized samples cultured in static **a**), and in perfusion **b**) conditions for 14 days. In the upper part of each panel, there are showing the seeding area (SA), low and high magnification (left and right, respectively). In the lower part, there are images corresponding to the internal section of the scaffold. Collagen III is stained in red, cytoskeleton in green, nuclei and silk fibroin scaffold are visible in blue. Scale bars for low magnification images (left column of each panel) = 1000 µm. Scale bars for high magnification images (right column of each panel) = 100 µm.

At first sight, the SA cells adhered on the sponge lamellae and among the fibrils of the yarns, without reaching the confluence. Indeed, in perfusion condition, some clusters of cells were visible

on the SA and the internal section images showed a slight cells penetration, occupying half of the entire section.

Collagen I and collagen III signals were quite hidden by the cytoskeleton ones in both cell culture conditions, in fact collagens were better visible in the high magnification images. From a qualitative point of view, it seems that in static condition, collagen III was slightly more visible than collagen I. This result reflects the qPCR values, in which the gene expression of Col III is slightly higher than the expression of Col I at day 14 in static condition. In perfusion condition, on the other hand, the gene expression followed the same trend even if collagens protein level signals were not so visible probably because covered by the cytoskeleton signal.

Figure 31 and 32 show the content of collagen I and III (respectively) after 28 days of culture in static and in perfusion conditions.

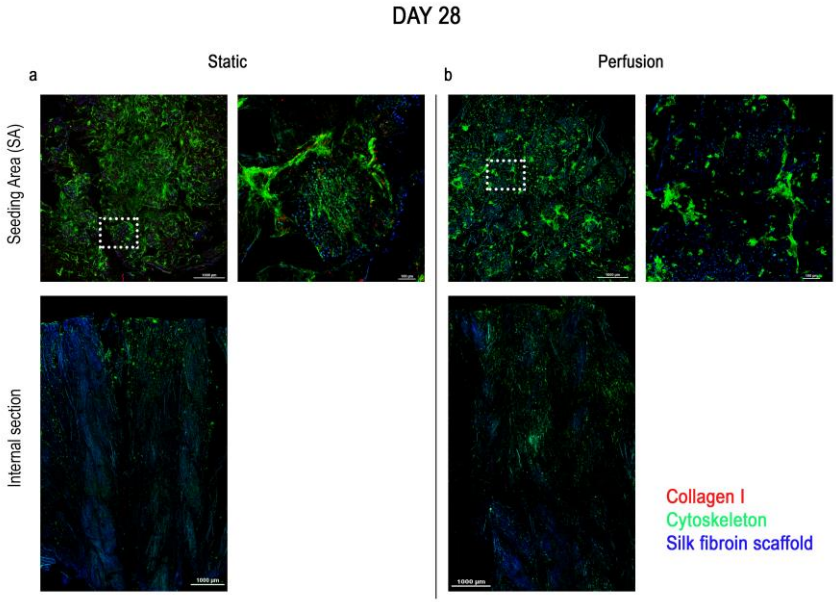

Figure 31: confocal images of functionalized samples cultured in static **a**), and in perfusion **b**) conditions for 28 days. In the upper part of each panel, there are showing the seeding area (SA), low and high magnification (left and right, respectively). In the lower part, there are images corresponding to the internal section of the scaffold. Collagen I is stained in red, cytoskeleton in green, nuclei and silk fibroin scaffold are visible in blue. Scale bars for low magnification images (left column of each panel) = 1000 µm. Scale bars for high magnification images (right column of each panel) = 100 µm.

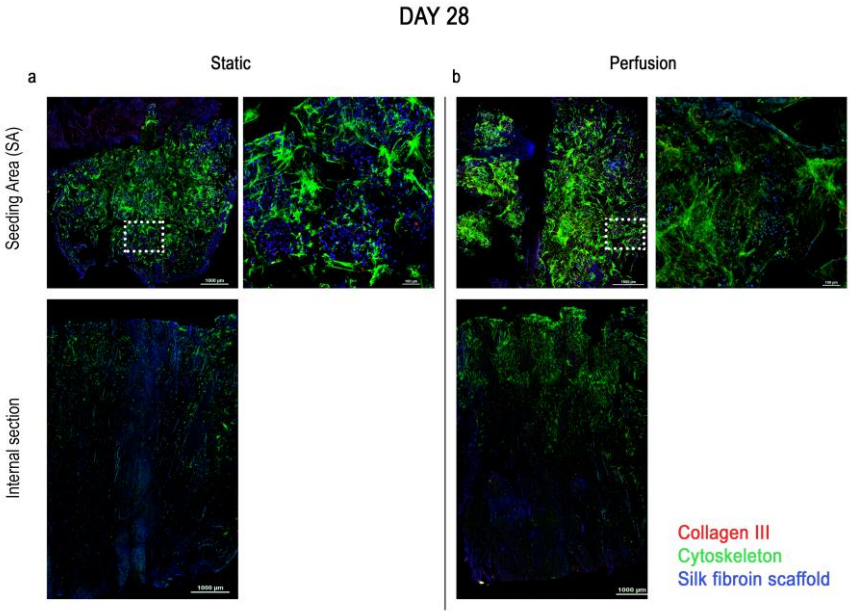

Figure 32: confocal images of functionalized samples cultured in static **a**), and in perfusion **b**) conditions for 28 days. In the upper part of each panel, there are showing the seeding area (SA), low and high magnification (left and right, respectively). In the lower part, there are images corresponding to the internal section of the scaffold. Collagen III is stained in red, cytoskeleton in green, nuclei and silk fibroin scaffold are visible in blue. Scale bars for low magnification images (left column of each panel) = 1000 µm. Scale bars for high magnification images (right column of each panel) = 100 µm.

As a general overview, in both figures it is possible to observe that the number of cells slightly increased, from day 14 to day 28, showing a slight AdMSCs proliferation. Also cell penetration along the scaffold slightly increased compared to the results

obtained after 14 days, even if the number of cells is not enough to completely populate the entire structure.

Figure 31 showed collagen I deposition, mainly visible at high magnification images, indicating a low expression or a signal hidden by the strong cytoskeleton fluorescence. The signal of collagen I seemed to be higher in static condition than the perfusion one, results that can be supported by the gene expression values shown in graph 9, where the amount of col I expressed is higher in static condition than the perfusion one, but not in a significant way. On the other hand, opposite situation is verified for collagen III deposition (Figure 32) that seemed more present in the perfusion condition, observing the high magnification images. Also in this case it is possible to compare the protein level with the gene level shown in the qPCR graph, where at day 28 the expression is significantly upregulated in the perfusion condition compared to the static one.

As a general comment, these results may indicate that the perfusion condition enhanced the cell migration through the structure of the scaffold. However, considering the results obtained from the gene expression values, it can be that the incorporation of the growth factor into the scaffold combined with the structural cues and the perfusion stimulation induced cell differentiation. This could be the reason why cells did not extensively proliferate in the scaffold structure, showing also no

significant differences in the metabolic activity (Graph 8), since they could be triggered toward tendon/ligament differentiation.

In Figure 33, is visible a representative image of the external area of the scaffold not functionalized and functionalized after 28 days of culture. In both static and perfusion conditions, there are no cells growing on the external part of the scaffold, they are all directed inwards. This means that, in both cases, the bioreactor chamber size, matching with the scaffold ones, did not give enough space for the cells to adhere and grow on the external area, but guided them across the construct. In particular, in the perfusion condition, the medium flow directs the cells through the entire scaffold, preventing the medium flow outside.

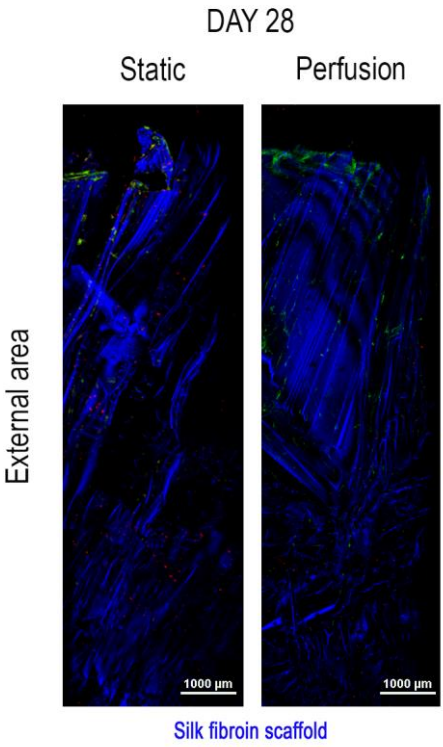

Figure 33 representative confocal images of samples not functionalized and functionalized, cultured in static and in perfusion conditions for 28 days. The images are showing the external area of the scaffold. Cell cytoskeleton is stained in green, nuclei and silk fibroin scaffold are visible in blue. Scale bars = 1000 µm.

4.3.5. In vivo study: evaluation of inflammatory response

One of the first events following the implantation of a biomaterial-scaffold is the interaction with inflammatory response and foreign-body reaction. The inflammatory process plays a crucial role in triggering the tissue regeneration procedure, starting with the exposure of the material to the body fluid and to the blood agents. This event activates numerous cell types, such as immune cells (including macrophages) able to induce the production of cytokines involved in the signalling pathways of the regenerative response [155,156]. Therefore, it is important to evaluate the impact of implanted scaffolds on inflammatory response in *in vivo* system, in particular nowadays subcutaneous implantation in small animals is indicative for forthcoming preclinical studies [157]. The histological analysis was performed on the retrieved scaffolds implanted in rats (Figure 34) at 2 and 4 weeks of implantation to observe the interaction between samples and tissue inflammatory response in *in vivo* study. The staining used were Hematoxylin and Eosin (H&E), where in a typical tissue, nuclei appeared blue, whereas the cytoplasm and the ECM have various degrees of pink staining, and ED-1 (or anti-CD68) that typically stains tissue macrophages, key players in the inflammation process, in brown.

Macrophages typically initiate the innate response of the immune system in their pro-inflammatory phenotype, called M1, which infiltrate and clean the wound from bacteria, foreign debris and dead cells. Then they polarized into the so called M2 phenotype, predominantly anti-inflammatory, which promote cell migration and proliferation to start the healing process [158].

Figure 35 shows the implanted scaffold surrounded by many cells. As a general overview, the brown staining of ED-1 is not particularly evident, but the H&E staining highlights cells, most probably inflammatory cells, mainly and homogeneously distributed around the implanted scaffold (S), at the interface with the tissue (T).

The images at 2 weeks post implant may indicate the stages of the innate immune response, where the macrophages are activated and led to the formation of granulation tissue [156]. Some giant cells are visible, indicating that the implanted scaffold caused a foreign body reaction. In the images after 4 weeks of implantation it is possible to observe the formation of later stages of granulation, that may have activated fibroblasts to produce a sort of thin fibrous capsule since there are cells more concentrated along the interface between the scaffold and the tissue, but also close to the baves composing the yarns (Figure 35). It seems that the multicomponent scaffolds were well tolerated by the host animal and induced the typical steps of an

innate immune response to an implanted material [158]. It is known that silk materials can cause a mild inflammatory response which should be reduced within few weeks after implantation. Similar behaviour of silk fibroin scaffold implanted *in vivo* was already found in literature, in which after 4 weeks silk fibroin did not elicit a strong inflammatory response [159]. Indeed, there are many variables that can influence a local inflammatory response (material structure, geometry, porosity, size, cell mobilization, etc.) [156,160,161], as well as the degradation rates, which mainly depend on the secondary structure of the protein and on the structure of the scaffold material. In fact, a porous scaffold is more prone to higher degradation rate, since cell infiltration (and macrophage recruitment) can easily occurred [162,163]. To evaluate more in detail the effect of the multicomponent scaffold implanted, longer time point analysis are needed to verify if the cell infiltration, visible in the images at 4 weeks, could lead either to integration in the host tissue or to the formation of fibrotic capsule.

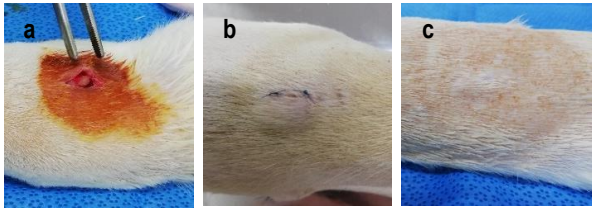

Figure 34: gross observation of wound healing after scaffold implantation under skin. a) skin just after the insertion of the samples under skin; b) wound healing after 10 days; c) skin almost recovered completely after 14 days.

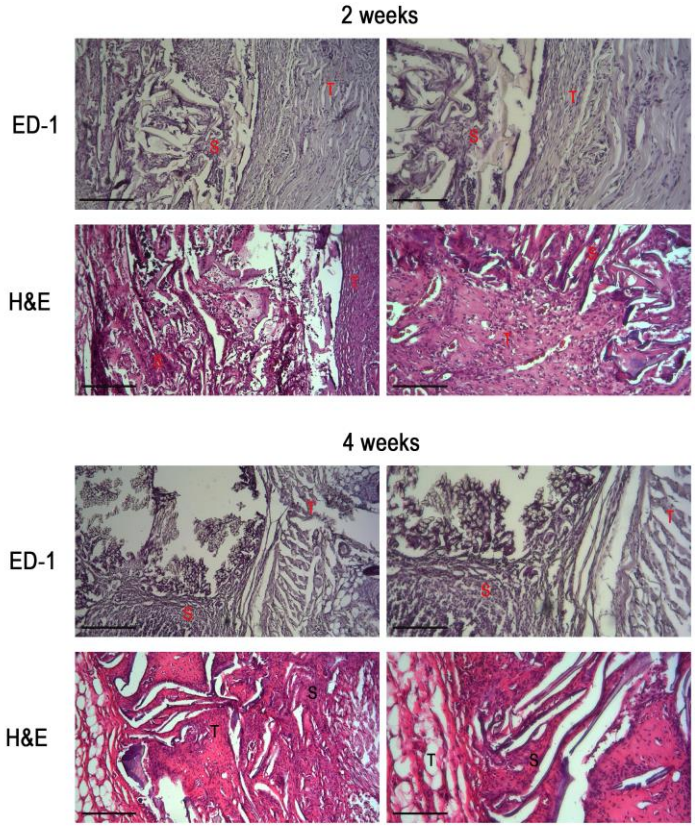

Figure 35: ED-1 and H&E staining of histological sections of scaffold implanted in vivo under skin for 2 and 4 weeks. '**S**' indicates scaffold, '**T**' indicates tissue. Scale bar = 300 µm.

4.4. Conclusions

Anterior cruciate ligament is one of the most injured ligaments in the knee [38]. Tissue engineering is trying to mimic its ECM to balance the mechanical properties and the biological performances of the native tissue. In this chapter, a multicomponent model scaffold was proposed, with the focus on the design, the fabrication and the biological role.

The importance of the matrix has been understood in recent works [61,83], where scaffolds for ligament regeneration made only of fibers, failed in promoting the tissue regeneration for the lack of void volume to let the cell ingrowth. For these reasons, we decided to combine the anisotropic silk fibroin sponge obtained in the previous chapter (chapter III), in combination with the insertion of native silk fibroin yarns, to obtain a model scaffold able to give the proper mechanical support but also to allow cell penetration for tissue regeneration. The material used was already shown in the previous chapter to be effective [61,70,83]. Tensile mechanical properties of silk fibroin yarns in dry and wet conditions were assessed to define the number of yarns needed to reach the adequate mechanical requirements that a model scaffold should have. The reported results, demonstrated that the multicomponent scaffold incorporation of 27 silk fibroin yarns can reach the mechanical properties of the native ACL (stiffness

and load at break) without offering enough void volume for the cell ingrowth. We decided to insert 12 yarns, able to ensure the double strength of a model scaffold during a normal daily rehabilitation activity after surgery [31] to overcome unexpected yarn failure. Despite the stiffness of the model scaffold is proportional to the number of yarns, using yarns with a lower twisting degree, an isostiff scaffold can be obtained. Moreover, the combination of silk fibroin yarns and lamellar sponge with elongated pores, could mimic the alignment of collagen molecules and the structure of the ECM resembling the native ligament tissue. In fact, the structural cues of the scaffold were able to induce cell alignment and distribution, following the directionality of the pores [93,125], but also cell migration and penetration, inducing the process of regeneration to start.

The use of the homemade bioreactor improved the cell culture medium perfusion, enhancing the nutrients supply inside and along the multicomponent scaffold [138], promoting cell proliferation and triggering the synthesis of ECM, mostly with the production of collagen III, after 28 days of culture.

However, the perfusion stimulation combined with the structural cues of the scaffold was not able to induce cell differentiation according to the results obtained from the gene expression analysis (Graph 5), meaning that the only mechanical stimuli were not enough to induce cell differentiation. For this reason,

we decided to improve our multicomponent model scaffold with the functionalization approach investigated in chapter 3 and in the work done in collaboration with prof. Van Griensven and colleagues [93]. The idea was to improve the bioactivity of the scaffold playing on the synergistic effect of a biomimetic scaffold, stem cells and heparin-based delivery of growth factor. Heparin was investigated for its versatility on functionalize a biomaterial scaffold and its affinity in binding growth factors [100], that allowed to create a low doses release system of growth factor over a period of 28 days of cell culture. The TGF-β2 growth factor, involved in the tendon/ligament development, was incorporated with high efficiency on the multicomponent silk fibroin scaffold. Its effect combined with the scaffold structure and porosity, in addition to the perfusion bioreactor stimulation, was able to lead AdMSCs through a differentiation lineage. In fact, the low amount of cells observed at the immunofluorescence images, could indicate that the AdMSCs did not show proliferation since they were intent on differentiating [164], considerations supported by the gene expression results (Graph 9).

Observing the biological characterization results obtained in this chapter, it is clearly evident that the combination of TGF-β2 with the multicomponent model scaffold and the perfusion stimulation, induced the upregulation of tendon/ligament

markers as well as the production of ECM components (collagens).

In addition, the histological evaluation of the *in vivo* inflammatory response revealed that the multicomponent scaffold implanted under skin resulted in a mild inflammatory response, supporting the competence of the silk based-scaffold [165] and inducing the formation of a granulation tissue.

Finally, this work gave a preliminary result based on a multicomponent scaffold functionalized and not functionalized with optimized structural, biological and biomechanical properties for ACL regeneration. It would be interesting to evaluate the effects of more cells seeded on the functionalized multicomponent scaffold, to evaluate the potential of completely populate the scaffold with differentiating AdMSCs thanks to the perfusion stimulation and the GF contribution.

Chapter V. Final remarks and future perspectives

This research work focused on the ligament tissue, with particular attention on the anterior cruciate ligament (ACL), one of the most injured ligaments in the knee [38]. The entire structure of ACL has remarkable structural properties, notably also considering the insertion site ligament-to-bone, a specialized tissue called enthesis [5]. Tissue Engineering (TE) is trying to discover the proper material and its functionalities to mimic the extracellular matrix (ECM) of this complex tissue, to combine the mechanical properties and biological characteristics of the native tissue. The material used in this work is silk fibroin. It has been widely demonstrated that this natural polymer is an effective and a good candidate for TE, since it is biocompatible, biodegradable and with interesting mechanical properties [70].

The first part of this thesis focuses on the enthesis regeneration. The results provided new insights on the effects of the combination of the topographical structure of the biphasic scaffold with biochemical cues provided by growth factors effect. In fact, the synergistic interactions between the scaffold heparin-functionalized able to increase growth factors affinity (TGF-β2 and GDF5) and the porosity gradient composing the construct, have induced stem cell differentiation (AdMSCs) through the

desired phenotypes typical of the transition region ligament-to-bone tissue [93].

The second part of the thesis focuses on the regeneration of the central ligament part. The results demonstrated that the insertion of native silk fibroin yarns leads to the fabrication of a multicomponent model scaffold with adequate mechanical requirements needed during a possible rehabilitation activity after surgery [31]. In addition, the role of the anisotropic fibroin sponge around the yarns resulted fundamental to provide void volume for cell ingrowth to start the regeneration process. The use of a homemade bioreactor was implemented to improve the cell culture medium perfusion through the model scaffold [138], in addition to the incorporation of TGF-β2 growth factor, able to induce cell migration and differentiation through a ligamentous lineage and promote synthesis of ECM molecules, thanks to the synergistic effect of mechanical and biochemical stimuli. The *in vivo* implantation of the scaffold showed a mild inflammatory, sustaining the competence of the silk based-scaffold [165].

Usually, the idea to fabricate a model scaffold for ligament tissue, rarely focuses the attention on its whole complex structure, considering also the insertion site to the bone tissue. For this reason, it was decided to dedicate attention on the insertion site, the enthesis, responsible for the integration of ligament-to-bone tissue, and to the central ligament part, which being at the center,

needs to support the mechanical requirements and promote tissue regeneration.

It would be interesting to evaluate the incorporation of the two structures investigated in chapter 3 and 4. Combining the multicomponent silk fibroin scaffold able to provide mechanical support with the yarns, with the porosity gradient resembling the insertion site of the ligament in to the bone. This complex structure could be able to offer the mechanical requirements and the void volume necessary to start the regeneration process, and in addition with the heparin functionalization able to retain low doses of GF and to induce AdMSCs differentiation, could lead to a full ACL model scaffold.

As a possible further future suggestion, it may be interesting to combine the mechanical-improved structure of the scaffold as a central ligament part with a recent method used to produce solid fibroin to improve the ligament-to-bone interphase. This new method corresponds to a low temperature sintering procedure based on a thermal-reflow to produce in fast-fashion monoliths of solid fibroin [166]. During the process, the solid sintered (at low temperature) fibroin can take the shape of the mold in which it is compressed, besides having demonstrated interesting mechanical properties and the ability to induce cell adhesion and proliferation [166]. For these reasons, monoliths of solid fibroin may

be modified with a proper mold to obtain a screw shape, that can act as an insertion site for a possible surgical implant, providing a new surgical treatment for ligament tissue regeneration.

List of Abbreviations and Acronyms

µCT: micro-Computed Tomography

ABC: Activated Biological Composite

ACL: Anterior Cruciate Ligament

AdMSCs: Adipose tissue-derived Mesenchymal Stem Cells

AEC:3-amino-9-ethylcarbazole

AM: Anterior-Medial

ANOVA: Analysis Of Variance

BMP: Bone Morphogenetic Protein

BPTB: Bone-Patellar Tendon-Bone

BSA: Bovine Serum Albumin

CCBR: Concentric Cylinder Bioreactor

Col: Collagen

D: Denier

DAPI: 4'6-diamidino-2-phenylindole

DI: Deionized

DMEM: Dulbecco's Modified Eagle Medium

DNA: Deoxyribonucleic Acid

ECM: Extracellular Matrix

ED-1: CD68 antibody

EDC:1-ethyl-3-(3dimethylaminopropyl) carbodiimide hydrochloride

En: Endotenon

Ep: Epitenon

EtOH: Ethanol

FBS: Fetal Bovine Serum

FCS: Fetal Calf Serum

FE-SEM: Field Emission-Scanning Electron Microscopy

GAG: Glycosaminoglycan

GDF5: Growth/differentiation factor 5

GFs: Growth Factors

H&E: Hematoxylin and Eosin

HA: Hyaluronic Acid

HA: Hydroxyapatite

HT: Hamstring Tendons

LAD: Ligament Augmentation Device

LARS: Ligament Advanced Reinforcement System

MeOH: Methanol

MES: (N-morpholino) ethanesulfonic acid

MF: Mineralized Fibrocartilage

MSCs: Mesenchymal Stem Cells

Na2CO3: Sodium Carbonate

NaCl: Sodium Chloride

NHS: N-hydroxysuccinimide

P/S: Penicillin/Streptomycin

PBS: Phosphate Saline Buffer

PCL: Polycaprolactone

PDS: Polydioxanone

PEG: Polyethylene Glycol

PGA: Polyglycolic Acid

PHB: Poly(3-hydroxybutyrate) (PHB),

PHBV: Poly(3-hydroxybutyrate-co-3-hydroxyvalerate)

PHUE-O3: Poly(3-hydroxyundecenoate)

PL: Posterior-Lateral

PLLA: Poly-L-lactic Acid

PP: Polypropylene

Pt/Pd: Platinum/Palladium

PT: Patellar-Tendon

PUUR: Poly(urethane urea)

qPCR: Quantitative Polymerase Chain Reaction

RGD: Arginine-Glycine-Aspartate

RSB: Rotating-Shaft Bioreactor

RT: Room Temperature

RWPV: Rotating Wall Perfusion Vessel Bioreactor

RWV: Rotating Wall Vessel

SA: Seeding Area

Scx: Scleraxis

SEM: Scanning Electron Microscopy

SF: Silk Fibroin

Sf: Subfascicular units

Sox9: SRY(Sex determing region)-box 9

TE: Tissue Engineering

TERM: Tissue Engineering and Regenerative Medicine

TGF-β2: Transforming Growth Factor-β2

TND: Tenomodulin

UF: Unmineralized Fibrocartilage

Chapter VI. Bibliography

1. Paschos NK, Howell SM. Anterior cruciate ligament reconstruction: Principles of treatment. *EFORT Open Rev*. 2016;1(11):398-408. doi:10.1302/2058-5241.1.160032
2. Leong NL, Petrigliano FA, McAllister DR. Current tissue engineering strategies in anterior cruciate ligament reconstruction. *J Biomed Mater Res - Part A*. 2014;102(5):1614-1624. doi:10.1002/jbm.a.34820
3. Takayama K, Kuroda R. Biological Augmentation of Anterior Cruciate Ligament Grafts. *Oper Tech Orthop*. 2017;27(1):33-37. doi:10.1053/j.oto.2017.01.007
4. Mahapatra P, Horriat S, Anand BS. Anterior cruciate ligament repair – past, present and future. *J Exp Orthop*. 2018;5(1). doi:10.1186/s40634-018-0136-6
5. Duthon VB, Barea C, Abrassart S, Fasel JH, Fritschy D, Ménétrey J. Anatomy of the anterior cruciate ligament. *Knee Surgery, Sport Traumatol Arthrosc*. 2006;14(3):204-213. doi:10.1007/s00167-005-0679-9
6. Wang JH-C. Mechanobiology of tendon. *J Biomech*. 2006;39(9):1563-1582. doi:10.1016/j.jbiomech.2005.05.011
7. Zantop T, Petersen W, Fu FH. Anatomy of the anterior

cruciate ligament. *Oper Tech Orthop*. 2005;15(1):20-28. doi:10.1053/j.oto.2004.11.011

8. Danylchuk KD, Finlay JB, Krcek JP. Microstructural organization of human and bovine cruciate ligaments. *Clin Orthop Relat Res*. 1978;NO.131:294-298. doi:10.1097/00003086-197803000-00048
9. Frank CB. Ligament structure and physiology. *J Musculoskelet Neuronal Interact*. 2004;4(2):199.
10. Strocchi R, de Pasquale V, Gubellini P, et al. The human anterior cruciate ligament: histological and ultrastructural observations. *J Anat*. 1992;180 (Pt 3:515-519. http://www.ncbi.nlm.nih.gov/pubmed/1487443%0Ahttp://www.pubmedcentral.nih.gov/articlerender.fcgi?artid=PMC1259652.
11. Bagnaninchi P, Yang Y, Haj AJ El, Maffulli N. Tissue engineering for tendon repair. *Br J Sport Med*. 2007;41. doi:10.1136/bjsm.2006.030643
12. Spiesz EM, Thorpe CT, Thurner PJ, Screen HRC. Structure and collagen crimp patterns of functionally distinct equine tendons, revealed by quantitative polarised light microscopy (qPLM). *Acta Biomater*. 2018;70:281-292. doi:10.1016/j.actbio.2018.01.034
13. Jamil T, Ansari U, Najabat Ali M, Mir M. A Review on Biomechanical and Treatment Aspects Associated with

Anterior Cruciate Ligament. *Irbm*. 2017;38(1):13-25. doi:10.1016/j.irbm.2016.10.002

14. Kuo CK, Marturano JE, Tuan RS. Novel strategies in tendon and ligament tissue engineering: Advanced biomaterials and regeneration motifs. *Sports Med Arthrosc Rehabil Ther Technol*. 2010;2:20. doi:10.1186/1758-2555-2-20
15. Laurencin CT, Freeman JW. Ligament tissue engineering: An evolutionary materials science approach. *Biomaterials*. 2005;26(36):7530-7536. doi:10.1016/j.biomaterials.2005.05.073
16. Zhao L, Thambyah A, Broom N. Crimp morphology in the ovine anterior cruciate ligament. *J Anat*. 2015;226(3):278-288. doi:10.1111/joa.12276
17. Diamant J, Keller A, Baer E, Litt M, Arridge RG. Collagen; ultrastructure and its relation to mechanical properties as a function of ageing. *Proc R Soc London Ser B Biol Sci*. 1972;180(60):293-315. doi:10.1098/rspb.1972.0019
18. Vunjak-Novakovic G, Altman G, Horan R, Kaplan DL. Tissue Engineering of Ligaments. *Annu Rev Biomed Eng*. 2004;6(1):131-156. doi:10.1146/annurev.bioeng.6.040803.140037
19. Kastelic J, Palley I, Baer E. A STRUCTURAL MECHANICAL MODEL FOR TENDON CRIMPING *. *J*

Biomech. 1980;13:887-893.

20. Kastelic J, Galeski A, Baer E. The multicomposite structure of tendon. *Connect Tissue Res*. 1978;6(1):11-23. doi:10.3109/03008207809152283
21. Font Tellado S, Balmayor ER, Van Griensven M. Strategies to engineer tendon/ligament-to-bone interface: Biomaterials, cells and growth factors. *Adv Drug Deliv Rev*. 2015;94:126-140. doi:10.1016/j.addr.2015.03.004
22. Yang PJ, Temenoff JS. Engineering orthopedic tissue interfaces. *Tissue Eng - Part B*. 2009;15(2):127-141. doi:10.1089/ten.teb.2008.0371
23. Benjamin M, Kumai T, Milz S, Boszczyk BM, Boszczyk AA, Ralphs JR. The skeletal attachment of tendons - Tendon "entheses." *Comp Biochem Physiol - A Mol Integr Physiol*. 2002;133(4):931-945. doi:10.1016/S1095-6433(02)00138-1
24. Lu HH, Thomopoulos S. Functional attachment of soft tissues to bone: development, healing, and tissue engineering. *Annu Rev Biomed Eng*. 2013;15:201-226. doi:10.1146/annurev-bioeng-071910-124656
25. Font Tellado S, Bonani W, Balmayor ER, et al. *Fabrication and Characterization of Biphasic Silk Fibroin Scaffolds for Tendon/Ligament-to-Bone Tissue*

Engineering.; 2017. doi:10.1089/ten.tea.2016.0460

26. Resnick D, Niwayama G. Entheses and enthesopathy. Anatomical, pathological, and radiological correlation. *Radiology*. 1983;146(1):1-9. doi:10.1016/B978-0-7216-0081-9.50014-5

27. Moffat KL, Sun WHS, Pena PE, et al. Characterization of the structure-function relationship at the ligament-to-bone interface. *Proc Natl Acad Sci U S A*. 2008;105(23):7947-7952. doi:10.1073/pnas.0712150105

28. Genin GM, Kent A, Birman V, et al. Functional grading of mineral and collagen in the attachment of tendon to bone. *Biophys J*. 2009;97(4):976-985. doi:10.1016/j.bpj.2009.05.043

29. Woo SL-Y, Hollis JM, Adams DJ, Lyon RM, Takai S. Tensile properties of the human femur- anterior cruciate ligament-tibia complex The effects of specimen age and orientation. *Am J Sports Med*. 1991;19(3):217-225.

30. Schmidt EC, Chin M, Aoyama JT, Ganley TJ, Shea KG, Hast MW. Mechanical and Microstructural Properties of Pediatric Anterior Cruciate Ligaments and Autograft Tendons Used for Reconstruction. *Orthop J Sport Med*. 2019;7(1):1-12. doi:10.1177/2325967118821667

31. Dargel J, Gotter M, Mader K, Pennig D, Koebke J,

Schmidt-Wiethoff R. Biomechanics of the anterior cruciate ligament and implications for surgical reconstruction. *Strateg Trauma Limb Reconstr*. 2007;2(1):1-12. doi:10.1007/s11751-007-0016-6

32. Zantop T, Petersen W, Sekiya JK, Musahl V, Fu FH. Anterior cruciate ligament anatomy and function relating to anatomical reconstruction. *Knee Surgery, Sport Traumatol Arthrosc*. 2006;14(10):982-992. doi:10.1007/s00167-006-0076-z
33. Shaerf DA, Pastides PS, Sarraf KM, Willis-Owen CA. Anterior cruciate ligament reconstruction best practice: A review of graft choice. *World J Orthop*. 2014;5(1):23-29. doi:10.5312/wjo.v5.i1.23
34. Marrale J, Morrissey MC, Haddad FS. A literature review of autograft and allograft anterior cruciate ligament reconstruction. *Knee Surgery, Sport Traumatol Arthrosc*. 2007;15(6):690-704. doi:10.1007/s00167-006-0236-1
35. Sharp JW, Kani KK, Gee A, Mulcahy H, Chew FS, Porrino J. Anterior cruciate ligament fixation devices: Expected imaging appearance and common complications. *Eur J Radiol*. 2018;99(September 2017):17-27. doi:10.1016/j.ejrad.2017.12.006
36. Beasley LS, Weiland DE, Vidal AF, et al. Anterior cruciate ligament reconstruction: A literature review of the

anatomy, biomechanics, surgical considerations, and clinical outcomes. *Oper Tech Orthop*. 2005;15(1):5-19. doi:10.1053/j.oto.2004.11.003

37. Mohtadi NG, Chan DS, Dainty KN, Whelan DB. Patellar tendon versus hamstring autograft for anterior cruciate ligament rupture in adults. *Cochrane Database Syst Rev*. 2006;(9). doi:10.1002/14651858.cd005960
38. Satora W, Królikowska A, Czamara A, Reichert P. Synthetic grafts in the treatment of ruptured anterior cruciate ligament of the knee joint. *Polym Med*. 2017;47(1):55-59. doi:10.17219/pim/76819
39. Langer R, Vacanti J. Tissue engineering. *Science (80-)*. 1993;260(5110):920-926. doi:10.1126/science.8493529
40. Viola J, Lal B, Hicks D, Grad O. The Emergence of Tissue Engineering as a Research Field. 2003.
41. Williams D. Benefit and risk in tissue engineering. *Mater Today*. 2004;7(5):24-29. doi:10.1016/S1369-7021(04)00232-9
42. Williams DF. Definitions in biomaterials: proceedings of a consensus conference of the European Society for Biomaterials. *Elsevier Sci Ltd*. 1987;Vol. 4.
43. Bronner F, Farach-Carson MC, Mikos AG, eds. *Engineering of Functional Skeletal Tissues*. Vol 3. London: Springer London; 2007. doi:10.1007/978-1-

84628-366-6

44. Williams DF. On the mechanisms of biocompatibility. *Biomaterials*. 2008;29(20):2941-2953. doi:10.1016/j.biomaterials.2008.04.023

45. Surrao DC, Waldman SD, Amsden BG. Biomimetic poly (lactide) based fibrous scaffolds for ligament tissue engineering. *Acta Biomater*. 2012;8(11):3997-4006. doi:10.1016/j.actbio.2012.07.012

46. Laurent C, Liu X, De Isla N, et al. Defining a scaffold for ligament tissue engineering: What has been done, and what still needs to be done. *J Cell Immunother*. 2018;4(1):4-9. doi:10.1016/j.jocit.2018.09.002

47. Nau T, Teuschl A. Regeneration of the anterior cruciate ligament: Current strategies in tissue engineering. *World J Orthop*. 2015;6(1):127-136. doi:10.5312/wjo.v6.i1.127

48. Yilgor C, Yilgor Huri P, Huri G. Tissue engineering strategies in ligament regeneration. *Stem Cells Int*. 2012. doi:10.1155/2012/374676

49. Yates EW, Rupani A, Foley GT, Khan WS, Cartmell S, Anand SJ. Ligament tissue engineering and its potential role in anterior cruciate ligament reconstruction. *Stem Cells Int*. 2012:11-14. doi:10.1155/2012/438125

50. Bhattarai N, Li Z, Gunn J, et al. Natural-Synthetic Polyblend Nanofibers for Biomedical Applications. *Adv*

Mater. 2009;21(27):2792-2797. doi:10.1002/adma.200802513

51. Yan Z, Yin H, Nerlich M, Pfeifer CG, Docheva D. Boosting tendon repair: interplay of cells, growth factors and scaffold-free and gel-based carriers. *J Exp Orthop*. 2018;5(1):1-13. doi:10.1186/s40634-017-0117-1
52. Petrigliano FA, Mcallister DR, Wu BM. Tissue Engineering for Anterior Cruciate Ligament Reconstruction : A Review of Current Strategies. 2006;22(4):441-451. doi:10.1016/j.arthro.2006.01.017
53. Lu HH, Cooper JA, Manuel S, et al. Anterior cruciate ligament regeneration using braided biodegradable scaffolds: In vitro optimization studies. *Biomaterials*. 2005;26(23):4805-4816. doi:10.1016/j.biomaterials.2004.11.050
54. Cooper JA, Lu HH, Ko FK, Freeman JW, Laurencin CT. Fiber-based tissue-engineered scaffold for ligament replacement: Design considerations and in vitro evaluation. *Biomaterials*. 2005;26(13):1523-1532. doi:10.1016/j.biomaterials.2004.05.014
55. Freeman JW, Woods MD, Cromer DA, Wright LD, Laurencin CT. Tissue engineering of the anterior cruciate ligament: The viscoelastic behavior and cell viability of a novel braid-twist scaffold. *J Biomater Sci Polym Ed*.

2009;20(12):1709-1728.
doi:10.1163/156856208X386282

56. Buma P, Kok HJ, Blankevoort L, Kuijpers W, Huiskes R, Van Kampen A. Augmentation in anterior cruciate ligament reconstruction — a histological and biomechanical study on goats. 2004;28:91-96. doi:10.1007/s00264-003-0515-0

57. Noyes FR, Grood ES. The Strength of the Anterior and Rhesus Cruciate Monkeys Ligament in Humans. *J Bone Jt Surgery, Ser A*. 1976;58(8):1074–1082.

58. Liljensten E, Gisselfalt K, Edberg B, Bertilsson H, Flodin P. Studies of polyurethane urea bands for ACL reconstruction. *J Mater Sci Mater Med*. 2002;13:351-359.

59. Rathbone S, Furrer P, Lubben J, Zinn M, Cartmell S. Biocompatibility of polyhydroxyalkanoate as a potential material for ligament and tendon scaffold material. 2009. doi:10.1002/jbm.a.32641

60. Irie T, Majima T, Sawaguchi N, Funakoshi T, Nishimura S, Minami A. Biomechanical and histologic evaluation of tissue engineered ligaments using chitosan and hyaluronan hybrid polymer fibers : A rabbit medial collateral ligament reconstruction model. 2011:111-117. doi:10.1002/jbm.a.32938

61. Teuschl A, Heimel P, Nürnberger S, Van Griensven M,

Redl H, Nau T. A novel silk fiber-based scaffold for regeneration of the anterior cruciate ligament: Histological results from a study in sheep. *Am J Sports Med*. 2016;44(6):1547-1557. doi:10.1177/0363546516631954

62. Li H, Fan J, Sun L, Liu X, Cheng P, Fan H. Functional regeneration of ligament-bone interface using a triphasic silk-based graft. *Biomaterials*. 2016;106:180-192. doi:10.1016/j.biomaterials.2016.08.012

63. Bettinger CJ, Langer R, Borenstein JT. Engineering substrate topography at the Micro- and nanoscale to control cell function. *Angew Chemie - Int Ed*. 2009;48(30):5406-5415. doi:10.1002/anie.200805179

64. Ishikawa H, Koshino T, Takeuchi R, Saito T. Effects of collagen gel mixed with hydroxyapatite powder on interface between newly formed bone and grafted Achilles tendon in rabbit femoral bone tunnel. 2001;22:1689-1694.

65. Robertson WJ, Hatch JD, Rodeo SA. Evaluation of Tendon Graft Fixation Using a -BSM Calcium Phosphate Cement. 2007;23(10):1087-1092. doi:10.1016/j.arthro.2007.04.007

66. Paxton JZ, Donnelly K, Keatch RP, Baar K. Engineering the Bone – Ligament Interface Using Polyethylene Glycol

Diacrylate Incorporated with Hydroxyapatite. *Tissue Eng Part A*. 2009;15(6). doi:10.1089/ten.tea.2008.0105

67. Spalazzi JP, Dagher E, Doty SB, Guo XE, Rodeo SA, Lu HH. In vivo evaluation of a multiphased scaffold designed for orthopaedic interface tissue engineering and soft tissue-to-bone integration. *J Biomed Mater*. 2008:1-12. doi:10.1002/jbm.a.32073

68. Spalazzi JP, Doty SB, Moffat KL, Levine WN, Lu HH. Development of Controlled Matrix Heterogeneity on a Triphasic Scaffold for Orthopedic Interface Tissue Engineering. *Tissue Eng*. 2006;12(12):3497-3508.

69. Carletti E, Motta A, Migliaresi C. Scaffolds for Tissue Engineering and 3D Cell Culture. In: Haycock JW, ed. *3D Cell Culture: Methods in Molecular Biology*. Vol 695. Methods in Molecular Biology. Totowa, NJ: Humana Press; 2011:17-39. doi:10.1007/978-1-60761-984-0_2

70. Vepari C, Kaplan DL. Silk as a Biomaterial. *Prog Polym Sci*. 2007;32(8-9):991-1007. doi:10.1016/j.progpolymsci.2007.05.013

71. Motta A, Maniglio D, Migliaresi C, et al. Silk fibroin processing and thrombogenic responses. *J Biomater Sci Polym Ed*. 2009;20(13):1875-1897. doi:10.1163/156856208X399936

72. Santo VE, Gomes ME, Mano JF, Reis RL. Controlled

release strategies for bone, cartilage, and osteochondral engineering-part i: Recapitulation of native tissue healing and variables for the design of delivery systems. *Tissue Eng - Part B Rev*. 2013;19(4):308-326. doi:10.1089/ten.teb.2012.0138

73. Mitchell AC, Briquez PS, Hubbell JA, Cochran JR. Engineering growth factors for regenerative medicine applications. *Acta Biomater*. 2016;30:1-12. doi:10.1016/j.actbio.2015.11.007

74. Padaki N V., Das B, Basu A. *Advances in Understanding the Properties of Silk*. Elsevier Ltd.; 2015. doi:10.1016/B978-1-78242-311-9.00001-X

75. Kaplan D, Adams WW, Farmer B, Viney C. Silk : Biology , Structure , Properties , and Genetics. 1994:2-16.

76. Altman GH, Diaz F, Jakuba C, et al. Silk-based biomaterials. *Biomaterials*. 2003;39:401-416. doi:10.1016/s0142-9612(02)00353-8

77. Teuschl AH, Van Griensven M, Redl H. Sericin removal from raw bombyx mori silk scaffolds of high hierarchical order. *Tissue Eng - Part C Methods*. 2014;20(5):431-439. doi:10.1089/ten.tec.2013.0278

78. Rockwood DN, Preda RC, Yücel T, Wang X, Lovett ML, Kaplan DL. Materials Fabrication from Bombyx mori Silk Fibroin. *Nat Protoc*. 2013. doi:10.1038/nprot.2011.379

79. Motta A, Fambri L, Migliaresi C. Regenerated silk fibroin films: Thermal and dynamic mechanical analysis. *Macromol Chem Phys*. 2002;203(10-11):1658-1665. doi:10.1002/1521-3935(200207)203:10/11<1658::AID-MACP1658>3.0.CO;2-3

80. Valluzzi R, Gido SP, Muller W, Kaplan DL. Orientation of silk III at the air-water interface. *Int J Biol Macromol*. 1999;24(2-3):237-242. doi:10.1016/S0141-8130(99)00002-1

81. Liu B, Song Y wei, Jin L, et al. Silk structure and degradation. *Colloids Surfaces B Biointerfaces*. 2015;131:122-128. doi:10.1016/j.colsurfb.2015.04.040

82. Motta A, Maniglio D, Migliaresi C, et al. Silk fibroin processing and thrombogenic responses. *J Biomater Sci Polym Ed*. 2009;20(13):1875-1897. doi:10.1163/156856208X399936

83. Altman GH, Horan RL, Lu HH, et al. Silk matrix for tissue engineered anterior cruciate ligaments. *Biomaterials*. 2002;23(20):4131-4141. doi:10.1016/S0142-9612(02)00156-4

84. Horan RL, Collette AL, Lee C, Antle K, Chen J, Altman GH. Yarn design for functional tissue engineering. *J Biomech*. 2006;39:2232-2240. doi:10.1016/j.jbiomech.2005.07.007

85. Horan RL, Toponarski I, Boepple HE, Weitzel PP, Richmond JC, Altman GH. Design and characterization of a scaffold for anterior cruciate ligament engineering. *J Knee Surg*. 2009;22(1):82-92. doi:10.1055/s-0030-1247730

86. Hohlrieder M, Teuschl AH, Cicha K, van Griensven M, Redl H, Stampfl J. Bioreactor and scaffold design for the mechanical stimulation of anterior cruciate ligament grafts. *Biomed Mater Eng*. 2013;23(3):225-237. doi:10.3233/BME-130746

87. Liu H, Fan H, Toh SL, Goh JCH. A comparison of rabbit mesenchymal stem cells and anterior cruciate ligament fibroblasts responses on combined silk scaffolds. *Biomaterials*. 2008;29:1443-1453. doi:10.1016/j.biomaterials.2007.11.023

88. Fan H, Liu H, Wong EJW, Toh SL, Goh JCH. In vivo study of anterior cruciate ligament regeneration using mesenchymal stem cells and silk scaffold. *Biomaterials*. 2008;29:3324-3337. doi:10.1016/j.biomaterials.2008.04.012

89. Chen X, Qi Y, Wang L, et al. Ligament regeneration using a knitted silk scaffold combined with collagen matrix. *Biomaterials*. 2008;29:3683-3692. doi:10.1016/j.biomaterials.2008.05.017

90. Panas-perez E, Gatt CJ, Dunn MG. Development of a silk and collagen fiber scaffold for anterior cruciate ligament reconstruction. *J Mater Sci*. 2013;24:257-265. doi:10.1007/s10856-012-4781-5

91. Fan H, Liu H, Toh SL, Goh JCH. Anterior cruciate ligament regeneration using mesenchymal stem cells and silk scaffold in large animal model. *Biomaterials*. 2009;30(28):4967-4977. doi:10.1016/j.biomaterials.2009.05.048

92. Altman G, Horan R, Weitzel P, Richmond J. The use of long-term bioresorbable scaffolds for anterior cruciate ligament repair. *J Am Acad Orthop Surg*. 2008;16:177-187.

93. Font Tellado S, Chiera S, Bonani W, et al. Heparin functionalization increases retention of TGF-β2 and GDF5 on biphasic silk fibroin scaffolds for tendon/ligament-to-bone tissue engineering. *Acta Biomater*. March 2018. doi:10.1016/J.ACTBIO.2018.03.017

94. Calejo I, Costa-Almeida R, Reis RL, Gomes ME. A Physiology-Inspired Multifactorial Toolbox in Soft-to-Hard Musculoskeletal Interface Tissue Engineering. *Trends Biotechnol*. 2019;38(1):83-98. doi:10.1016/j.tibtech.2019.06.003

95. Cicione C, Muinos-Lopez E, Hermida-Gomez T,

Fuentes-boquete I, Diaz-Prado S, Blanco FJ. Alternative protocols to induce chondrogenic differentiation : transforming growth factor- b superfamily. 2015;16:195-207. doi:10.1007/s10561-014-9472-7

96. Silva C, Carretero A, Soares da Costa D, Reis RL, Novoa-Carballal R, Pashkuleva I. Design of protein delivery systems by mimicking extracellular mechanisms for protection of growth factors. *Acta Biomater*. 2017;63:283-293. doi:10.1016/j.actbio.2017.08.042

97. Balmayor ER. Targeted delivery as key for the success of small osteoinductive molecules. *Adv Drug Deliv Rev*. 2015;94:13-27. doi:10.1016/j.addr.2015.04.022

98. Lee K, Silva EA, Mooney DJ. Growth factor delivery-based tissue engineering: General approaches and a review of recent developments. *J R Soc Interface*. 2011;8(55):153-170. doi:10.1098/rsif.2010.0223

99. Martino MM, Briquez PS, Maruyama K, Hubbell JA. Extracellular matrix-inspired growth factor delivery systems for bone regeneration. *Adv Drug Deliv Rev*. 2015;94:41-52. doi:10.1016/j.addr.2015.04.007

100. Rider CC, Mulloy B. Heparin, heparan sulphate and the TGF- Cytokine superfamily. *Molecules*. 2017;22(5):1-11. doi:10.3390/molecules22050713

101. Lorda-Diez CI, Montero JA, Martinez-Cue C, Garcia-

Porrero JA, Hurle JM. Transforming growth factors β coordinate cartilage and tendon differentiation in the developing limb mesenchyme. *J Biol Chem*. 2009;284(43):29988-29996. doi:10.1074/jbc.M109.014811

102. Guo X, Wang X-F. Signaling cross-talk between TGF-βBMP and other pathways. *Cell Res*. 2009;19(1):71-88. doi:10.1038/cr.2008.302.

103. Pryce BA, Watson SS, Murchison ND, Staverosky JA, Dünker N, Schweitzer R. Recruitment and maintenance of tendon progenitors by TGFBsignaling are essential for tendon formation. *Development*. 2009;136(8):1351-1361. doi:10.1242/dev.027342

104. Killian ML, Thomopoulos S. Scleraxis is required for the development of a functional tendon enthesis. *FASEB J*. 2016;30(1):301-311. doi:10.1096/fj.14-258236

105. Dyment NA, Breidenbach, Andrew P. Schwartz AG, Russell RP, et al. GDF5 PROGENITORS GIVE RISE TO FIBROCARTILAGE CELLS THAT MINERALIZE VIA HEDGEHOG SIGNALING TO FORM THE ZONAL ENTHESIS. 2015;405(1):96-107. doi:10.1016/j.ydbio.2015.06.020

106. Schneider S, Unger M, Van Griensven M, Balmayor ER. Adipose-derived mesenchymal stem cells from

liposuction and resected fat are feasible sources for regenerative medicine. *Eur J Med Res*. 2017;22(1):1-11. doi:10.1186/s40001-017-0258-9

107. Oliveira AL, Sun L, Kim HJ, et al. Aligned Silk-Based 3D Architectures for Contact Guidance in Tissue Engineering. *Acta Biomater*. 2012;8(4):1530-1542. doi:10.1016/j.actbio.2011.12.015

108. Hutmacher DW. Scaffolds in tissue engineering bone and cartilage. *Biomater Silver Jubil Compend*. 2000;21:175-189. doi:10.1016/B978-008045154-1.50021-6

109. Di Luca A, Szlazak K, Lorenzo-Moldero I, et al. Influencing chondrogenic differentiation of human mesenchymal stromal cells in scaffolds displaying a structural gradient in pore size. *Acta Biomater*. 2016;36:210-219. doi:10.1016/j.actbio.2016.03.014

110. Sakiyama-Elbert SE. Incorporation of heparin into biomaterials. *Acta Biomater*. 2014;10(4):1581-1587. doi:10.1016/j.actbio.2013.08.045

111. Leong NL, Arshi A, Kabir N, et al. In vitro and in vivo evaluation of heparin mediated growth factor release from tissue-engineered constructs for anterior cruciate ligament reconstruction. *J Orthop Res*. 2015;33(2):229-236. doi:10.1002/jor.22757

112. Jha AK, Mathur A, Svedlund FL, Ye J, Yeghiazarians,

Yerem Healy KE. Molecular Weight and Concentration of Heparin in Hyaluronic Acid-based Matrices Modulates Growth Factor Retention Kinetics and Stem Cell Fate. *J Control Release*. 2015;209:308-316. doi:10.1016/j.jconrel.2015.04.034

113. Manning C, Schwartz A, Liu W, et al. Controlled delivery of mesenchymal stem cells and growth factors using a nanofiber scaffold for tendon repair. *Acta Biomater*. 2013;9(6):6905-6914. doi:10.1016/j.actbio.2013.02.008
114. Lee SJ, Bae MS, Lee DW, et al. The use of heparin chemistry to improve dental osteogenesis associated with implants. *Carbohydr Polym*. 2017;157:1750-1758. doi:10.1016/j.carbpol.2016.11.062
115. Caliari SR, Harley BAC. Structural and biochemical modification of a collagen scaffold to selectively enhance MSC tenogenic, chondrogenic, and osteogenic differentiation. *Adv Healthc Mater*. 2014;3(7):1086-1096. doi:10.1002/adhm.201300646
116. Motta A, Foss C, Migliaresi C. Tailoring silk-based matrices for tissue regeneration. *ACS Symp Ser*. 2013;1135:281-299. doi:10.1021/bk-2013-1135.ch017
117. Wang Y, Kim HJ, Vunjak-Novakovic G, Kaplan DL. Stem cell-based tissue engineering with silk biomaterials. *Biomaterials*. 2006;27(36):6064-6082.

doi:10.1016/j.biomaterials.2006.07.008

118. Kew SJ, Gwynne JH, Enea D, et al. Synthetic collagen fascicles for the regeneration of tendon tissue. *Acta Biomater*. 2012;8(10):3723-3731. doi:10.1016/j.actbio.2012.06.018

119. Murugan R, Ramakrishna S. Design strategies of tissue engineering scaffolds with controlled fiber orientation. *Tissue Eng*. 2007;13(8):1845-1866. doi:10.1089/ten.2006.0078

120. Li W-JW-J, Tuli R, Okafor C, et al. A three-dimensional nanofibrous scaffold for cartilage tissue engineering using human mesenchymal stem cells. *Biomaterials*. 2005;26(6):599-609. doi:10.1016/j.biomaterials.2004.03.005

121. Aznar-Cervantes SD, Vicente-Cervantes D, Meseguer-Olmo L, Cenis JL, Lozano-Pérez AA. Influence of the protocol used for fibroin extraction on the mechanical properties and fiber sizes of electrospun silk mats. *Mater Sci Eng C*. 2013;33(4):1945-1950. doi:10.1016/j.msec.2013.01.001

122. Cho HJ, Ki CS, Oh H, Lee KH, Um IC. Molecular weight distribution and solution properties of silk fibroins with different dissolution conditions. *Int J Biol Macromol*. 2012;51(3):336-341. doi:10.1016/j.ijbiomac.2012.06.007

123. Callone E, Dirè S, Hu X, Motta A. Processing Influence on Molecular Assembling and Structural Conformations in Silk Fibroin: Elucidation by Solid-State NMR. *ACS Biomater Sci {&} Eng*. 2016;2(5):758-767. doi:10.1021/acsbiomaterials.5b00507

124. Ali U, Zhou Y, Wang X, Lin T. Electrospinning of Continuous Nanofiber Bundles and Twisted Nanofiber Yarns. 2008.

125. Domingues RMA, Chiera S, Gershovich P, Motta A, Reis RL, Gomes ME. Enhancing the Biomechanical Performance of Anisotropic Nanofibrous Scaffolds in Tendon Tissue Engineering: Reinforcement with Cellulose Nanocrystals. *Adv Healthc Mater*. 2016;5(11):1364-1375. doi:10.1002/adhm.201501048

126. Laranjeira M, Domingues RMA, Costa-Almeida R, Reis RL, Gomes ME. 3D Mimicry of Native-Tissue-Fiber Architecture Guides Tendon-Derived Cells and Adipose Stem Cells into Artificial Tendon Constructs. *Small*. 2017;13(31):1-13. doi:10.1002/smll.201700689

127. Shuakat MN, Lin T. Recent Developments in Electrospinning of Nanofiber Yarns. 2014;14(2):1389-1408. doi:10.1166/jnn.2014.9197

128. Gokarneshan N. Textiles in Tissue Engineering -A Review of Some Significant Trends. *Curr Trends Fash*

Technol Text Eng. 2018;4(1):1-6. doi:10.19080/ctftte.2018.04.555630

129. Tamayol A, Akbari M, Annabi N, Paul A, Khademhosseini A, Juncker D. Fiber-based tissue engineering: Progress, challenges, and opportunities. *Biotechnol Adv*. 2013;31(5):669-687. doi:10.1016/j.biotechadv.2012.11.007

130. Akbari M, Tamayol A, Laforte V, et al. Composite Living Fibers for Creating Tissue Constructs Using Textile Techniques. 2014;24:4060-4067. doi:10.1002/adfm.201303655

131. Guilak F, Butler DL, Goldstein SA, Baaijens FPT. Biomechanics and mechanobiology in functional tissue engineering. *J Biomech*. 2014. doi:10.1016/j.jbiomech.2014.04.019

132. Zhao J, Griffin M, Cai J, Li S, Bulter PEM, Kalaskar DM. Bioreactors for tissue engineering: An update. *Biochem Eng J*. 2016;109:268-281. doi:10.1016/j.bej.2016.01.018

133. Martin I, Wendt D, Heberer M. The role of bioreactors in tissue engineering. *Trends Biotechnol*. 2004;22(2):80-86. doi:10.1016/j.tibtech.2003.12.001

134. Chen HC, Hu YC. Bioreactors for tissue engineering. *Biotechnol Lett*. 2006;28(18):1415-1423. doi:10.1007/s10529-006-9111-x

135. Kahn CJF, Vaquette C, Rahouadj R, Wang X. A novel bioreactor for ligament tissue engineering. *Biomed Mater Eng*. 2008;18(4-5):283-287. doi:10.3233/BME-2008-0538

136. Sikavitsas VI, Temenoff JS, Mikos AG. Biomaterials and bone mechanotransduction. *Biomaterials*. 2001;22(19):2581-2593. doi:10.1016/S0142-9612(01)00002-3

137. Cartmell SH, Porter BD, García AJ, Guldberg RE. Effects of Medium Perfusion Rate on Cell-Seeded Three-Dimensional Bone Constructs in Vitro. *Tissue Eng*. 2003;9(6):1197-1203. doi:10.1089/10763270360728107

138. Levorson-Wright EJ, Santoro M, Kasper FK, Mikos AG. Scaffolds: Flow perfusion bioreactor design. In: *Comprehensive Biomaterials II*. Vol 5. ; 2017:1-17. doi:10.1016/B978-0-12-803581-8.10072-4

139. Kasper FK, Liao J, Kretlow JD, Sikavitsas VI, Mikos AG. Flow perfusion culture of mesenchymal stem cells for bone tissue engineering. *StemBook*. 2008:1-18. doi:10.3824/stembook.1.18.1

140. Alvarez-Barreto JF, Linehan SM, Shambaugh RL, Sikavitsas VI. Flow perfusion improves seeding of tissue engineering scaffolds with different architectures. *Ann Biomed Eng*. 2007;35(3):429-442. doi:10.1007/s10439-

006-9244-z

141. Melchels FPW, Tonnarelli B, Olivares AL, et al. The influence of the scaffold design on the distribution of adhering cells after perfusion cell seeding. *Biomaterials*. 2011;32(11):2878-2884. doi:10.1016/j.biomaterials.2011.01.023

142. Coulson-Thomas VJ, ferreira tarsis. Dimethylmethylene Blue Assay (DMMB). *Bio-protocol*. 2014;4(18):e1236. doi:10.21769/BioProtoc.1236

143. O'Brien J, Wilson I, Orton T, Pognan F. Investigation of the Alamar Blue (resazurin) fluorescent dye for the assessment of mammalian cell cytotoxicity. *Eur J Biochem*. 2000;267(17):5421-5426. doi:10.1046/j.1432-1327.2000.01606.x

144. Dinstein Y, Li Y, Dai DX-Q. *Biomechanical Engineering of Textiles and Clothing*. Woodhead Publishing; 2006.

145. Kolafik J, Migliaresi C, Stol M, Nicolais L. Mechanical properties of model synthetic tendons. 1981;15(September 1980):147-157. doi:https://doi.org/10.1002/jbm.820150204

146. Morrison JB. THE MECHANICS OF THE KNEE JOINT IN RELATION TO NORMAL WALKING. *J Biomech*. 1970;3(April 1969).

147. Schulze-Tanzil G, Al-Sadi O, Ertel W, Lohan A.

Decellularized Tendon Extracellular Matrix—A Valuable Approach for Tendon Reconstruction? *Cells*. 2012;1(4):1010-1028. doi:10.3390/cells1041010

148. Deville S, Saiz E, Nalla RK, Tomsia AP. Freezing as a Path to Build Complex Composites. *Science (80-)*. 2006;311.

149. Kundu B, Rajkhowa R, Kundu SC, Wang X. Silk fibroin biomaterials for tissue regenerations. *Adv Drug Deliv Rev*. 2013;65(4):457-470. doi:10.1016/j.addr.2012.09.043

150. Al-Nasiry S, Geusens, Hanssens M, Luyten C, Pijnenborg R. The use of Alamar Blue assay for quantitative analysis of viability , migration and invasion of choriocarcinoma cells. 2007;22(5):1304-1309. doi:10.1093/humrep/dem011

151. Präbst K, Engelhardt H, Ringgeler S, Hübner H. Colorimetric Proliferation Assays. *Basic Color Prolif Assays MTT, WST, Resazurin*. 2017;1601:1-17. doi:10.1007/978-1-4939-6960-9

152. Shukunami C, Takimoto A, Nishizaki Y, et al. Scleraxis is a transcriptional activator that regulates the expression of Tenomodulin, a marker of mature tenocytes and ligamentocytes. *Sci Rep*. 2018;8(1):1-17. doi:10.1038/s41598-018-21194-3

153. Wagner ER, Bravo D, Dadsetan M, et al. Ligament Tissue Engineering Using a Novel Porous Polycaprolactone Fumarate Scaffold and Adipose Tissue-Derived Mesenchymal Stem Cells Grown in Platelet Lysate. *Tissue Eng - Part A*. 2015;21(21-22):2703-2713. doi:10.1089/ten.tea.2015.0183

154. Fan H, Liu H, Toh SL, Goh JCH. Enhanced differentiation of mesenchymal stem cells co-cultured with ligament fibroblasts on gelatin/silk fibroin hybrid scaffold. *Biomaterials*. 2008;29(8):1017-1027. doi:10.1016/j.biomaterials.2007.10.048

155. Karin M, Clevers H. Reparative inflammation takes charge of tissue regeneration. *Nature*. 2016;529(7586):307-315. doi:10.1038/nature17039

156. Thurber AE, Omenetto FG, Kaplan DL. In vivo bioresponses to silk proteins. *Biomaterials*. 2015;71:145-157. doi:10.1016/j.biomaterials.2015.08.039

157. Khorramirouz R, Go JL, Noble C, et al. A novel surgical technique for a rat subcutaneous implantation of a tissue engineered sca ff old. *Acta Histochem*. 2018;120(3):282-291. doi:10.1016/j.acthis.2018.02.010

158. Corradetti B. *The Immune Response to Implanted Materials and Devices*. (Corradetti B, ed.).; 2017. doi:10.1007/978-3-319-45433-7

159. Liu H, Ge Z, Wang Y, Toh SL, Sutthikhum V, Goh JCH. Modification of sericin-free silk fibers for ligament tissue engineering application. *J Biomed Mater Res - Part B Appl Biomater*. 2007;82(1):129-138. doi:10.1002/jbm.b.30714

160. Woodward SC. Physiological and biochemical evaluation of implanted polymers. *Ann N Y Acad Sci*. 1968;146(1):225-250. doi:10.1111/j.1749-6632.1966.tb45498.x

161. Sussman EM, Halpin MC, Muster J, Moon RT, Ratner BD. Porous implants modulate healing and induce shifts in local macrophage polarization in the foreign body reaction. *Ann Biomed Eng*. 2014;42(7):1508-1516. doi:10.1007/s10439-013-0933-0

162. Holland C, Numata K, Rnjak-Kovacina J, Seib FP. The Biomedical Use of Silk: Past, Present, Future. *Adv Healthc Mater*. 2019;8(1). doi:10.1002/adhm.201800465

163. Li C, Guo C, Fitzpatrick V, et al. Design of biodegradable, implantable devices towards clinical translation. *Nat Rev Mater*. 2020;5(1):61-81. doi:10.1038/s41578-019-0150-z

164. Correia C, Bhumiratanaa S, Yan L-P, et al. Development of silk-based scaffolds for tissue engineering of bone from human adipose derived stem cells. *Acta Biomater*. 2012;8(7):2483-2492. doi:10.1016/j.actbio.2012.03.019

165. Meinel L, Hofmann S, Karageorgiou V, et al. The inflammatory responses to silk films in vitro and in vivo. *Biomaterials*. 2005;26(2):147-155. doi:10.1016/j.biomaterials.2004.02.047

166. Bucciarelli A, Chiera S, Quaranta A, Yadavalli VK, Motta A, Maniglio D. A Thermal-Reflow-Based Low-Temperature , High-Pressure Sintering of Lyophilized Silk Fibroin for the Fast Fabrication of Biosubstrates. *Adv Funct Mater*. 2019;1901134:1-13. doi:10.1002/adfm.201901134

Scientific Production

Review in preparation, entitled "The role of silk fibroin in recent TE applications for ACL/ligament-to-bone interface regeneration"

Manuscripts in International Journals

Bucciarelli A, **Chiera S**, Quaranta A, Yadavalli VK, Motta A, Maniglio D., A Thermal-Reflow-Based Low-Temperature , High-Pressure Sintering of Lyophilized Silk Fibroin for the Fast Fabrication of Biosubstrates, Adv Funct Mater. **2019**;1901134:1-13. doi:10.1002/adfm.201901134.

Font Tellado S, **Chiera S**, Bonani W, Patrina S.P. Poh, Claudio Migliaresi, Antonella Motta, Elizabeth R. Balmayor, Martijn van Griensven, Heparin functionalization increases retention of TGF-β2 and GDF5 on biphasic silk fibroin scaffolds for tendon/ligament-to-bone tissue engineering, Acta Biomater. March **2018**. doi:10.1016/J.ACTBIO.2018.03.017.

Domingues RMA, **Chiera S**, Gershovich P, Motta A, Reis RL, Gomes ME. Enhancing the Biomechanical Performance of Anisotropic Nanofibrous Scaffolds in Tendon Tissue

Engineering: Reinforcement with Cellulose Nanocrystals. Adv Healthc Mater. **2016**; 5 (11): 1364-1375 doi:10.1002/adhm.201501048 (production in master thesis)

Participation to congresses and schools

S. Chiera, W. Bonani, D. Maniglio, A. Motta, C. Migliaresi, *Design of a multicomponent silk fibroin scaffold for ligament regeneration*, Achilles Conference, 8-11th July 2019; Porto, Portugal (ORAL COMMUNICATION)

S. Chiera, W. Bonani, D. Maniglio, A. Motta, C. Migliaresi, *Design of a new bioactive matrix to guide ligament regeneration*, TICME conference, 12-15th June 2019; Trento, Italy (POSTER)

S. Chiera, W. Bonani, A. Motta, C. Migliaresi, *Design of a new bioactive matrix to guide ligament regeneration*, TERMIS EU Conference, 27-31th May 2019; Rhodes, Greece (ORAL COMMUNICATION)

S. Chiera, W. Bonani, D. Maniglio, A. Motta, C. Migliaresi, *Equine collagen scaffold as rotator cuff support*, Comprehensive Summer school on Tissue Engineering, 18-23rd June 2018; Trento, Italy (ORAL COMMUNICATION)

S. Chiera, W. Bonani, A. Motta, C. Migliaresi, *Characterization of textile silk fibers for tendon tissue engineering applications*, Bone-tec conference, 12-14th October 2017; Munich, Germany (ORAL COMMUNICATION)

Internship

September-December 2019: internship as visiting PhD student; under the supervisor of Prof. Gilson Khang; Department of Engineering of Chonbuck National University, Jeonju, South Korea. Research activities focused on *in vitro* and *in vivo* evaluation of silk fibroin scaffold for tissue engineering applications.

Acknowledgements

I would like to thank my PhD supervisors, Professor Antonella Motta and Professor Claudio Migliaresi, for giving me the opportunity to conduct my PhD research, with precious mentoring and support through the years. I am grateful to Professor Devid Maniglio and Doctor Walter Bonani for sharing their valuable scientific knowledge and for giving me important suggestions. Thanks to all the members of BIOtech Research Center, in particular to our technician Lorenzo Moschini for his technical support.

I would like also to thank Prof. Dr. Matijn Van Griensven, Dr. Elisabeth Rosado Balmayor for making our collaboration possible and for giving me the opportunity to enrich my research, especially the work done together with Sonia Font Tellado, but also with Sandra Schneider.

A special thanks to Prof. Khang for his supervision and kindness during my internship at Chonbuck National University and to his collaborators, in particular Hunhwi Cho.

Thanks to REMIX" Project, G.A. 778078 H2020-MSCA-RISE2017 for having partially financially supported my research project.

A special thanks to all collaborators and colleagues along this journey.